Dekan der Fakultät für Biologie: Prof. Dr. Dierk Reiff
Promotionsvorsitzender: Prof. Dr. Andreas Hiltbrunner
Betreuer der Arbeit:
Referent:
Koreferent:
Drittprüfer:
Datum der mündlichen Prüfung:

Inaugural-Dissertation zur Erlangung des Doktorgrades der Fakultät für Biologie der Albert-Ludwigs Universität Freiburg im Breisgau und der Fakultät für Informatik der KTH Stockholm

Characterisation of inputs and outputs of striatal medium spiny neurons in health and disease

Author:
Marko Filipović
born in
Belgrade, Serbia

Supervisors:

Prof. Arvind Kumar

Prof. Gilad Silberberg

Prof. Ad Aertsen

Prof. Jeanette Hällgren Kotaleski

A thesis submitted in fulfilment of the requirements for the degree of Doctor of Philosophy in the

Albert-Ludwigs Universität Freiburg im Breisgau, (Faculty of Biology)
and for the degree of PhD in Computer Science in
KTH, Royal Institute of Technology, Stockholm, (Dept. of Computational Science and Technology, School of Electrical Engineering and Computer Science)

Thesis printed in Sweden by US-AB, Stockholm, November 2019

Declaration of Authorship

I, Marko Filipović, declare that this thesis titled, 'Characterisation of inputs and outputs of striatal medium spiny neurons in health and disease' and the work presented in it are my own. I confirm that:

- This work was done wholly or mainly while in candidature for a research degree at this University.
- Where any part of this thesis has previously been submitted for a degree or any other qualification at this University or any other institution, this has been clearly stated.
- Where I have consulted the published work of others, this is always clearly attributed.
- Where I have quoted from the work of others, the source is always given. With the exception of such quotations, this thesis is entirely my own work.
- I have acknowledged all main sources of help.
- Where the thesis is based on work done by myself jointly with others, I have made clear exactly what was done by others and what I have contributed myself.

Signed: _____

Date: _____

Abstract

Striatal medium spiny neurons (MSNs) play a crucial role in various motor and cognitive functions. They are separated into those belonging to the direct pathway (dMSNs) and the indirect pathway (iMSNs) of the basal ganglia, depending on whether they express D1 or D2 type dopamine receptors, respectively. In this thesis I investigated the input processing of both MSN types, the characteristics of dMSN outputs, and the effect that aberrant iMSN activity has on the subthalamic nucleus-globus pallidus externa (STN-GPe) network.

In order to verify a previous result from a computational study claiming that dMSNs should receive either more or stronger total input than iMSNs, I performed an analysis of *in vivo* whole-cell MSN recordings in healthy and dopamine (DA) depleted (6OHDA) anesthetized mice. To test this prediction, I compared subthreshold membrane potential fluctuations and spike-triggered average membrane potentials of the two MSN types. I found that dMSNs in healthy mice exhibited considerably larger fluctuations over a wide frequency range, as well as significantly faster depolarization towards the spiking threshold than iMSNs. However, these effects were not present in recordings from 6OHDA animals. Together, these findings strongly suggest that dMSNs do receive stronger total input than iMSNs in healthy condition.

I also examined how different concentrations of dopamine affect neural trial-by-trial (or response) variability in a biophysically detailed compartmental model of a direct-pathway MSN. Some of the sources of trial-by-trial variability include synaptic noise, neural refractory period, and ongoing neural activity. The focus of this study was on the effects of two particular properties of the synaptic input: correlations of synaptic input rates, and the balance between excitatory and inhibitory inputs (E-I balance). The model demonstrates that dopamine is in general a significant diminisher of trial-by-trial variability, but that its efficacy depends on the properties of synaptic input. Moreover, input rate correlations and changes in the E-I balance by themselves also proved to have a marked impact on the response variability.

Finally, I investigated the beta-band phase properties of the STN-GPe network, known for its exaggerated beta-band oscillations during Parkinson's disease (PD). The current state-of-the-art computational model of the network can replicate both transient and persistent beta oscillations, but fails to capture the beta-band phase alignment between the two nuclei as seen in human recordings. This was particularly evident during simulations of the PD condition, where STN or GPe were receiving additional stimulation in order to induce pathological levels of beta-band activity. Here I show that by manipulating the percentage of the neurons in either population that receives stimulation it is possible to increase STN-GPe phase difference heterogeneity. Furthermore, a similar effect can be achieved by adjusting synaptic transmission delays between the two populations. Quantifying the difference between human recordings and network simulations, I provide the set of parameters for which the model produces the greatest correspondence with experimental results.

Zusammenfassung

"Striatal Medium Spiny Neurons" (MSNs) spielen eine essentielle Rolle in verschiedensten Motor- und kognitiven Funktionen. Sie werden unterschieden in solche, die dem direkten (dMSNs) und dem indirekten (iMSNs) Signalweg der Basalganglien zugeordnet werden, abhängig davon ob sie D1- oder D2-typ Dopaminrezeptoren exprimieren. In dieser Arbeit untersuche ich die Eingangsverarbeitung beider MSN-Typen, die Charakteristiken von dMSN-Ausgängen, sowie den Effekt, den anomale iMSN-Aktivität auf das "Subthalamischer Nucleus-Globus Pallidus Externa" (STN-GPe)-Netzwerk hat.

Um die Ergebnisse einer vorangehenden rechnergestützten (computational) Studie zu verifizieren, die den Anspruch erhebt, dass dMSNs entweder mehr, oder stärkeren Eingang als iMSNs bekommen sollten, habe ich in-vivo Ganzzellen-MSN-Messdaten in gesunden und Dopamin (DA)-abgereicherten (6OHDA) anästhesierten Mäusen analysiert. Um diese Vorhersage zu prüfen, habe ich Schwankungen des Membranpotentials unterhalb der Feuerschwelle und Spike-induzierte mittlere Membranpotentiale jener beiden MSN-Typen verglichen. Ich fand heraus, dass in gesunden Mäusen sMSNs deutlich größere Schwankungen über eine große Frequenzspanne, sowie eine signifikant schnellere Depolarisation hin zur Feuerschwelle zeigen als iMSNs dies tun. In Messdaten von 6OHDA-Versuchstieren hingegen waren diese Effekte nicht zu beobachten. Diese beiden Befunden zusammengenommen legen nahe, dass in gesundem Zustand dMSNs stärkeren Gesamteingang erhalten als iMSNs.

Zudem habe ich untersucht inwiefern verschiedene Dopaminkonzentrationen neurale "trial-by-trial"-variabilität bzw. Antwort-Variabilität in einem biophysikalisch detaillierten Kompartiment-Modell von dMSNs beeinflussen. Quellen von trial-by-trial-Variabilität sind unter anderem synaptisches Rauschen, neurale Refraktionszeit und fortlaufende neurale Aktivität. Der Schwerpunkt dieser Studie lag auf dem Effekt zweier bestimmter Eigenschaften von synaptischem Eingang: Zum einen Korrelationen von synaptischen Eingangsraten, zum anderen die Balance zwischen anregenden und hemmenden Eingängen ("E-I-balance"). Das Modell zeigt, dass Dopamin im allgemeinen die trial-by-trial-Variabilität erheblich verringert, aber seine Wirkungskraft von den Eigenschaften des synaptischen Eingangs abhängt. Darüber hinaus hat es sich herausgestellt, dass Korrelationen der Eingangsraten und Änderungen in der E-I-Balance für sich genommen ebenfalls deutlichen Einfluss auf die Antwortvariabilität haben.

Schließlich habe ich die Beta-Band Phaseneigenschaften des STN-GPe Networks untersucht, von welchem bekannt ist, dass im Falle von Parkinson (PD) in übersteigertem Maße Beta-Band Oszillationen stark erhöht sind. Der mathematische Modell nach aktuellem Stand der Wissenschaft ist in der Lage sowohl das transiente, sowie auch anhaltende Beta-Oszillationen zu replizieren, scheitert aber daran die Beta-Band-Phasenbeziehung zwischen den zwei Nuklei zu erfassen, wie sie in Messungen am Menschen beobachtet wird. Dies war besonders deutlich ersichtlich bei Simulationen des Parkinson-Zustands, bei welchen STN oder GPe zusätzlich stimuliert werden um pathologische Niveaus von Beta-Band-Aktivität zu herbeizuführen. Durch diese Ergebnisse zeige ich, dass durch Anpassen des Bruchteils – wie viele Neuronen derjenigen der beiden Populationen die Stimulation erhält, tatsächlich stimuliert werden – es möglich ist, die Heterogenität der STN-GPe-Phasendifferenzen zu erhöhen. Ein ähnlicher Effekt kann erreicht werden, in dem

man die synaptischen Transmissionszeiten zwischen den beiden Populationen anpasst. Um die Diskrepanz zwischen Daten aus Messungen am Menschen und Daten aus Netzwerksimulationen zu quantifizieren, liefere ich Parameterwerte für die die Ergebnisse des Modells die größte Übereinstimmung mit den experimentellen Daten zeigen.

Abstrakt

Striatala medium spiny neuroner (MSNs) spelar en stor roll för olika motoriska och kognitiva funktioner. Beroende på huruvida dessa neuroner uttrycker dopaminreceptorer av D1- eller D2-typ, klassificeras de som tillhörande den direkta (dMSN) respektive den indirekta (iMSN) vägen genom basala ganglierna. I denna avhandling undersöker jag hur inputet från kortex till de två typerna av MSNs processas och jag karakteriserar aktiviteten från dMSNs, samt undersöker även vilken effekt avvikande iMSN aktivitet ger upphov till i det basala ganglienätverk som består av den subthalamiska kärnan (STN) och globus pallidus externa (GPe).

För att verifiera resultaten från en tidigare modelleringsstudie, som predicerat att dMSNs erhåller fler eller får starkare inputs från kortex jämfört med iMSNs, analyserade jag in vivo data från MSN 'wholecell' registreringar gjorda i nedsövda möss som antingen tillhört en kontrollgrupp (friska möss) eller en grupp där dopamin (DA) reducerats m.h.a. 6OHDA. För att testa modellprediktionen jämförde jag subtröskliga membranpotentialfluktuationer och spik-triggade medelvärdesbildade membranpotentialer från de två typerna av MSNs. Jag upptäckte att dMSNs från kontrollgruppen uppvisade avsevärt större fluktuationer över ett brett frekvensintervall och också hade en snabbare depolarisering mot spiktröskeln jämfört med iMSNs. Dessa effekter syntes dock inte i experimentella data från de djur som behandlats med 6OHDA. Sammantaget tyder dessa observationer på att dMSNs i friska möss får starkare kortexinput än iMSNs.

Jag använde även en biofysikaliskt detaljerad kompartmentmodell av en dMSN för att undersöka hur olika dopaminkoncentrationer påverkar responsvariabiliteten vid upprepade försök. Synaptiskt brus, neuronens refraktärperiod såväl som den pågående nätverksaktiviteten kan utgöra orsaker till responsvariabiliteten. I den här studien fokuserade vi på effekten av två egenskaper hos synapsinputet: korrelationer mellan synapsernas aktiveringsfrekvens, och balansen mellan de excitatoriska och inhibitoriska inputen (E-I balansen). Modellen visar att dopamin generellt förminskar responsvariabiliteten signifikant, men att effekten beror på synapsinputets egenskaper. Dessutom fann jag att både korrelationer i inputfrekvensen och förändringar i E-I balansen hade en stark inverkan på responsvariabiliteten

Slutligen undersökte jag STN-GPe nätverkets egenskaper vad gäller faskopplingen i beta-bandsområdet, vilket är intressant eftersom oscillationer med beta-bandsfrekvenser ses vid Parkinson's sjukdom (PD). Dagens state-of-the-art nätverksmodeller kan reproducera både transienta och persistenta betaoscillationer, men kan inte fånga den faskoppling mellan STN och GPe inom beta-bandet som ses i data från människa. Detta är särskilt tydligt vid simulering av PD, när STN eller GPe stimuleras extra för att inducera patologiska nivåer av beta-bandsaktivitet. Jag visar att genom att ändra den andel av neuronerna i de två kärnorna som stimuleras, är det möjligt att öka heterogeniciteten i fasskillnaden mellan STN och GPe. Dessutom kan en liknande effekt även erhållas genom att ändra fördröjningen i synapserna mellan de två populationerna. Genom att kvantifiera skillnaderna mellan humana data och nätverkssimuleringarna kunde jag bestämma den uppsättning parameterar där modellen producerar den största likheten med de experimentella resultaten.

Publications

1. Chapter 2 is published in the Journal of Neurophysiology as
   Direct Pathway Neurons in Mouse Dorsolateral Striatum In Vivo Receive Stronger Synaptic Input than Indirect Pathway Neurons
   Marko Filipović, Maya Ketzef, Ramon Reig, Ad Aertsen, Gilad Silberberg, Arvind Kumar

2. Chapter 3 will be submitted as
   Modulatory effects of dopamine on dynamical space of direct pathway striatal neurons: a simulation study
   Marko Filipović, Robert Lindroos, Jeanette Hellgren-Kotaleski, Arvind Kumar

3. Chapter 4 is a part of the ongoing work that will be submitted in the future.

Acknowledgements

During these utterly transformative seven years I was very lucky to do actual science under the supervision of Prof. Arvind Kumar and Prof. Gilad Silberberg. It has been an incredible ride, filled with triumphs and frustrations and discoveries that will hopefully be of some use to future researchers. Through it all, Arvind provided both excitation and inhibition where needed, balancing his inputs in accordance to my outputs. His advice, support, and scientific zeal improved my critical thinking, skills in research, writing and general workflow. But of course, how could it have been any different — he's a Kumar after all! I am also very grateful to Gilad for accepting me to his lab, supporting me in a crucial moment and teaching me what a life of an experimentalist is like. Without that experience I don't think I would have come to appreciate all the aspects of neuroscience that I have. Thank you Gilli!

I would also like to thank Prof. Jeanette Hellgren-Kotaleski and Prof. Ad Aertsen for their crucial feedback on my work at different stages, and for discussions that we shared. Whatever the quality of this thesis, it is that much better for their input.

A huge part of my PhD life was spent in Bernstein Center Freiburg, and I am not sure that there is a better place for scientific work than there. I extend my most heartfelt thanks to the lovely and helpful staff of BCF who had to deal with my problems more than they would have wished: Janina Kirsch, Gundel Jäger, Fiona Siegfried, Katrin Pansa, Liliane Merz, Birgit Ahrens, and Uwe Grauer. I would also like to thank Prof. Stefan Rotter for his advice, when I occasionally popped into his office with random questions. Finally, I would like to acknowledge the generous funding of the Erasmus Mundus program "EuroSPIN", without which none of this would have been possible.

What made my stay at BCF special even more were wonderful discussions and nights out with: Alejandro (Bujan), Julia, Salvatore, Nebojša, Marco (sorry for all the noise!), Han, Luiz, Robin, Diego&Stephanie, Wenqing, Taskin, Sima, Simon, Ioannis, Antje, Félix (Tiago), Felix (Hoffmann), Renato, Sadra, Sarah, Fereshteh, Benjamin (I still owe you 2 or 3 beers), Michael (Prettyboy), and Gunnar. I will miss you all sorely, folks.

Special place in my heart is reserved for the "Basal Gang", for many a wonderful discussion and a night of gaming: Jyotika (man, I owe you *so* much!), Sebastian, Martin, Carlos, Lars (damn your boardgame savvy!), Alejandro (Jimenez), Amin, Mohammadreza, and Robert. You folks made me fall in love with this amazing and infuriating brain structure. Shame on you!

A very special shoutout to two of the people I quite accidentally befriended to an unexpected degree: Stojan Jovanović and Martin Angelhuber. I love you both!

A part of my PhD was spent in beautiful Stockholm, where I met such a bunch of great people I doubt I'll meet again: Maya (you rock!), Yvonne, Robert (man, did I bother you all the time or what), Kai (I still don't worry about it!), Matthijs, Josje, Ramon, Wioleta, Ylva, Martino, Jovana, Georgios, Florian, Peter, Daniel, and Anu.

I will never forget the time and memories I share with Milena, who was there through thick and thin and who supported me no matter what. I owe her more than I can every repay.

Also, a big fat kiss to all my friends back home: Bujke, Dača, Koči, Neša, Reba, Kara, Proka, Voca. You may have been out of sight, but never out of mind!

And finally, without the love and support of my family, I am honestly not sure if I could have finished this. My parents, Milan and Olga, and my grandparents, Jaša and Zdenka, sacrificed a lot to get both my brother and myself to where we are. I am forever indebted to them. Speaking of my brother Aleksa, a shoutout to him for continuing to surprise me with his achievements. And I thought I was the smart one! No matter, I'm still uglier than him, that counts for something.

Contents

List of Figures

List of Tables

To my grandma and grandpa. I wish they could have seen this day.
To my family.

Mojoj baki i mom deki, voleo bih da su dočekali ovaj dan.
Mojoj porodici.

Chapter 1

Introduction

The basal ganglia (BG) is a set of interconnected subcortical nuclei involved in several critical brain functions, including action selection, motor control, and reinforcement learning (Figure 1.1*A*) (Averbeck and Costa, 2017, Groenewegen, 2003). Their dysfunction is implicated in such pathologies as Parkinson's disease (PD), Huntington's disease, and other movement-related disorders, but also addictive behavior, depression, anxiety, and similar (Albin et al., 1989, Miller, 2007). Given this, understanding both function and dysfunction of the BG is of supreme importance not just for neuroscience, but also for medicine and other related fields.

The main input station and the largest nucleus of the basal ganglia is the striatum – "the striped body", named for its patterned white-and-grey matter appearance. The striatum receives direct input from multiple cortical and thalamic regions, with different upstream areas innervating different striatal sections (Wall et al., 2013).

Anatomically, the striatum is a complex and fairly large brain structure composed of ventral and dorsal sections. The ventral striatum consists of the nucleus accumbens and the olfactory tubercle, and is associated with limbic system and reward-related behavior (Tremblay et al., 2009). The dorsal striatum is divided into the caudate nucleus and the putamen that are separated by a layer of white matter called the internal capsule, and is involved in motor function and associative learning (Anderson et al., 2017, Groenewegen, 2003). Both striatal sections are targets of dopamine (DA) neurons, with the ventral striatum being innervated from the ventral tegmental area in the midbrain (mesolimbic pathway), and the dorsal striatum receiving dopaminergic projections from substantia nigra pars compacta (SNc), another of the BG nuclei (Ikemoto, 2010, Lammel et al., 2011, Lynd-Balta and Haber, 1994).

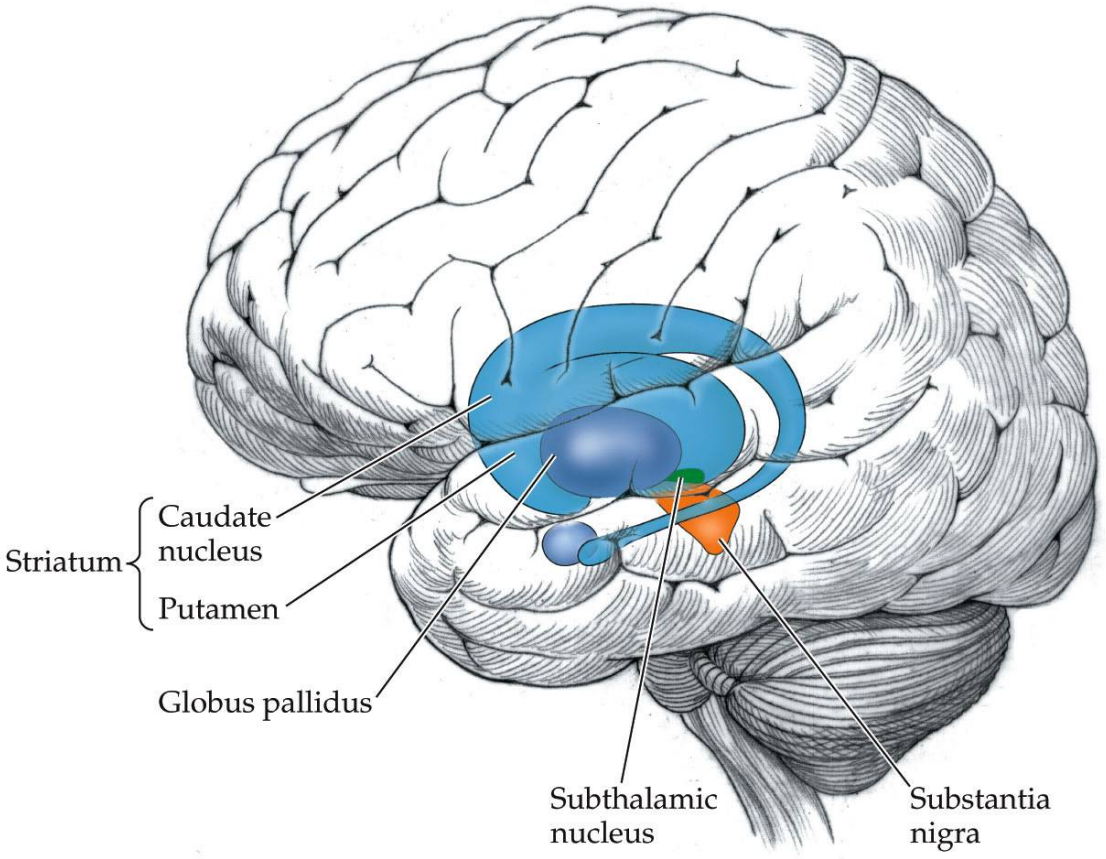

Fig 1.1. The basal ganglia with their constituent nuclei. Figure taken from `https://beyondthedish.wordpress.com/tag/basal-ganglia/`.

The most prominent targets for dopamine afferents are medium spiny neurons (MSNs), the principal neurons of the striatum that comprise 95% of its total neuronal population. MSNs are GABAergic cells that receive excitatory inputs from cortex and thalamus and inhibitory inputs from several different types of striatal interneurons, as well as lateral inhibitory connections from other MSNs. This makeup makes the striatal network a purely inhibitory one, driven only by excitation coming from upstream brain areas. Additionally, MSNs are divided into two groups based on which dopamine receptor they express: D1-type MSN group that includes D1 and D5 receptors and whose excitability is increased by the presence of dopamine, and D2-type MSNs that express D2, D3, and D4 receptors that get suppressed with increased DA levels. The two MSN types are also the originators of the "direct" and "indirect" neural pathways of the basal ganglia that are thought to regulate action selection and voluntary movement (Figure 1.2) (Gerfen and Scott Young, 1988, Nambu, 2004). D1-type MSNs are associated with the direct pathway, and are thus often abbreviated as "dMSNs", while D2-type MSNs are considered to be a part of the indirect pathway and are similarly called "iMSNs". This is also the notation that is going to be used throughout this thesis.

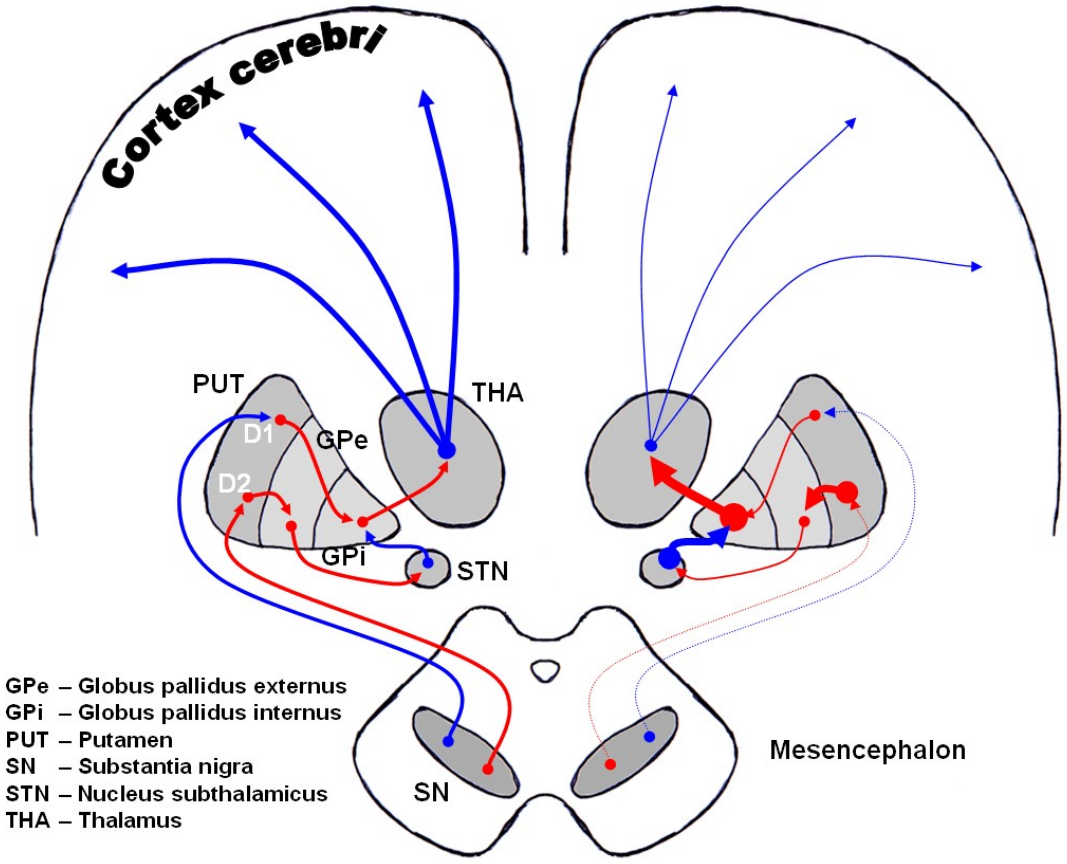

Fig 1.2. Functional pathways in the basal ganglia. Blue connections indicate stimulation, and red arrows suppression of the target. The left side of the figure represents a human brain in normal conditions, whereas the right side shows the changes in connection strengths during Parkinson's disease. Figure taken from `https://commons.wikimedia.org/wiki/File:DA-loops_in_PD.jpg`.

1.1 A short history of the striatal research

While the structure, composition, and the assumed function of the striatum as described above are textbook knowledge today, the road to these discoveries was very long. Indeed, it started already in the 2nd century AD with Claudius Galenus, a Greek physician and surgeon in the Roman Empire also known as Galen of Pergamon. He was the first to leave a written record of basal forebrain structures that he named glutia (buttocks) (Parent, 2012). Yet, it wasn't until the 16th century and the Flemish anatomist Andreas Vesalius that the first illustrations including delineations of the basal ganglia structures could be found (Figure 1.3*A*). Even though Vesalius's work was of great importance, he didn't provide any specific labeling of BG nuclei. This was remedied by Thomas Willis who, apart from coining the term "neurology", had very detailed drawings of the basal ganglia made for his 1664 treatise *Cerebri anatome* (Figure 1.3*B*). Giving a special focus to the structure he named corpus striatum, he hypothesized that it had a crucial role in the control of motor behavior (Parent, 2012). Over the span of the

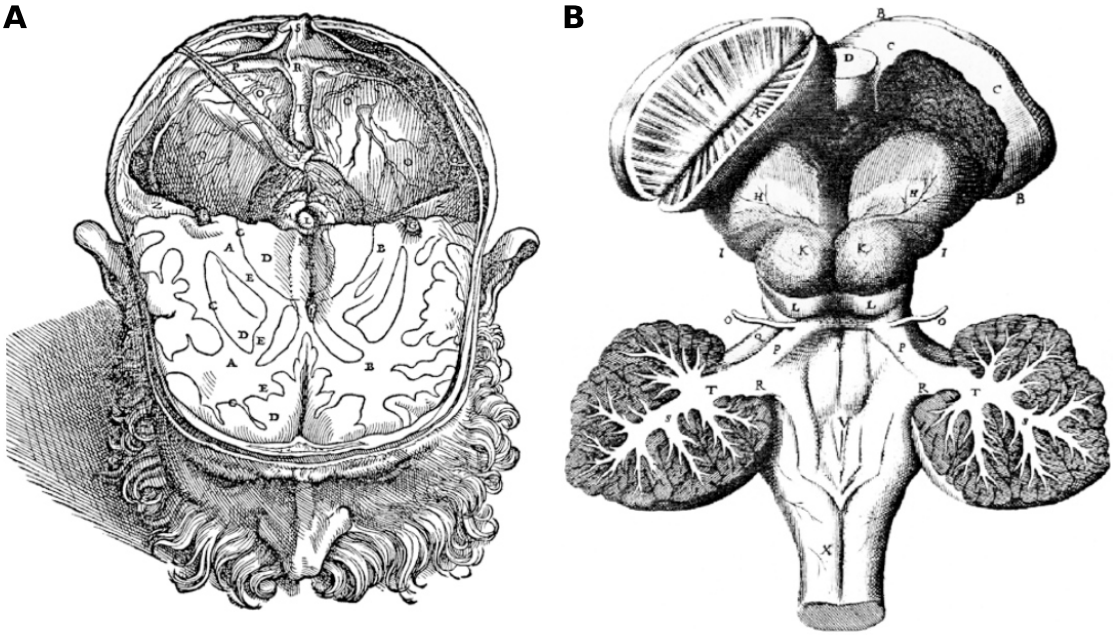

Fig 1.3. Graphical representations of the BG of old. ***A*** Andreas Vesalius's depiction of the BG from the 16th century, showing a horizontal section through the human brain. Putamen and thalamus can be recognized in the right hemisphere in the sections labeled with the letter D, and tracts of white matter labeled with E and roughly corresponding to internal capsule can be seen separating them. ***B*** Depiction of the BG found in Thomas Willis's 17th century text *Cerebri anatome*. Corpus striatum on the right side has been bisected to expose the eponymous striations. Figures taken from Parent (2012).

next two centuries, several prominent European anatomists and physiologists further improved on the knowledge of basal ganglia, providing ever more detailed illustrations and delineating many of the discrete BG nuclei. However, only with the work of Karl Friedrich Burdach in the 19th century was that the striatum received more attention. In his seminal work *Vom Baue und Leben des Gehirns*, published in three parts between 1819 and 1826, Burdach recognized that caudate nucleus and putamen were different structures divided by the internal capsule. He also described the globus pallidus (GPe), substantia nigra (SN), claustrum, and the external capsule, with the subthalamic nucleus (STN) being the only one of BG constituents left unexplored (Parent, 2012).

Even though the caudate and putamen were now treated as separate nuclei, a common embryonic origin of the two structures was discovered by Carl Wernicke (1876), and their identical structures together with a connecting region described by Charles Foix and Ion Nicolesco (1925). Finally, Cécile and Oskar Vogt (1941) and one of their students, Harald Brockhaus (1942), established the single term "striatum" for all elements that were previously considered individual parts of the corpus striatum: the caudate nucleus, the putamen, and the narrow bridge of grey matter that connected them called "fundus striati" (Percheron et al., 1994).

A quite fascinating aspect of the history of striatal research is the discovery of cortico-striatal connections. Namely, already in the second half of the 19th century Theodor Meynert (1871) and Jules Bernard Luys (1882) speculated about the striatum being the source of the motor tract in the brain, which consequently necessitated the presence of a cortico-striatal connection. However, during this period several anatomical experiments performed by Jean Martin Charcot (1876), Paul Flechsig (1877), and Wernicke (1880) demonstrated the existence of the pyramidal tract and its independence with respect to the basal ganglia. This resulted in the rejection of the idea of a cortico-striatal connection for the following 80 years, with many of the prominent neurophysiologists and anatomists of the first half of the 20th century (Joseph Jule Dejerine, S.A.K. Wilson, M.A. Souques, Foix, Nicolesco) denying its existence (Percheron et al., 1994). The whole issue stemmed from the fact that the cortico-striatal axons are very fine and – most importantly – not myelinated, while the staining methods used in that period were myelin-based. This of course prevented the anatomists from observing the presence of such connections. Not until an influential topographical study of Janet Kemp and Thomas Powell in 1970 was the cortico-striatal projection explicitly identified Jones (1999).

The history of striatal pathophysiology began with the description of caudate atrophy in Huntington's disease (although it is contested whether the initial discovery was made by G. Anton in 1896, or by Alois Alzheimer in 1911), and continued with the Vogts who were convinced of the major role of the basal ganglia in motor disorders (Percheron et al., 1994).

Chief among BG pathologies, Parkinson's disease was described a century earlier (original essay reproduced in Parkinson 2002), but its mechanism was an enigma until 1970s. An aspect of PD that was known at the start of the 20^{th} century was the dying out of neurons of substantia nigra pars compacta (SNc), and different lesion experiments have provided several different explanations of the cause of the disease. At the 1921 meeting of the Society of Neurology devoted to Parkinsonian symptoms, proponents of each of these explanations came to a head: the "nigrists", the "pallidists", the "rubrists", and the "mixed" group. Over the following decades, several of the prominent researchers (including the Vogts and Wilson) changed their opinions and came to believe that it was indeed a pallidal lesion that was responsible for PD. Only in 1971 had the research by Raymond Escourolle and associates revealed for the first time the dopaminergic nature of nigro-striatal connection and the effectiveness of the L-Dopa treatment in alleviating Parkinsonian symptoms (Percheron et al., 1994).

While anatomical studies provided much knowledge about the structure of the basal ganglia they weren't able to provide much insight into its function. Nevertheless, their involvement with motor function was established based on efferent projections from the

globus pallidus that terminate in the ventral thalamus, which in turn projects to the motor cortex (DeLong, 1971). With the advent of extracellular single-unit recordings in 1957 (Gusel'nikov, 1957, Hubel, 1957, Ricci et al., 1957) and other more involved techniques later on, studies in both anesthetized (Denny-Brown, 1962, Jung and Hassler, 1960, Adey and Dunlop, 1960) and moving (Travis and Sparks, 1967, DeLong, 1971) animals paved the way for the first functional maps of the basal ganglia circuitry. During the 1980s, anatomical and physiological studies pointed towards the existence of at least two separate BG-thalamocortical loops based on the origin of cortical afferents to different portions of the striatum (Figure 1.4*A*) (Alexander et al., 1986). By the end of the decade, with the discovery that striatal medium spiny neurons belonging to striatonigral pathway express D1 dopamine receptor and those belonging to striatopallidal pathway express D2 dopamine receptor, the full description of the BG circuitry was almost complete (Figure 1.4*B*) (Albin et al., 1989). Finally, Alexander and Crutcher (1990) proposed a schema that for the first time brought forward the notion of "direct" and "indirect" pathways (Figure 1.4*C*). This box-and-arrow plot is, with smaller or larger modifications, still in use to this day.

The following thirty years of research brought much more detailed knowledge of the function and dysfunction of the basal ganglia and its main input station, the striatum. And while we are still discovering new aspects of this circuitry, the focus of modern-day investigations are on describing the correlates of behavior and functional deficits in the electrophysiological activity of the BG nuclei.

1.2 Neural correlates of brain function and dysfunction in the basal ganglia

The functions of the basal ganglia are as varied as they are complex. The BG is primarily known as a motor control processing hub, receiving inputs from sensory and motor cortices, limbic structures, as well as thalamus (Wall et al., 2013), and being involved in action selection: choosing an action sequence to perform based on internal state of the system and external conditions (Balleine et al., 2007, Redgrave et al., 1999). Action selection has been the subject of many computational studies investigating potential neural substrates that would support such a mechanism (Bahuguna et al., 2015, Bissonette and Roesch, 2015, Gurney et al., 2001a,b, Guthrie et al., 2009, Morita et al., 2016, Tomkins et al., 2014), as well as experimental ones examining the role of dopamine in selecting an appropriate action (Howard et al., 2017, Surmeier et al., 2009, Tai et al., 2012). Some of these studies were also conducive for practical implementations in robotic agents (Bahuguna et al., 2019b).

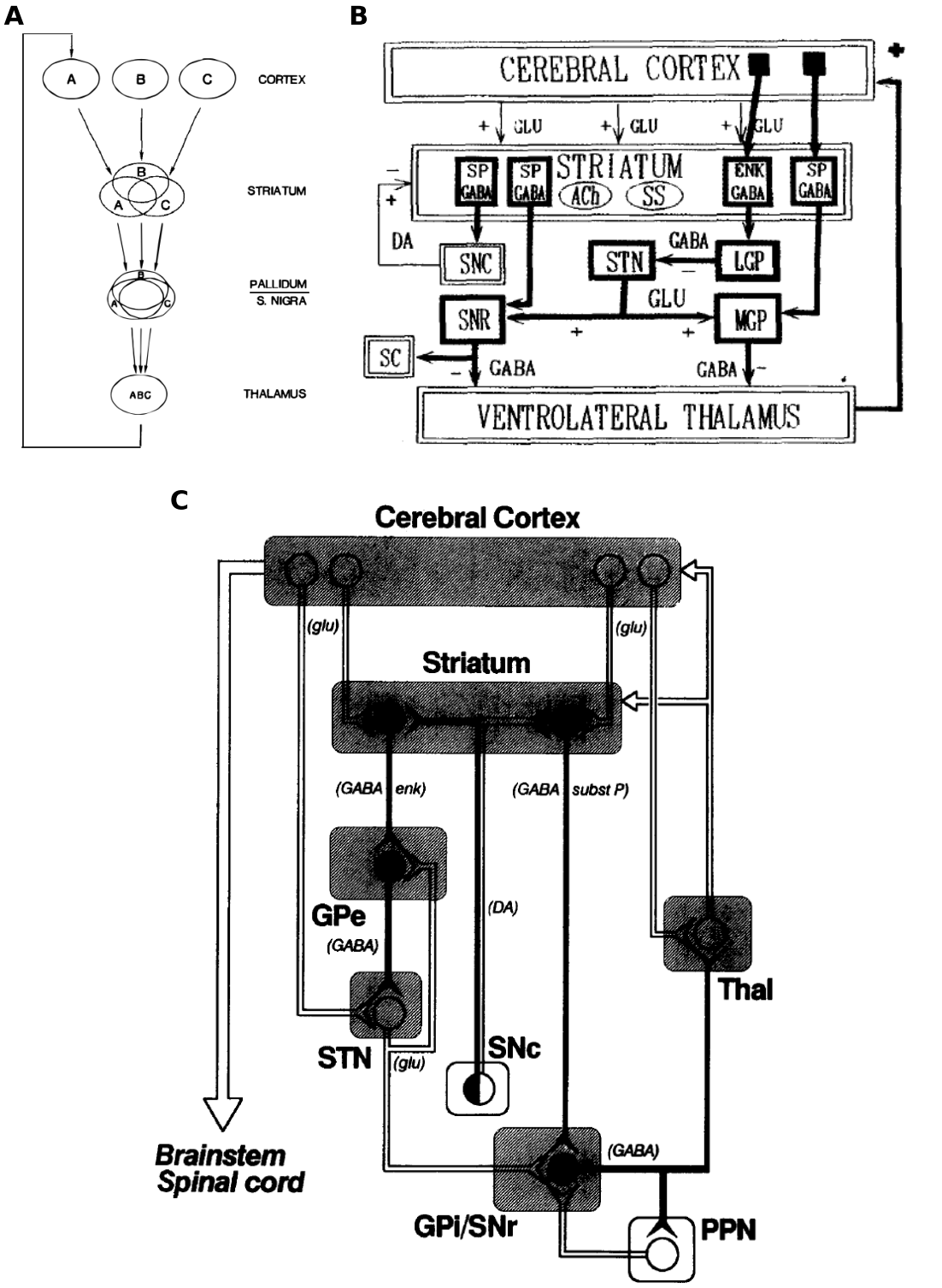

Fig 1.4. Evolution of functional box-and-arrow maps of the BG. ***A*** Probably the first functional diagram of the BG circuitry, from Alexander et al. (1986). While then-hypothesized "funnel" structure of BG-thalamocortical connectivity is prominent, here was also the fist time that the presence of multiple parallel loops within BG was proposed (denoted with A, B, and C). ***B*** A more complete functional map of the BG in healthy brain, taken from Albin et al. (1989). In this seminal study several different variants of this circuitry were proposed, depending on which BG pathology was discussed. ***C*** The first box-and-arrow plot where direct and indirect pathways of the BG were directly mentioned, taken from Alexander and Crutcher (1990). This same configuration of boxes, with some minor modifications, is still in use to this day.

The basal ganglia is also a part of the brain's limbic system, playing a crucial role in association and reinforcement learning. It is now a well established fact that phasic striatal dopamine release after a stimulus or an event represents reward prediction error, with the spike in striatal DA concentration encoding a reward better than the prediction, maintained levels of DA encoding no prediction error, and a DA concentration dip encoding omission of a predicted reward (Schultz et al., 1997, Schultz, 2016). The literature covering different aspects of this mechanism is rich, both in its experimental (e.g. Cox et al. 2015, Kasanova et al. 2017) and theoretical treatment (e.g. Daw et al. 2005, Frank 2004). Reinforcement learning is also an interesting research topic in the context of the many disorders of the basal ganglia (Keiflin and Janak, 2015, Maia and Frank, 2011).

Considering the complexity of the BG system and the functions it performs, it is not surprising that it finds itself at the center of a multitude of brain disorders (Albin et al., 1989). The most prominent of these is certainly Parkinson's disease, the second most common neurodegenerative disorder after Alzheimer's disease (McGregor and Nelson, 2019). In PD, the loss of dopaminergic neurons leads to hypoactivity of dMSNs and hyperactivity of iMSNs, causing a severe disbalance of the direct and indirect pathways and a host of symptoms such as tremor, bradykinesia, rigidity, etc. (Albin et al., 1989, DeLong, 1990). The treatment through dopamine precursor L-DOPA, while effective, also results in its own set of issues for the majority of the PD patients (Carvalho et al., 2017).

Involvement of the basal ganglia in other disorders also bears a brief mention:

- Tourette's syndrome: seen specifically as a disorder of the striatum. Although there are currently several competing hypotheses of the precise mechanism of Tourette's, they are all linked with increased binding of the dopamine transporter and its effect on MSNs (Albin and Mink, 2006, Hienert et al., 2018).
- Huntington's disease: characterized by the direct loss of iMSNs and the resulting disbalance of direct and indirect pathways (Andre et al., 2011, Barry et al., 2018).
- Schizophrenia: elevated striatal DA levels and abnormal cortico-striatal reward processing have been heavily implicated in the pathogenesis of its symptoms (Deserno et al., 2016, Garofalo et al., 2017).
- Impulsive, compulsive, and addictive behaviors: while the origins of these types of disorders are complex and can affect multiple brain regions, most of them include alterations of the mesolimbic dopaminergic system or changes in DA receptor availability that directly affect the striatum and the balance of the two BG pathways (Barlow et al., 2018, Yager et al., 2015).

It is obvious that a common thread through most of these disorders is some form of breakdown of dopaminergic signaling in the striatum and the consequent (electro)physiological adaptations and aberrant input-output processing of medium spiny neurons. Therefore, expanding our knowledge of MSNs is paramount for proper understanding of the function and dysfunction of the basal ganglia as a whole.

1.3 Research questions

Striatal medium spiny neurons have been the focus of much attention over the years, especially in the context of dopaminergic modulation and its dysfunction during Parkinson's disease (for detailed reviews, see (Silberberg and Bolam, 2015, Tritsch and Sabatini, 2012, Zhai et al., 2018)). Crucially, apart from different dopamine receptors they express, both anatomical and electrophysiological dichotomies have been found between direct and indirect pathway MSNs (Gertler et al., 2008). Furthermore, the entire striatal connectome is asymmetrical, with dMSNs being preferentially targeted by striatal fast-spiking interneurons (FSIs), and iMSNs forming stronger connections to dMSNs than vice versa (Planert et al., 2010, Taverna et al., 2008). However, until recently not much has been known about relative strength of excitatory inputs to the two MSN types. A series of studies performed *in vitro* has suggested that afferent synapses differ between dMSNs and iMSNs (Doig et al., 2010, Lei et al., 2004, Wall et al., 2013), and more recently, provided more conclusive evidence that dMSNs receive stronger corticostriatal and thalamostriatal inputs compared to iMSNs. A theoretical study by Bahuguna et al. (2015) also postulated that, considering the asymmetry in striatal connectivity, in order for dMSN and iMSN activities to be properly balanced it is required that direct-pathway neurons receive either more or stronger excitatory input (Figure 1.5). Here I provide the first evidence from *in vivo* whole-cell recordings in anesthetized animals that dMSNs indeed do receive stronger total input, and that this difference is attenuated in 6OHDA lesioned mice. This work is explained briefly in the section *Differential input to MSNs* and then in detail in Chapter 2.

Medium spiny neuron outputs have mostly been considered in the context of direct and indirect pathway processing, and global changes to their average firing rates triggered by the loss of midbrain dopamine neurons during PD. By contrast, the question I explore briefly in *Response variability of MSNs* and more deeply in Chapter 3 revolves around the variability of dMSN output firing rates in response to synaptic input. Response —or trial-by-trial —variability, is a well-established neural property (Faisal et al., 2008, Shadlen and Newsome, 1998), and its sources have been traced to synaptic noise (Faisal et al., 2008, Mainen and Sejnowski, 1995), refractory period (Kara et al., 2000), and

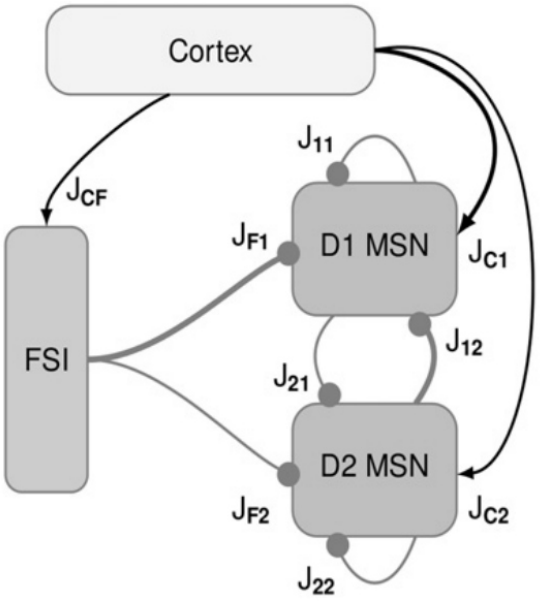

Fig 1.5. Schematic of the striatal connectome. Thickness of the connections denotes its strength. Note the proposed increased strength of cortico-dMSN connection as opposed to cortico-iMSN one. Figure taken from Bahuguna et al. (2015).

ongoing neural activity (Arieli et al., 1996). However, to the best of my knowledge, there has been no study of the influence of input rate correlations and the changes in excitation-inhibition balance on neural response variability. In combination with these input modalities, I also examine how dopaminergic modulation specific to dMSNs leads to changes in their output variability, and thus directly impacts their function in both health and disease.

Finally, MSNs through their efferents connect and direct the dynamics of the downstream BG nuclei. Specifically, indirect pathway MSN projections onto globus pallidus externa have a direct impact on the STN-GPe network, with an increase of iMSN output inhibiting GPe neurons and inducing elevated levels of beta-band activity. It has been suggested in both experimental and theoretical studies that hyperactivity of iMSNs in dopamine-depleted striatum is directly responsible for generation of pathological beta-band oscillations that arises during PD (Corbit et al., 2016, Kondabolu et al., 2016, Kumar et al., 2011). Indeed, a network model from our laboratory captures well this dynamics (Kumar et al., 2011, Mirzaei et al., 2017); however, it is unable to reproduce the STN-GPe phase alignment integral to beta-band activities of the two nuclei, as recorded in human PD patients (Cagnan et al., 2015). In Chapter 4 I propose a modification of the STN-GPe network model that enables the system to partially capture this phase alignment, and quantify the correspondence between the simulated and the experimentally obtained data. This topic is briefly covered in the section *Phase alignment heterogeneity in STN-GPe network*.

1.4 Methods

In this thesis I used numerical simulations, signal processing methods, and statistical analyses to explore properties of MSNs and of the STN-GPe network.

Numerical simulations were used in Chapters 3 and 4, but in different capacities. In Chapter 3 a compartmental biophysically detailed model of a single direct-pathway MSN was used to explore its output response variability over different trials and various levels of dopamine for three distinct input modalities: when excitatory and inhibitory inputs were independent, when their mean rates were correlated over different trials, and when their balance was modified. We performed a thorough literature search in order to quantify and properly model the modulatory effects of dopamine on a D1-receptor expressing MSN. More detailed description of the model and the methodology underlying its construction can be found in Lindroos et al. (2018).

In Chapter 4 I extended an already existing numerical network model of the STN-GPe circuit (Kumar et al., 2011, Mirzaei et al., 2017) to study the emergence of phase heterogeneity of beta-band oscillations in both control and stimulated (Parkinsonian) conditions. I performed a grid-search over different stimulation configurations to find a set of parameters that would provide the best match with the data obtained from human patients (Cagnan et al., 2015), quantified by an error measure derived from residual sum of squares (RSS).

Signal processing was used in Chapters 2 and 4. In both chapters I used filtering and power spectral analysis to obtain relevant signals either from in vivo recorded membrane potentials (Chapter 2), or from population PSTHs (Chapter 4). Additionally, I employed Hilbert transform in Chapter 4 to obtain envelope and phase data of beta-band signal, as well as beta-burst thresholding technique described in Tinkhauser et al. (2017a). For Chapter 2 I have devised an elaborate post-hoc method of estimating the effective membrane time constant based on combined approach of numerical simulations, spectral analysis of recorded data, and analysis of the filtering properties of neural membranes.

Finally, in Chapter 2 I have devised and implemented a hard-thresholding algorithm for detection of up- and down-states in MSN recordings, and implemented a method for extraction of spike-triggered averages described in Léger et al. (2005).

The compartmental model was implemented in NEURON simulator with PyNN Python interface (Hines and Carnevale, 1997, Hines, 2009). Network simulations were implemented in NEST simulator (http://nest-initiative.org) (Peyser et al., 2017). For Chapter

2 data analysis was performed in MATLAB R2016a (Mathworks, Inc.), and for Chapter 3 and 4 in Python 2.7 with various open source libraries, such as NumPy, SciPy, Matplotlib, etc.

1.5 Summary of the results

1.5.1 Differential input to MSNs

The striatum is the main input structure of the basal ganglia, and its principal cells are GABAergic medium spiny neurons. MSNs comprise around 95% of striatal neuronal population, and are divided into two main types depending on whether they express D1 or D2 dopamine receptors. D1R-expressing MSNs (dMSNs) belong to the direct pathway of the basal ganglia, projecting directly to globus pallidus interna (GPi), which releases the thalamus from inhibition and allows movement to initiate. Conversely, D2R-expressing MSNs (iMSNs) are part of the indirect pathway and project to globus pallidus externa (GPe), whose inhibition in turn disinhibits subthalamic nucleus (STN), which then excites GPi, thus finally inhibiting the thalamus and stopping a movement. The balance of activity of the two basal ganglia pathways is crucial for its proper function Cui et al. (2013), and one of its determinants is the synaptic input to the striatum. It is known that both MSN types receive convergent excitatory input from the majority cortical and some of the thalamic areas (Wall et al., 2013). In the recent years there has been an attempt to uncover whether there are any differences in the type of input that dMSNs and iMSNs receive. Numerous conflicting studies tried to answer this question (Arias-García et al., 2017, Deng et al., 2015, Doig et al., 2010, Lei et al., 2004, Mallet, 2006, Wall et al., 2013), until Parker et al. (2016) provided strong evidence from *in vitro* recordings in mice that both cortical and thalamic inputs are biased to dMSNs.

However, significant differences exist between recordings performed in brain slices and those obtained from living animals. *In vitro* research, while essential, has some important shortcomings: recorded neurons have much reduced connectivity due to the plane of cutting, and their membrane is mostly hyperpolarized due to lack of synaptic inputs. As a consequence, synaptic conductances measured *in vivo* can be very different from those *in vitro* (Destexhe et al., 2003). Thus, in Chapter 2 I proceed to analyze whole-cell MSN membrane voltage recordings obtained from anesthetized mice, and to show for the first time *in vivo* that in synaptically-driven up-states dMSNs receive either stronger or more total input than iMSNs. While it should be noted that, due to the nature of the recordings, it has been impossible to determine whether this difference is caused by an increase in excitatory or inhibitory inputs, the end result still provides experimental

support for the previous theoretical prediction made by Bahuguna et al. (2015). In addition, I demonstrate that the difference in MSN up-state inputs is attenuated in the case of dopamine depletion, a find which corresponds to the similar one in a previous study in MSN down-states (Ketzef et al., 2017). Finally, the analysis in this study also indicates that MSNs in up-states operate in a synaptically driven high-conductance regime akin to that seen in pyramidal neurons, which resembles the awake state of an animal (Destexhe et al., 2003, Haider et al., 2013).

1.5.2 Response variability of MSNs

Noise is omnipresent in the central nervous system (CNS) (Shadlen and Newsome, 1998). One of its aspects at the neuronal level is trial-by-trial (or response) variability, defined as differences between responses that are observed when the same experiment is repeated in the same specimen —or in our case, in the same neuron (Faisal et al., 2008). This type of variability has two main sources. One arises from deterministic responses to variable initial conditions: if the initial condition of a neural system differs between trials, the resulting outputs will also differ. A perfect example for this source of noise was described by Arieli et al. (1996), who described how response variability in cat local field potentials (LFP) was the result of superposition of the deterministic evoked signal and the current state of the ongoing activity. The second source are stochastic fluctuations in the neural signal itself, exemplified by noise in membrane and synaptic conductances (Faisal et al., 2008, Mainen and Sejnowski, 1995, Schreiber et al., 2004).

Neural response variability is usually quantified by Fano factor (FF), which scales the response variance with its mean. A perfectly regular neuron would have Fano factor of zero, while a highly variable Poissonian neuron would have FF of one. Throughout the CNS there are examples of highly variable neurons with FFs exceeding one, but also of others which are closer to zero, sometimes to be found even in the same region (Faisal et al., 2008).

In Chapter 3 I employ Fano factor to measure how neuronal trial-by-trial variability is influenced for different synaptic input modalities. For this purpose I am using a biophysically detailed compartmental model of a direct pathway MSN with realistic dopaminergic modulation (Lindroos et al., 2018). I test how a dMSN responds over trials to repeated synaptic stimulation, with E and I input rates drawn either from independent or correlated distributions, and what are the effects of changes in input E-I balance on the trial-by-trial variability. I combine these two input modalities with dopaminergic modulation to further investigate how dMSN behaves in dopamine depleted conditions

(such as during PD), and how for very high DA concentrations (which can occur during reinforcement learning).

During the course of this study I find that dopamine generally acts as a significant diminisher of trial-by-trial variability, but that its efficacy in this respect is dependent on the properties of synaptic input. Moreover, input rate correlations and changes in E-I balance prove to have by themselves a significant impact on the response variability, with an increase in correlations decreasing the variability, and the change in E-I balance having a more complex effect. Both of these input modalities are further complicated in the situation where dopamine levels are not fixed but are fluctuating.

1.5.3 Phase alignment heterogeneity in STN-GPe network

During the course of Parkinson's disease, dopaminergic neurons located in substantia nigra pars compacta (SNc) gradually die off, severely limiting the supply of dopamine to the basal ganglia. Dopamine depletion initially results in hyperactivity of iMSNs and hypoactivity of dMSNs, which in turn leads to the loss of balance between the direct and indirect BG pathways and the dysfunction of basal ganglia as a whole. On the exterior, these changes manifest as tremor in extremities, bradykinesia, stooped posture, and other Parkinsonian symptoms.

One of the effects of PD is an increase in beta-band (15-35 Hz) LFP power of BG, caused by oscillations between STN and GPe (Brown et al., 2001). The source of these pathological beta oscillations is, however, contested. One hypothesis is the disbalance in the inputs to the STN-GPe circuitry, through the strengthening of the indirect pathway and increased inhibition of GPe, or through increased input to the STN (Kumar et al., 2011). Another suggestion is that the origin of oscillations lies within the STN-GPe network itself, in the disrupted reciprocal connectivity between the two nuclei (Tachibana et al., 2011, Mirzaei et al., 2017). Both of these approaches have received theoretical treatment, and the resulting network model successfully reproduced beta-band activity in both normal and PD conditions (Kumar et al., 2011, Mirzaei et al., 2017). However, in Chapter 4 I show that this model is unable to capture the heterogeneity of STN-GPe beta-band phase alignment that has been observed in recordings from human PD patients (Cagnan et al., 2015). I proceed to demonstrate that by stimulating only a certain percentage of STN and/or GPe populations the network model can exhibit the full heterogeneity of STN-GPe phase difference distributions, and furthermore, that the choice of the synaptic transmission delays has a significant impact on these beta-band phase profiles. What is more, I show that the resulting phase profiles show a not inconsiderable degree of overlap with those recorded in PD patients, for a particular

choice of model parameters. The major benefit of this modification is that it improves the model by bringing it more in line with experimental findings, while keeping it tractable for analysis by tools such as mean field theory (Bahuguna, 2017).

1.6 Key advancements

The overview of the key findings described in this thesis are as follows:

- I provide experimental evidence that dMSNs receive either more or stronger synaptic input than iMSNs, and that this difference between the two MSN types is attenuated in dopamine-depleted animals. While similar claims have been made for *in vitro* preparations in the past, this is the first such finding from *in vivo* recordings. This result also gives a direct support to the previously established theoretical prediction, and in combination with it, contributing an important piece of information for future theoretical and modelling studies. (See Chapter 2).

- I propose an explanation of the response variability of dMSNs for different levels of dopaminergic modulation. I show how the trial-by-trial variability is affected in a nonmonotonic way from DA depletion (that is, in a PD-like condition) to very high DA concentrations (such as during reward learning). Moreover, I show how different synaptic input paradigms, such as input rate correlations and changes in excitation-inhibition input balance, can directly influence dMSN variability in non-trivial manner. I hypothesize that these effects provide additional context to reinforcement and motor learning. (See Chapter 3)

- I propose a version of the STN-GPe network model that exhibits STN-GPe beta-band phase alignment heterogeneity similar to that as seen in human Parkinson patients. The previous versions of the model efficiently explained the generation of beta-band oscillations in this circuit, but could not capture the interplay of STN and GPe beta-band phase activity, nor the entire phase spectrum that the currently proposed model can. I demonstrate that by stimulating only a certain percentage of both STN and GPe populations, the model can generate SNT-GPe phase difference profiles that approach those in experimental recordings. Furthermore, I found that the choice of synaptic delay parameter is one of the major factors of phase difference heterogeneity. Importantly, these results give support to the notion of the presence of multiple processing channels in individual BG nuclei. (See Chapter 4)

Chapter 2

Direct pathway neurons in mouse dorsolateral striatum *in vivo* receive stronger synaptic input than indirect pathway neurons

Marko Filipović[*1,2], Maya Ketzef[*3], Ramon Reig[4], Ad Aertsen[2], Gilad Silberberg[3], Arvind Kumar[1,2†]

[*] **These two authors contributed equally to this work**

[1] **Dept. of Computational Science and Technology, School of Computer Science and Communication, KTH Royal Institute of Technology, Stockholm, Sweden**

[2] **Bernstein Center Freiburg and Faculty of Biology, University of Freiburg, Germany**

[3] **Dept. of Neuroscience, Karolinska Institutet, Stockholm, Sweden**

[4] **Instituto de Neurociencias, Consejo Superior de Investigaciones Científicas & Universidad Miguel Hernandez, San Juan de Alicante, Spain**

2.1 Introduction

The striatum is the largest nucleus in the basal ganglia (BG) and acts as its main input structure. GABAergic medium spiny neurons (MSNs) are the striatal projection neurons and constitute about 95 % of the striatal neuronal population. D1 type dopamine

receptor expressing MSNs (dMSNs) project to the substantia nigra pars reticulata and globus pallidus interna and constitute the 'direct pathway', whereas D2 type dopamine receptor expressing MSNs (iMSNs) project to the globus pallidus externa and constitute the 'indirect pathway'. A balance in the activity of the two pathways is essential for correct functioning of the BG, and is disrupted in BG-related pathologies such as Parkinson's disease (PD). To understand how the direct and indirect pathways shape BG function, we need to quantify both the upstream excitatory inputs into the striatum and the recurrent inhibitory connections within and between dMSNs and iMSNs.

The dMSNs and iMSNs differ in their connectivity: iMSN to dMSN connectivity (13 %) is much higher than dMSN to iMSN (4.5 %), whereas dMSN to dMSN connectivity (7 %) is much lower than iMSN to iMSN (23 %) (Taverna et al., 2008, Planert et al., 2010). Moreover, GABAergic fast-spiking interneurons (FSIs) connect preferentially to dMSNs compared to iMSNs (53 % vs. 36 %) (Gittis et al., 2010). That is, dMSNs receive overall more inhibition than iMSNs. Despite these differences, both dMSNs and iMSNs exhibit similar average activity in awake behaving animals (Cui et al., 2013, Sippy et al., 2015).

Using a computational model we recently predicted that dMSNs should receive stronger excitatory input than iMSNs (either through more synapses, stronger synapses, or stronger input rates and/or correlations), so that both dMSNs and iMSNs may have comparable firing rates (Bahuguna et al., 2015). Recent *ex vivo* recordings suggest that cortico-striatal synapses on dMSNs may be stronger than those on iMSNs (Parker et al., 2016) (however, see Lei et al. (2004), Kress et al. (2013), Doig et al. (2010), Deng et al. (2015)). While this data supports the theoretical predictions, it is well known that *in vivo* synaptic conductances can be very different from *ex vivo* measurements (Destexhe et al., 2003).

Even though it is hard to estimate the full strength and numbers of individual synapses impinging on dMSNs and iMSNs experimentally, a relative difference in the total input to the two neuron types can be estimated by analyzing *in vivo* intracellular membrane potential fluctuations. In particular, the variance (or the spectral power) of the membrane potential fluctuations is proportional to the square of the synaptic strength (Kuhn et al., 2004). That is, by comparing the spectra of sub-threshold membrane potential *in vivo* we can test whether dMSNs indeed receive stronger total input than iMSNs, as was theoretically predicted (Bahuguna et al., 2015).

Therefore, we recorded and analyzed the *in vivo* membrane potentials of dMSNs and iMSNs from healthy and dopamine-depleted anaesthetized mice using whole-cell patch clamp recordings. These neurons exhibited alternating periods of high and low activity (called up- and down-states, respectively), characteristic of recordings in animals under ketamine-induced anaesthesia (Wilson and Kawaguchi, 1996). We found that dMSNs

exhibited higher spectral power in their up-states than iMSNs over a wide range of frequencies in healthy mice. In addition, bilateral whisker stimulation in healthy animals showed that sensory inputs evoked larger responses in dMSNs than in iMSNs. Despite these differences, the membrane time constants of the two MSN types were not significantly different. Therefore we can conclude that the observed stronger membrane potential fluctuations are indicative of stronger synaptic inputs and/or higher input correlations. Finally, we found that dopamine depletion abolished the difference in spectral power of up-state membrane potential fluctuations between dMSNs and iMSNs, highlighting the role of dopamine in maintaining the activity balance between the direct and indirect pathways.

Thus, our study provides the first experimental *in vivo* evidence of stronger synaptic input to the direct-pathway of the mouse dorsolateral striatum, and demonstrates that this difference is attenuated in dopamine-depleted animals.

2.2 Methods

Experimental Methods

Ethics approval. All experiments were performed according to the guidelines of the Stockholm municipal committee for animal experiments under an ethical permit to G.S. (N12/15). D1-Cre (EY262 line) or D2-Cre (ER44 line, GENSAT) mouse line were crossed with the Channelrhodopsin (ChR2)-YFP reporter mouse line (Ai32, Jackson laboratory) to induce expression of ChR2 in either dMSNs or iMSNs, respectively. Mice of both sexes were housed under a 12-hour light-dark cycle with food and water ad libitum. All experiments were carried out during the light phase.

6OHDA lesioning. Mice (12 males and females 8-10 weeks of age) were anesthetized with isoflurane and mounted in a stereotaxic frame (David Kopf Instruments, Tujunga, California). The mice received one unilateral injection of 1 µL of 6OHDA-HCl (3.75 µg/µL dissolved in 0.02 % ascorbic acid) into the medial forebrain bundle (MFB), according to the following coordinates (Paxinos and Franklin, 2004): antero-posterior −1.2 mm, medio-lateral 1.2 mm and dorso-ventral −4.8 mm. After surgery, all mice were injected with Temgesic (0.1 mg/kg, Reckitt Benckiser, Berkshire, England) and allowed to recover for at least 2 weeks. Sham and unlesioned mice (n = 21 of both sexes) served as controls, their data were pooled after no differences were found between the groups. Only 6OHDA injected mice that showed rotational behavior (Santini et al., 2007) were used in our experiments (see Ketzef et al. 2017 for more details).

In vivo recordings. Experiments were conducted as described previously (Reig and Silberberg, 2014, Ketzef et al., 2017). Briefly, 2-3 weeks post-lesioning, mice were anesthetized by intraperitoneal (IP) injection of ketamine (75 mg/kg) and medetomidine (1 mg/kg) diluted in 0.9 % NaCl. To maintain mice under anaesthesia, a third of the dose of ketamine was injected intraperitonally approximately every 2 hours or in case the mouse showed response to pinching or changes in EcoG patterns. Mice were tracheotomized, placed in a stereotactic frame, and received oxygen enriched air throughout the recording session. Core temperature was monitored with a feedback-controlled heating pad (FHC) and kept on 36.5±0.5 °C. Patch clamp recordings were performed in the dorsolateral striatum since the sensory and motor areas project topographically onto it (McGeorge and Faull, 1989). The skull was exposed and a craniotomy was drilled (Osada success 40) 3.5-4 mm lateral to the bregma, and the dura was removed. Patch pipettes were pulled with a Flaming/Brown micropipette puller P-1000 (Sutter Instruments). Pipettes (7-10 MΩ, borosilicate, Hilgenberg), back-filled with intracellular solution, were inserted with a ∼1500 mbar positive pressure to a depth of about 2 mm from the surface, after which the pressure was reduced to 30-35 mbar. The pipette was advanced in 1 µm steps in depth (35 degrees angle), in voltage clamp mode. When a cell was encountered, the pressure was removed to form a Gigaseal, followed by application of a ramp of increasing negative pressure until a cell opening was evident. Recordings were performed in current clamp mode. Intracellular solution contained (in mM): 130 K-gluconate, 5 KCl, 10 HEPES, 4 Mg-ATP, 0.3 GTP, 10 Na2-phosphocreatine, and 0.2-0.3 % neurobiotin or biocytin (pH = 7.25, osmolarity ∼285 mOsm). The exposed brain was continuously covered by 0.9 % NaCl to prevent drying. Signals were amplified using a MultiClamp 700B amplifier (Molecular Devices) and digitized at 20 kHz with a CED acquisition board and Spike 2 software (Cambridge Electronic Design).

Optogenetic identification of in vivo recorded neurons. To obtain on line identification of whole-cell recorded neurons, we used the optopatcher (Katz et al., 2013) (A-M systems, WA USA). Computer controlled pulses of blue light (7 mW LED, 470 nm, Mightex systems) were delivered through an optic fiber inserted into the patch-pipette while recording the responses in whole-cell configuration (Fig. 2.1*A*). Light steps (500 ms) were delivered every 2-5 seconds with increasing intensity between 20 to 100 % of full LED power (2.1 mW at the tip of the fiber). Positive cells responded to light stimulation by step-like depolarization with or without firing, whereas negative cells did not show any response (Fig. 2.1*B*, and see Ketzef et al. (2017) for full characterization).

Whisker stimulation. Air puffs were delivered by a picospritzer (Picospritzer III, Parker Hannifin) through plastic tubes (1 mm diameter) positioned up to a centimeter from the mouse's whiskers. Air puff stimulations (15 ms) were delivered at 0.2 Hz and at least

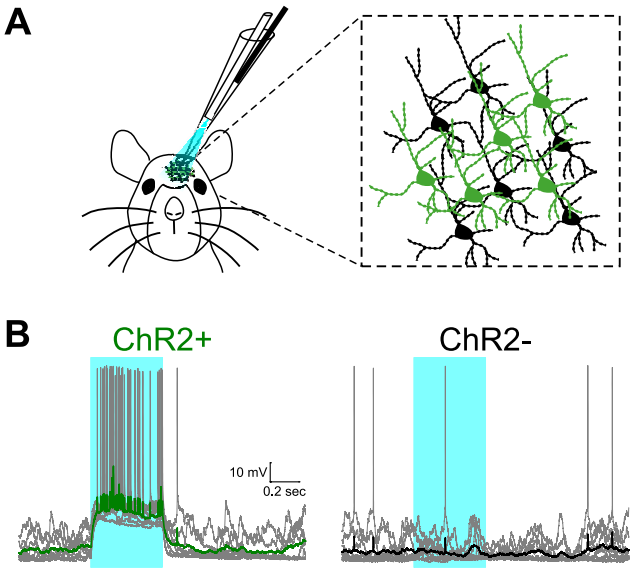

Fig 2.1. MSNs classification using the optopatcher. To facilitate the classification of MSNs as belonging to either the direct (dMSN) or indirect (iMSN) pathway in vivo, we utilized an optogenetic approach. In either D1-Cre or D2-Cre animals crossed with ChR2 reporter mouse, we selectively expressed ChR2 in dMSNs or iMSNs, respectively. Using the optopatcher, we could deliver focal light stimulation to the recorded cell and classify its identity 'online' during whole cell patch recordings. ***A*** Illustration of the experimental approach (*left*). In anesthetized mice, the optopatcher is introduced through the craniotomy. The optic fiber is inserted into the patch pipette and light application is focal. MSNs of both pathways are intermingled (*right*), positive cells (green) express ChR2 and YFP, whereas negative cells (black) do not. ***B*** Whole cell patch recording from positive (*left*) and negative (*right*) cells in a D2-ChR2 mouse. When the blue light is activated (470 nm, 0.5 s), positive cells depolarize immediately, whereas negative cells are not affected. Each example shows 10 repetitions (gray), overlaid by the average trace (green for positive and black for negative cells).

30 responses were acquired for each stimulation condition. The air pressure was set to 103.4-137.9 kPa (15-20 PSI).

2.2.1 Data Analysis

Up- and down-state detection. The detection of up- and down-states was done offline using an automated algorithm. The data collection was done independent of the up-down state detection algorithm and its parameters. For each membrane potential recording, we used a short time window (20-100 ms, depending on the noise level in the recording) to identify sudden transitions in the membrane potential with an amplitude sufficiently large to cross the cell-specific up-state or down-state thresholds. Upon detection of such a transition, we classified the following voltage period as an up-state or a down-state (Fig. 2.2*A*). The next sufficiently large membrane potential transition in the opposite direction marked the ending of that state. State thresholds were determined by finding the two main peaks of the bimodal voltage histogram of the entire trace, and by empirically adjusting these thresholds for the best detection rate (see also Léger et al. (2005) and Fucke et al. (2011)). In cells where the overall baseline voltage level fluctuated over

time, we either used only the most stable section of the recording or discarded the entire recording. All states with a duration shorter than 40 ms were discarded from the analysis (Mukovski et al., 2007).

For the purpose of characterizing the sub-threshold membrane potential dynamics analysis we excluded all up-states during which spiking occurred (however see the Fig. 2.4 where we considered spikes). Moreover, we also excluded a state from further analysis if one or more of the following criteria was met: (1) an up-state was interrupted by a down-state shorter than 25 ms (both states were discarded), (2) the mean membrane potential of a down-state exceeded the global average down-state potential for that cell by more than 3 %, (3) a recording artefact was present, or (4) a whisker stimulation trigger occurred either during the state or 200 ms preceding the state.

Finally, for all remaining states, we removed 5 % of the data, from the start of the state and before the end of the state, to minimize the impact of state transitions on the measured variables.

Power spectral density (PSD) estimation. The PSD estimate of an up-state membrane voltage trace was determined by first subtracting the mean potential from the remainder of the trace, and then by applying the MATLAB periodogram function with Bartlett-Hann windowing. The minimal detectable frequency in individual up-state PSDs was set as the inverse of the duration of that state. For each cell, all such up-state PSD estimates were averaged to obtain a single power spectral density curve (Fig. 2.2*B*, gray traces). When comparing PSDs across cell groups (dMSNs vs. iMSNs), we constructed a grand-average PSD for each group by averaging over PSDs of individual cells (Fig. 2.2*B*, color traces). Frequencies below 5 Hz were disregarded because we observed only few up-states longer than 200 ms. Additionally, all frequency content between 45 and 55 Hz was removed to avoid power line contamination. We restricted the higher frequency range to 150 Hz, adopting this as the upper limit of the high-gamma band in our study.

Experimental data suggest that in a variety of behavioral conditions, both ongoing and evoked activity show modulation in specific frequency bands (Buzsáki, 2006). Therefore, we divided PSD estimates obtained in this manner into five standard frequency bands: sub-α (5-8 Hz), α (8-13 Hz), β (13-30 Hz), low-γ (30-70 Hz), and high-γ (70-150 Hz), to determine whether MSNs are attuned to receive specific frequency inputs from the cortex. We also analyzed the spectra by splitting it into low and high frequency bands (i.e. 5-13 Hz and 13-150 Hz). To calculate the total power within any one frequency band for each cell, we isolated the section of interest of the PSD estimate and integrated the area under the curve.

Due to very low levels of spectral power during the down-states, the line noise power precluded any meaningful PSD comparison across the two cell groups.

Effective membrane time constant estimation. We estimated the effective membrane time constant τ_m from the *in vivo* membrane potential fluctuations by the following method. For a narrow enough voltage range, the membrane of a neuron can be approximated as a linear low-pass filter. Then, for that narrow voltage range, τ_m is directly proportional to the membrane capacitance and inversely related to the total membrane conductance. Thus, to minimize non-linear voltage-dependent effects, to account for the voltage dependence of τ_m (Kuhn et al., 2004), and to be able to treat the neuron membrane as a linear low-pass filter, we first binned the average membrane potentials of all states in 0.5 mV wide bins. Then we estimated the power spectral density of individual states belonging to each bin and averaged over the estimates in order to reduce noise, as explained in the previous section. Further noise reduction was achieved by smoothing the averaged PSD estimate with a Gaussian kernel, and the resulting curve was used to extract the cutoff frequency f_c, calculated as the point where the maximal value of the smoothed PSD estimate fell to one half (-3 dB point, Fig. 2.3*A*). The initial effective membrane time constant τ_m^{ini} was then calculated as $1/(2\pi f_c)$. We repeated this procedure for a series of narrow voltage ranges across different instances of up- and down-states within a single cell, in order to avoid non-linearities induced by large excursions of the effective membrane conductance.

The smoothing of the average PSD estimate introduces a shift of the -3 dB point, leading to an erroneous estimation of the effective membrane time constant. The magnitude and sign of the error depend, in a non-linear fashion, on the width of the Gaussian kernel used for smoothing in the frequency domain, and the duration of the original signal in the time domain. To account for this error, we numerically determined a correction term τ_m^C, which we could then add to the initially estimated value τ_m^{ini}, to obtain the final MSN membrane time constant estimate τ_m. This correction term was calculated as follows. We constructed multiple surrogate "neuronal" time series by filtering Gaussian white noise signals of different durations through a set of low-pass Butterworth filters (third order, zero-phase) with predetermined cutoff frequencies. Thus, for each of the surrogate time series we knew the actual time constant (τ^{actual}) of the underlying low-pass filter. We then proceeded to make an initial estimate of the time constant (τ^{ini}) as described above, using a single fixed value for the kernel width of the Gaussian smoothing function ($k_w = 12$). The error term was then defined as $\tau^C = \tau^{actual} - \tau^{ini}$. Using this approach, we obtained the correction term τ^C for signals of different durations and filters with different time constants. Next, we defined τ^C as a function of τ^{ini} and signal duration (Fig. 2.3*B*) to obtain the correction term τ_m^C for our estimates of the MSN

membrane time constant. Finally, the effective MSN membrane time constant τ_m was determined by adding the corresponding τ_m^C to the initial estimate τ_m^{ini}.

The main weakness of this method stems from the necessity of averaging the spectral data over many trials of sufficient duration and power. That is, for the most precise estimation, the trials (states) should preferably be at least 250 ms long, and the input to the neurons should have rich enough frequency content to uncover the membrane cutoff frequency (comparable to injecting white noise into the *in vitro* recorded neuron).

Due to the underlying approximations and limitations of the method, the estimated values of the membrane time constants should not be treated as actual, precise values of those neurons' τ_m. Nevertheless, our approach does return consistent and comparable results across different cells when applied to the recorded data. Moreover, our analysis employing the τ_m estimation procedure uncovers differences in membrane time constant of the down-states similar to those previously reported in Ketzef et al. (2017) (Fig. 2.3*D*).

Spike-triggered average (STA) calculations. For every recorded neuron that spiked we extracted 12 ms of the pre-spike voltage traces. The duration of this particular time window was chosen as it roughly represents the average membrane integration window for synaptic input in the up-states, based on the estimations of the effective membrane time constants across different cell groups (Fig. 2.3*D*). For every cell, spikes were identified in the voltage trace, and the intervals from 0.25 ms before to 5 ms after the spike events were removed from the trace. The spiking threshold was then determined as the largest fluctuation of the first derivative of the remaining trace. The times when the derivative of the full trace crossed the threshold were taken as spike onset times. For the purpose of calculating the average of these pre-spike voltage traces (STA), we did not include any spikes occurring during state transitions, that initiated less than 12 ms after the start of an up-state, or which were occurred earlier than 17 ms after the previous spike in the same up-state. The remaining pool of spikes was divided into those that were the result of spontaneous neuronal activity and those that arose as the consequence of whisker stimulation. If, after these selections. the pool contained at least three spikes, the STA was calculated.

The STAs were compared using a permutation test. For each group comparison we collected all the cell-average traces into a single pool, shuffled their indices, and generated randomized groups by drawing as many traces from this common shuffled pool as the original groups had. For each such generated randomized group, we constructed a grand-average STA. We repeated this process 1,000 times. Significance lines were determined as the 2.5 % and 97.5 % of the voltage distributions of the random grand-average traces for each time point. The range of voltage distributions differed between groups when the number of traces belonging to randomized groups for a single comparison was different

(e.g., for the comparison of spontaneous vs. evoked iMSN STAs, we had 11 spontaneous and 4 evoked cell-average traces). This difference is reflected in the voltage ranges depicted in the graphs, but it does not affect the validity of the permutation test.

Statistical methods. Unless noted otherwise, the data are presented as mean ± SEM and were tested for normality using the Shapiro-Wilk test. Normally distributed data were tested by the unpaired two-sample Student's t-test, and non-normally distributed data by the Wilcoxon rank-sum test (ttest2 and ranksum in MATLAB, respectively). The significance level α was set to 0.05. In the case of PSD comparison over different frequency bands (Fig. 2.2*D*), the results were corrected for multiple testing by the Holm-Bonferroni correction (Holm, 1979), and both the corrected α-level (α_{HB}) and the calculated p-value are reported.

All data analyses were performed using custom scripts written in MATLAB R2016a (Mathworks, Inc.).

2.3 Results

To estimate the relative strength of excitatory synaptic inputs to striatal neurons, we obtained *in vivo* whole-cell patch clamp recordings of MSNs from the dorsolateral striatum in control (dMSN $n = 26$, iMSN $n = 18$, total $n = 44$) and 6OHDA lesioned mice (dMSN $n = 16$, iMSN $n = 12$, total $n = 28$). We used optogenetic stimulation to classify MSNs online during the recording session as belonging to either the direct or indirect pathway using the optopatcher (Katz et al., 2013). Both dMSNs and iMSNs showed slow-wave membrane potential oscillations (up- and down-states), characteristic of neurons recorded in animals under ketamine-induced anesthesia (Wilson and Kawaguchi, 1996) (Fig. 2.2*A*). During the up-state, MSNs receive barrages of excitatory inputs from the neocortex and the thalamus. We, therefore, analyzed the variance and spectrum of the up-state membrane potential traces to assess the respective synaptic inputs to the two MSN types.

2.3.1 dMSNs have higher spectral power in up-state than iMSNs

If a neuron soma is treated as a simple linear integrator, the mean and variance of the subthreshold membrane potential fluctuations is primarily determined by the firing rate, the number of excitatory and inhibitory inputs to a given cell, and their synaptic

strength (Kuhn et al., 2004):

$$\begin{aligned} \mu_v &= U_r + \lambda_e \int \mathrm{EPSP}(t) - \lambda_i \int \mathrm{IPSP}(t)dt \\ \sigma_v^2 &= \lambda_e \int \mathrm{EPSP}(t)^2 dt + \lambda_i \int \mathrm{IPSP}(t)^2 dt \end{aligned} \tag{2.1}$$

where μ_v and σ_v^2 are the voltage-dependent mean and variance of the membrane potential, U_r is the resting membrane potential, λ_e and λ_i are the rates of excitatory and inhibitory inputs, respectively, and $EPSP(t)$ and $IPSP(t)$ describe the temporal shape of excitatory and inhibitory post-synaptic potentials.

From Eq. 2.1 it is clear that excitatory and inhibitory inputs have an opposite effect on the mean of the membrane potential of a cell receiving synaptic input. By contrast, because the calculation of the variance involves the square of the PSPs kernel, an increase in either excitatory or inhibitory inputs always results in an increase of the variance of the membrane potential (Eq. 2.1). Against this background, consider two neurons, n_s and n_w, receiving inputs via stronger and weaker synapses, respectively. The excitatory and inhibitory inputs to these two neurons can be tuned such that both n_s and n_w have the same mean membrane potential. However, due to the stronger synaptic weights and, hence, larger post-synaptic potentials, the neuron n_s will exhibit a larger membrane potential variance than the neuron n_w. This example illustrates that the mean membrane potential is not an adequate measure for the overall synaptic input, but by comparing the variances it is possible to determine if two neurons receive different amounts of synaptic inputs. This requires that the two neurons receive uncorrelated synaptic inputs and that their membrane time constants are similar.

Since the variance in time-domain equals the power spectral density (PSD) in frequency domain (Parseval's theorem), the PSD gives an estimate of the variance for every frequency in the signal (Papoulis and Pillai, 2002). Therefore, we measured the PSD of the membrane potential for every detected up- and down-state of a cell (Fig. 2.2*A*, see Methods).

For each MSN type we constructed a grand-average PSD estimate for both control and 6OHDA conditions (Fig. 2.2*B*). Direct comparison of these grand-averages revealed that dMSNs had consistently higher PSD than iMSNs over all examined frequency bands under control conditions. In particular, in three prominent, higher-frequency bands (β: 13-30 Hz, $Z = 2.47$, $p = 0.0135$, $\alpha_{HB} = 0.0167$; low-γ: 30-70 Hz, $t_{(42)} = 2.72$, $p = 0.0095$, $\alpha_{HB} = 0.01$; and high-γ: 70-150 Hz, $Z = 2.57$, $p = 0.01$, $\alpha_{HB} = 0.0125$) dMSNs showed significantly higher power than iMSNs (Fig. 2.2*C*, top left). Because the total power spectral density of the membrane potential in a selected frequency band equals the variance of the membrane potential in that frequency band (Papoulis and Pillai,

2002), the heightened power of dMSN up-state membrane potentials in control animals is indicative of stronger voltage fluctuations as compared to iMSNs. Unlike under control conditions, in the DA-depleted striatum we found no difference in the spectral power of up-state membrane potential fluctuations of dMSNs and iMSNs (across all bands $p > 0.69$, Fig. 2.2*C*, top right). Comparison of the up-state control vs. DA-depleted conditions revealed a significant difference in dMSN α-band (8-13 Hz) power ($Z = 2.71$, $p = 0.0068$, $\alpha_{HB} = 0.01$). DA depletion did not affect the spectral power of iMSN (control vs. DA-depleted conditions across all bands had p-values above corrected alpha levels).

In down-states, there was no significant difference in spectral power of dMSNs and iMSNs in either condition (the calculated p-values were always above corrected alpha levels), except in a single case: dMSNs in control vs. DA-depleted conditions expressed significance in the high-γ band ($Z = 2.60$, $p = 0.0092$, $\alpha_{HB} = 0.0125$).

Finally, to verify that the effect we observed was not just an artefact of dividing the power spectrum into an arbitrary number of bands, we repeated our statistical analysis for the low (5-13 Hz) and high (13-150 Hz) frequencies separately. We found that the difference between dMSN and iMSN up-states in control condition was preserved in the high frequencies ($Z = 2.66$, $p = 0.078$, $\alpha_{HB} = 0.025$), while it was non-existent in the low frequencies (p-value above corrected alpha level). Similarly, dMSN up-state differences between control and DA-depleted conditions were still present only in the low frequencies ($t_{(40)} = 2.44$, $p = 0.019$, $\alpha_{HB} = 0.025$). However, in the down-states the differences between dMSN control and DA-depleted conditions were now visible both in low ($Z = 2.32$, $p = 0.02$, $\alpha_{HB} = 0.025$) and in high ($t_{(40)} = 2.29$, $p = 0.027$, $\alpha_{HB} = 0.05$) frequencies, presumably because of a more forgiving value of Holms-Bonferroni correction term.

Given that up-states are thought to be primarily synaptically driven (Wilson and Kawaguchi, 1996, Stern et al., 1997), our results indicate that the increased power of dMSNs, especially in the higher-frequency bands, compared to iMSNs in the control case stems from stronger total input to direct pathway striatal neurons. Furthermore, our results suggest that in dopamine-depleted conditions, the total input to dMSNs is either significantly reduced and/or is more similar to the input to iMSNs.

2.3.2 MSN membrane time constant does not underlie the differences in high-frequency power

The difference in high-frequency power between dMSNs and iMSNs may be caused by a difference in the time constants of the two neuron types. We estimated the effective time

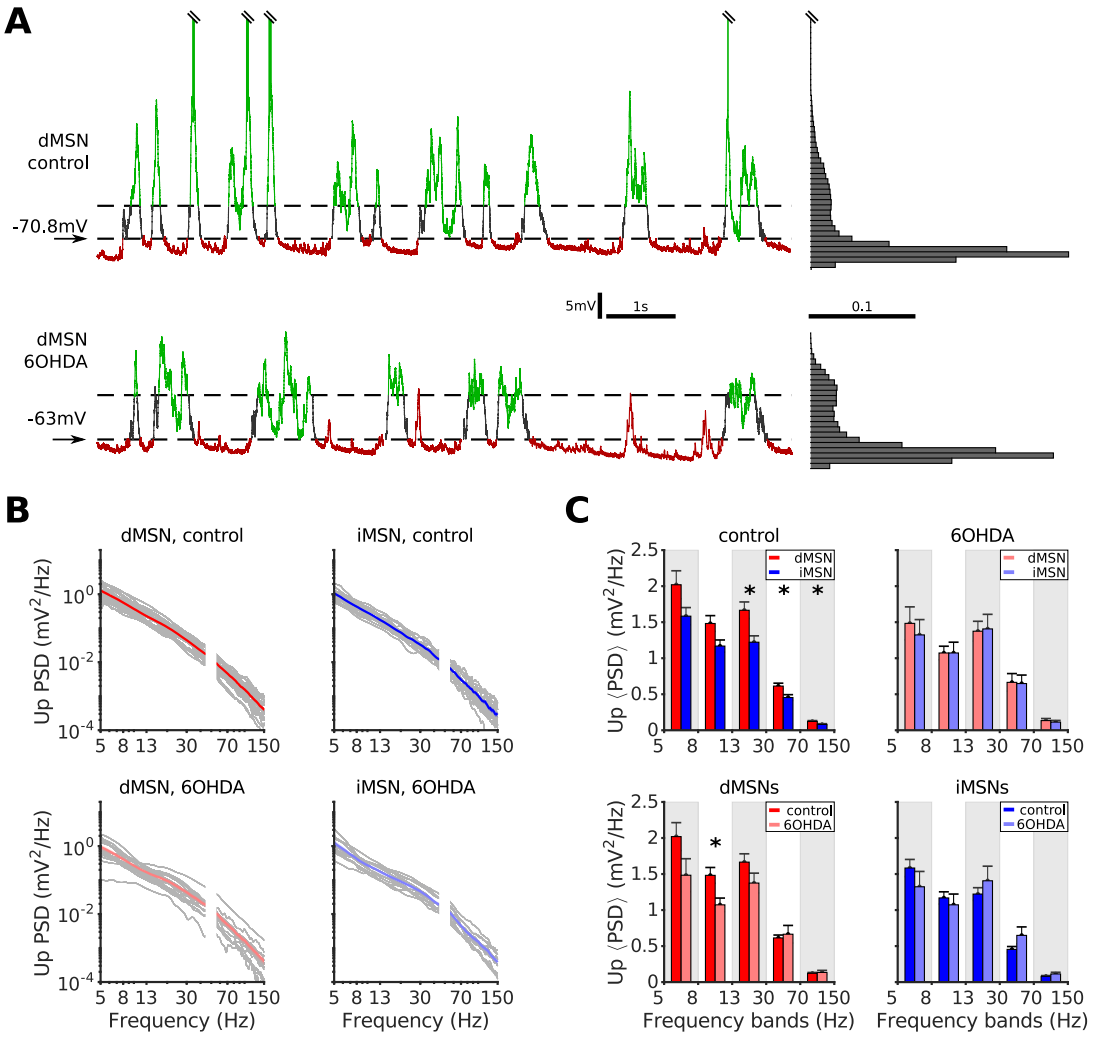

Fig 2.2. dMSNs carry more power than iMSNs during up-states in control conditions. ***A*** *Left*: Ten seconds of membrane potential recordings for a dMSN in control (upper trace) and 6OHDA (lower trace) conditions, exhibiting up- and down-states (green and red, respectively). Dashed lines represent the two cell-specific voltage thresholds used for state classification (see Methods). *Right*: Distributions of membrane potential values for the entire recordings of the two neurons shown at *left*. Note the characteristic bimodality of the up- and down-states. ***B*** Grand-average PSD estimates of up-states for all dMSNs and iMSNs in control (*top*, red and blue, respectively) and 6OHDA (*bottom*, light red and light blue, respectively) conditions. Grey traces represent average up-state PSD estimates of individual neurons. Frequencies between 45 and 55 Hz were removed to avoid power line contamination (see Methods). ***C*** Comparison of grand-average PSD estimates in different frequency bands. dMSNs exhibited higher power spectral density than iMSNs in control conditions in beta ($p = 0.0135$, $\alpha_{HB} = 0.0167$), low-gamma ($p = 0.0095$, $\alpha_{HB} = 0.01$), and high-gamma bands ($p = 0.0103$, $\alpha_{HB} = 0.0125$; dMSN $n = 26$, iMSN $n = 18$ for all three bands), indicating either stronger or more frequent synaptic input. dMSNs also showed increased PSD in control versus 6OHDA for the 8-13 Hz band ($p = 0.0087$, $\alpha_{HB} = 0.01$). Test statistics were corrected using the Holm-Bonferroni procedure.

constant using the spectrum of the membrane potential fluctuations (see Methods).

We found that the effective time constants for both dMSNs and iMSNs in the up-states were smaller than in the down-states (Table 2.1, Fig. 2.3*C*). On average, the ratio of down-state to up-state effective membrane time constant across all groups was 1.92

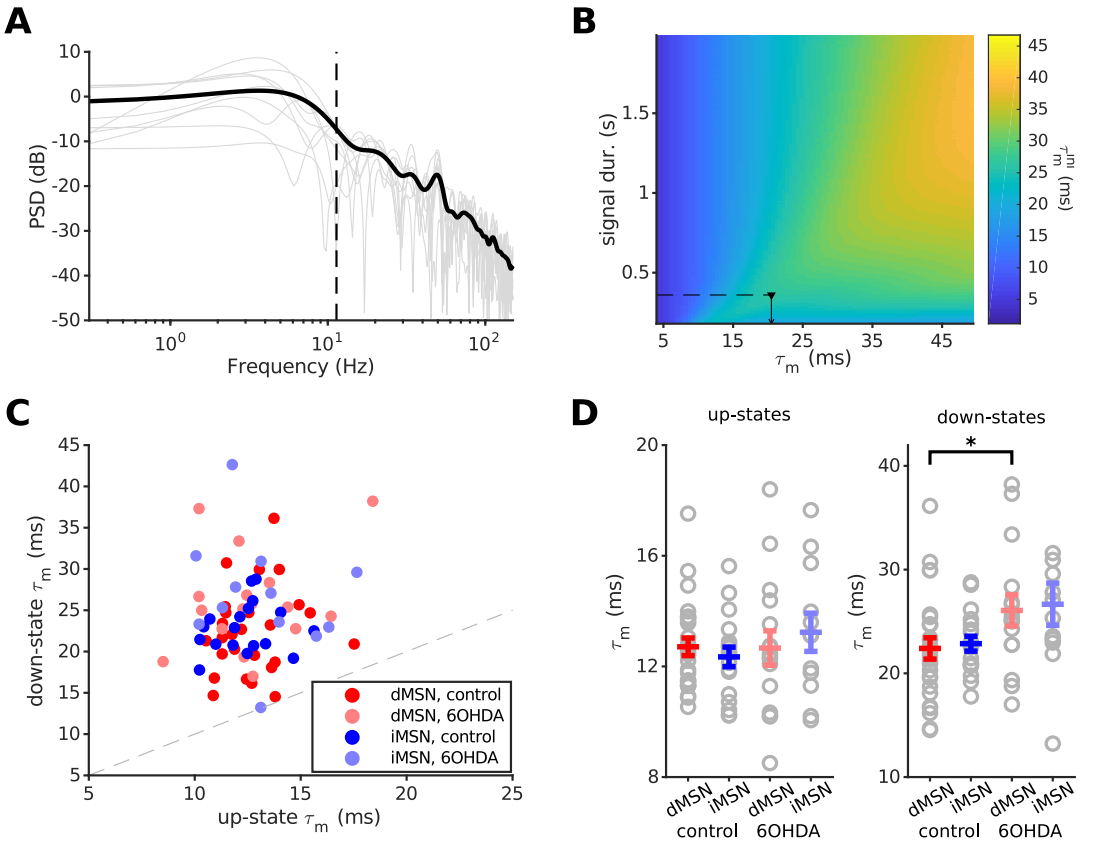

Fig 2.3. No difference in effective membrane time constant between dMSNs and iMSNs in up-states. ***A*** Example of the effective membrane time constant estimation in a dMSN, for all up-states with the mean membrane potential falling into a single 0.5 mV voltage bin. PSD estimates of individual up-states (grey) were averaged and smoothed (black trace), and the initial membrane time constant τ_m^{ini} was estimated as the point where the maximal power decreased by −3 dB (black dashed line). ***B*** Two-dimensional representation of the matrix used in the τ_m correction procedure. Depending on the average duration of all up-states within one voltage level, the initial τ_m^{ini} was corrected by the appropriate value to obtain the final τ_m estimate (see Methods). The black dashed line and the marker represent the data depicted in *A*. ***C*** Up-state vs. down-state τ_m for all neurons regardless of the cell type or physiological condition; the dashed line represents equality. It is clear that τ_m in the up-states is smaller than in the down-states, indicating a high-conductance regime due to synaptic bombardment, similar to that in neocortical neurons (Paré et al., 1998, Destexhe et al., 1999, Léger et al., 2005). ***D*** There is no significant difference in up-state τ_m between dMSNs and iMSNs, either in control or 6OHDA conditions. This suggests that the differences in up-state membrane power are not the result of differences in membrane dynamics between dMSNs and iMSNs. In down-states, 6OHDA dMSNs had higher τ_m than the control cells ($p = 0.044$). Data are shown as mean±SEM. Control dMSNs and iMSNs are in red and blue, respectively, whereas 6OHDA dMSNs and iMSNs are in light red and light blue, respectively. $^*p < 0.05$

(Fig. 2.3*D*, dMSN control 1.76, iMSN control 1.85, dMSN 6OHDA 2.06, iMSN 6OHDA 2.01). This is similar to the case of neocortical neurons, which also show a shorter time constant in up-states (Paré et al., 1998, Destexhe et al., 1999, Léger et al., 2005). However, in MSNs this ratio is not as large as has been reported for neocortical neurons (Reig and Silberberg, 2014), presumably because of the closing of potassium inward rectifier (Kir) channels in MSNs, happening as the membrane depolarizes (Waters and Helmchen, 2006, Nisenbaum and Wilson, 1995).

Table 2.1. Comparison of the effective time constants of dMSNs and iMSNs in the up-states vs. down-states. For both MSN types, across both healthy and dopamine-depleted conditions, up-states exhibited significantly faster membrane dynamics than down-states.

		τ_m^{up} (ms)	τ_m^{down} (ms)	nr. samples	statistics	p-value
control	dMSN	12.7 ± 0.3	22.4 ± 1.0	26	-6.0 (Z)	1.8×10^{-9}
	iMSN	12.3 ± 0.3	22.8 ± 0.7	18	-13.1 (t_{34})	7.1×10^{-15}
6OHDA	dMSN	12.7 ± 0.6	26.1 ± 1.5	16	-8.2 (t_{30})	3.3×10^{-9}
	iMSN	13.2 ± 0.7	26.7 ± 2.0	12	-6.2 (t_{22})	2.8×10^{-6}

Further comparisons showed no significant difference between the up-state effective time constants of dMSNs and iMSNs in control or 6OHDA conditions (in all cases $p > 0.22$; Fig. 2.3D). However, in the down-states, the effective τ_m of dMSNs was slightly larger in the 6OHDA condition than in the control ($t_{(40)} = -2.08$, $p = 0.044$; control $n = 26$, 6OHDA $n = 16$), whereas such difference for the iMSNs was just above the significance level ($p = 0.052$; Fig. 2.3D). These results are partially consistent with previously reported measurements of input resistance using standard methods in MSN down-states (Ketzef et al., 2017).

Taken together, these results clearly suggest that the differences in the power spectra of up-state sub-threshold membrane potential fluctuations between dMSNs and iMSNs (Fig. 2.2D) are not the result of different membrane time constants of the two types of neurons. Moreover, the lower membrane time constant of MSNs in the up-state suggests that these neurons also operate in a relatively high conductance regime.

2.3.3 dMSNs receive stronger input from mouse sensory cortex than iMSNs

In the analysis so far we focused on subthreshold membrane potential sections, in which neurons did not fire action potentials during the up-states. To further test the hypothesis that dMSNs indeed receive stronger inputs than iMSNs, we investigated the membrane fluctuations leading to action potential discharges. To this end, we obtained the spike-triggered average (STA) of the membrane potential immediately preceding action potential discharge for each neuron (Fig. 2.3A-C). If dMSNs would indeed receive stronger inputs, we would expect the corresponding STA traces to approach the spike threshold with a steeper slope, compared to the STA traces of iMSNs. To better quantify this difference, we sub-divided the spikes of each neuron into those corresponding to spontaneous spiking activity and those evoked by whisker deflections with brief

air puffs. This STA analysis was only performed for healthy animals, as in our data MSNs recorded from DA-depleted mice elicited only a very small number of spikes, not sufficient for STA analysis.

Comparison of the grand-average STAs for the two MSN types upon bilateral whisker stimulation revealed that dMSNs indeed depolarized to the spike threshold much faster than iMSNs. For the spontaneously generated spikes, this applied as well, although the difference was less prominent. Comparing the average membrane potential 12 ms before spike time (the duration of the average up-state integration window shown in Fig. 2.3*D*), we found that dMSN membrane potentials were on average 1.3 mV more hyperpolarized than those of iMSNs, resulting in steeper depolarization slopes (k) preceding spike initiation (Fig. 2.4*D*, $t = -12$ ms; dMSN, -6.27 ± 0.34 mV, $k = 0.31$ mV/ms, $n = 10$; iMSN, -4.97 ± 0.53 mV, $k = 0.28$ mV/ms, $n = 10$). This difference was even bigger for whisker stimulation evoked spikes (Fig. 2.4*E*, $t = -12$ ms; dMSN, -9.95 ± 1.16 mV, $k = 0.58$ mV/ms, $n = 5$; iMSN, -6.01 ± 0.72 mV, $k = 0.34$ mV/ms, $n = 4$).

We further examined the STA differences between dMSNs and iMSNs by utilizing a permutation test (see Methods). When a grand-average STA trace would fall above 97.5 % or below 2.5 % voltage distribution line, we deemed that result significant. We found that the comparison of spontaneous dMSN and iMSN STAs yielded no significant difference. However, the evoked STA traces between dMSNs and iMSNs were markedly different (Fig. 2.4*F*). Furthermore, the additional input from the sensory cortex seems to have specifically targeted dMSNs, as their STA traces varied significantly between the spontaneous and evoked conditions, whereas no major change was observable for the same comparison of iMSNs (Fig. 2.4*G*).

Thus, the results of our STA analysis also support the notion that dMSNs receive stronger synaptic input than iMSNs in healthy animals.

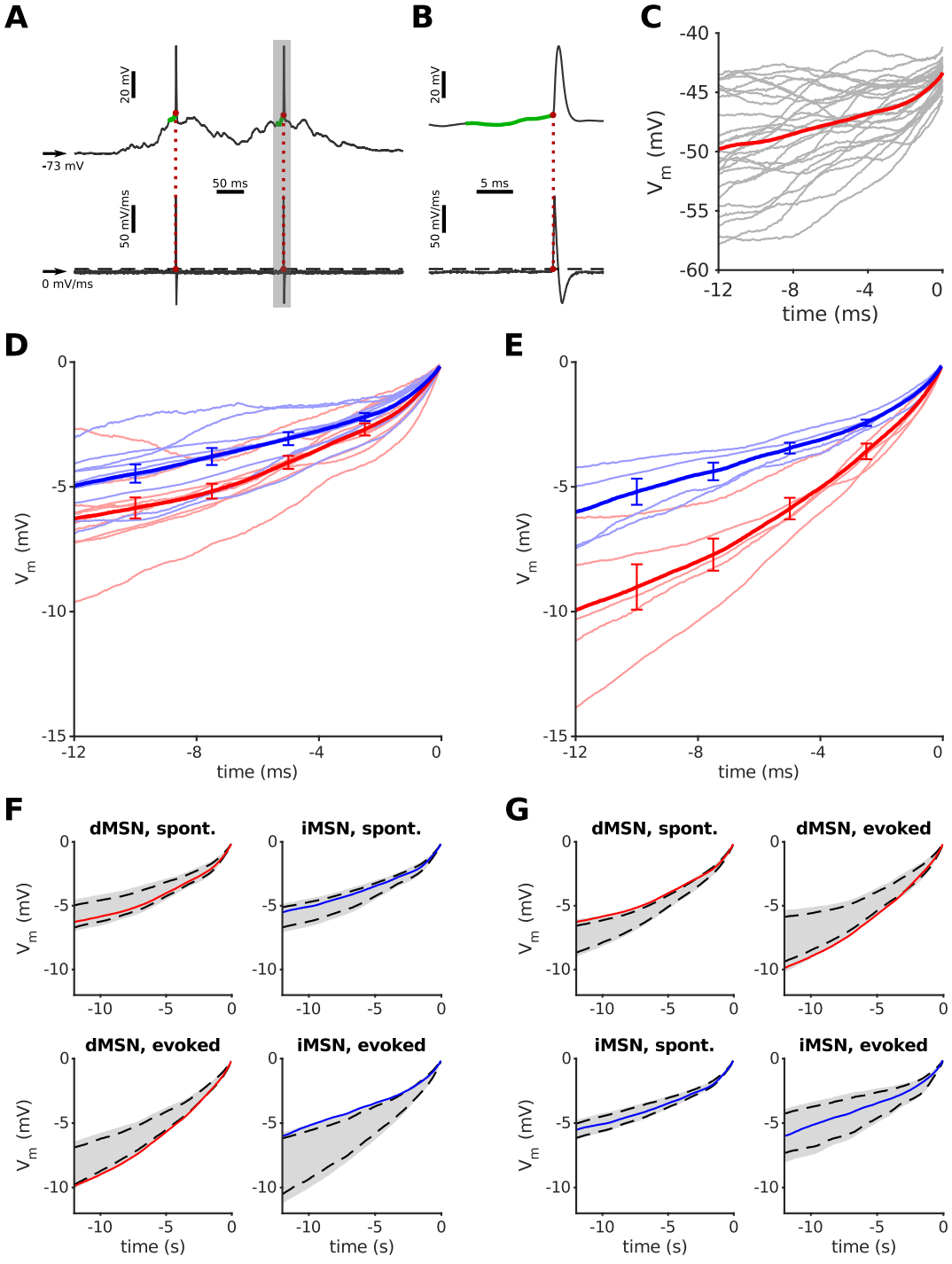
A
20 mV
-73 mV
50 ms
50 mV/ms
0 mV/ms
B
20 mV
5 ms
50 mV/ms
C
V_m (mV)
time (ms)
D
V_m (mV)
time (ms)
E
V_m (mV)
time (ms)
F
dMSN, spont.
iMSN, spont.
dMSN, evoked
iMSN, evoked
V_m (mV)
time (s)
G
dMSN, spont.
dMSN, evoked
iMSN, spont.
iMSN, evoked
V_m (mV)
time (s)

Fig 2.4. ***(preceeding page).*** **dMSNs accelerate faster towards firing threshold than iMSNs when receiving input from barrel cortex.** ***A*** Example of the estimation of the firing threshold and extraction of the pre-spike voltage trace. *Top*: membrane potential of a dMSN in the up-state; *bottom*: its first-order derivative dV/dt. The spiking threshold was determined as the highest voltage deflection seen in the derivative that didn't produce a spike (black dashed line); when the derivative crossed the threshold, this marked the start of an action potential (red dot). The voltage trace during 12 ms preceding the spike onset is marked in green. ***B*** Expanded view of the shaded area in *A*. ***C*** Example of calculating the spike-triggered average (STA, red curve) for the neuron in *A*. Gray traces are 12 ms pre-spike intervals from individual up-states producing a spike. ***D*** Comparison of grand-average STAs of dMSNs and iMSNs in control conditions (thick lines in red and blue, respectively) when action potentials were generated by spontaneous activity. Faint red and blue traces show STAs for individual neurons of corresponding MSN types. All traces were aligned to spike onset. Error bars represent SEM. ***E*** Same as in *D*, but the action potentials were generated by whisker stimulation and synaptic input from the barrel cortex. Note that the grand-average STA of dMSNs is accelerating faster toward spike onset, indicating stronger synaptic input to these neurons. ***F*** The permutation test shows that evoked dMSN and iMSN STAs differed significantly, by falling in the bottom and top 2.5 % of voltage distributions, respectively. However, no such difference was observed for spontaneous traces. ***G*** While there was no marked difference between spontaneous and evoked iMSN STAs, dMSN traces differed significantly across the two conditions.

2.4 Discussion

Here we provided evidence that *in vivo* dMSNs receive stronger synaptic input than iMSNs and that this difference is attenuated in dopamine-depleted animals. These findings were based on two observations: (1) dMSNs showed significantly higher spectral power than iMSNs in the up-states, especially in the higher-frequency bands (Fig. 2.2*C,D*), and (2) in both spontaneous and stimulus-induced spikes dMSNs membranes depolarized faster than iMSNs before reaching spike-threshold, as revealed by their STAs (Fig. 2.4). These results provide support for the theoretical prediction that direct-pathway MSNs in healthy state animals receive stronger synaptic input than iMSNs (Bahuguna et al., 2015). In addition, we showed by spectral analysis that the effective membrane time constant of MSNs during up-states is significantly shorter than in down-states, indicating that synaptic inputs affect the membrane conductance to a larger extent than hyperpolarization-activated conductances mediated by the Kir channels in MSNs.

Paired recordings in slices revealed that iMSNs form more and stronger synaptic connections onto dMSNs than they receive from them (Taverna et al., 2008, Planert et al., 2010). In addition, fast spiking interneurons also form more connections onto dMSNs than onto iMSNs (Planert et al., 2010, Gittis et al., 2010). Given these differences in connectivity, Bahuguna et al. (2015) predicted that dMSNs must receive more or stronger excitatory inputs if both dMSNs and iMSNs were to be co-activated (Cui et al., 2013) or have comparable activity levels in both ongoing and stimulus evoked activity (Sippy et al., 2015), as has been observed experimentally. Consistent with this prediction,

Parker et al. (2016) showed that, in healthy animals *in vitro*, dMSNs receive stronger excitatory input from both thalamo-striatal and cortico-striatal projections. They also showed that, while in 6OHDA leasioned animals corticostriatal projections remained largely unchanged, the ratio of dMSNs and iMSN AMPA currents in thalamic input decreased, suggesting that in DA-depleted mice thalamostriatal input to dMSNs became weaker.

Our findings that dMSNs receive stronger/more inputs is also consistent with the anatomical observation that dMSNs not only have larger dendritic area than iMSNs (Gertler et al., 2008) but also receive higher density of cortical inputs (Huerta-Ocampo et al., 2014). Therefore, if we combine out results with those of Gertler et al. (2008) and Huerta-Ocampo et al. (2014), it is plausible that dMSNs receive more synaptic inputs from the neocortex than iMSNs.

Here, we show that the disparity between the total inputs to dMSNs and iMSNs is also maintained *in vivo* in the up-states, which closely resemble the awake state of an animal (Destexhe et al., 2003, Haider et al., 2013). In our analysis we assumed that larger fluctuations in the membrane potential are a reflection of stronger synaptic weights and/or correlated inputs. Because both thalamus and cortex are co-activated in the up-states, we cannot distinguish between thalamo-striatal and cortico-striatal inputs. However, by selectively silencing thalamic inputs to the striatum (using optogenetic or chemogenetic approaches) it should be possible to determine the relative contributions of thalamo-striatal and cortico-striatal inputs *in vivo* following our approach. A limitation of our analysis is that we cannot separate excitatory from inhibitory inputs. In fact, an increase in either type of synaptic inputs can increase the membrane potential variance (Kuhn et al., 2004). However, our comparison of STAs suggests that dMSNs are more likely to receive stronger excitatory inputs because during both, spontaneous and stimulus-evoked activity, dMSNs depolarize faster to the action-potential threshold than iMSNs (Fig. 2.4).

The size of membrane potential fluctuations is affected by the mean membrane potential which determines the synaptic driving force and the membrane time constant (Kuhn et al., 2004). In our data we did not find a significant difference between the mean up-state membrane potentials of dMSNs and iMSNs in either control or 6OHDA conditions (in all cases $p > 0.138$, data not shown), and no significant difference in up-state τ_m estimations either (Fig. 2.3*D*). The latter is contrary to previous findings *in vitro*, where measurements of whole-cell capacitances and input resistances of dMSNs and iMSNs suggest that their membrane time constants are different (Gertler et al., 2008, Fieblinger et al., 2014). It should be born in mind, however, that under *in vivo* conditions the membrane properties are affected by the ongoing synaptic activity (Kuhn et al., 2004)

and that synaptic inputs can easily overcome the differences in the neuron membrane properties measured *in vitro* (Destexhe et al., 2003, 2007).

Furthermore, our data shows that in MSNs the effective membrane time constant in the up-states is on average 46 % smaller than in the down-states (Table 2.1, Fig. 2.3*C*), indicating a high-conductance state in striatal neurons in the presence of synaptic inputs, similar to that of neocortical neurons (Destexhe et al., 2003, Léger et al., 2005, Destexhe et al., 2007). That is, in the up-states, the membrane time constant is strongly influenced by synaptic inputs.

Finally, our results also provide new insights into how dopamine affects the total input to the MSNs. We found that in dopamine-depleted animals the differences in the inputs to the two MSN types decreased, so that both dMSNs and iMSNs received similar amounts of the total input. Such a decrease could be a consequence of reduction in excitatory and/or inhibitory input to the MSNs. Experimental data indicates that in the absence of dopamine thalamo-striatal excitatory inputs to dMSNs are weakened (Parker et al., 2016). However, there is also evidence that following DA depletion striatal fast spiking interneurons (FSIs, PV-expressing interneurons) undergo morphological changes that alter their target preference towards iMSNs (Gittis et al., 2010, Mallet, 2006). While the contribution of PV axonal remodelling is hard to assess, it may be a potential underlying mechanisms of the effect that we observe in lesioned animals. Although we cannot differentiate between the contribution of excitatory and inhibitory inputs by spectral analysis, the STA waveforms suggest that dMSNs and iMSNs receive unequal amount of excitatory inputs. Moreover, these results are consistent with our previous findings that in healthy animals dMSNs exhibit stronger response to contralateral sensory stimulation than iMSNs, and that these differences are diminished in dopamine-depleted mice (Reig and Silberberg, 2014, Ketzef et al., 2017). Thus, our results and previous findings (Ketzef et al., 2017) suggest that dopamine is important to maintain the difference in the total input to dMSNs and iMSNs.

While we have provided evidence for stronger total synaptic input to the dMSNs as compared to iMSNs, it is still unclear whether the extra input to the dMSNs is due to stronger excitatory (cortical and/or thalamic) inputs, more intense inhibition, or a combination thereof. Furthermore, it also not clear whether the larger membrane potential fluctuations in dMSNs are due to stronger synapses or to higher input correlations. More dedicated experiments involving selective correlated activation of cortical and thalamic neurons will help resolving these questions.

2.5 Acknowledgements

We thank Dr. Jyotika Bahuguna, Dr. Rita Almeida, Matthijs Dorst, Michael Zohar and Yvonne Johansson for their technical support and advice. This work was funded in parts by: the EU Erasmus Mundus Joint Doctorate Program 'EUROSPIN', The International Graduate Academy (IGA) of the Freiburg Research Services (to Marko Filipović), the Swedish Research Council (Research Project Grant, StratNeuro), the Swedish Brain Foundation (Hjärnfonden) Grant, Wallenberg Fellowship (to G. Silberberg), Parkinsonfonden grant (to Arvind Kumar), and the German Research Foundation (DFG#1086 BrainLinks BrainTools) (to Ad Aertsen and Arvind Kumar).

2.6 Author contributions

Marko Filipović and Arvind Kumar conceived and designed the project in this chapter. Maja Ketzef, Ramon Reig, and Gilad Silberberg designed and performed the experiments. Marko Filipović and Maja Ketzef implemented and perfomed data analysis. Marko Filipović and Arvind Kumar interpreted the results.

Chapter 3

Modulatory effects of dopamine on trial-by-trial variability of direct pathway striatal neurons: a simulation study

Marko Filipović[1,2], Robert Lindroos[3], Jeanette Hellgren-Kotaleski[3,4], Arvind Kumar[1,2]

[1] Dept. of Computational Science and Technology, School of Computer Science and Communication, KTH Royal Institute of Technology, Stockholm, Sweden

[2] Bernstein Center Freiburg and Faculty of Biology, University of Freiburg, Germany

[3] Department of Neuroscience, Nobel Institute for Neurophysiology, Stockholm, Sweden

[4] Science for Life Laboratory, School of Electrical Engineering and Computer Science, KTH Royal Institute of Technology, Solna, Sweden

3.1 Introduction

The principal cells of the striatum are medium spiny neurons (MSNs). Based on the dopamine (DA) receptor they express, they are assigned either to D1R-expressing direct-pathway group (dMSNs), or D2R-expressing indirect-pathway group (iMSNs). As a neuromodulator, dopamine is known to play a crucial role in the function and dysfunction

of the basal ganglia as a whole, being integral in such mechanisms as reinforcement learning, action selection, motor control, addictive behavior, etc. For MSNs in particular, DA modulation is complex and multifaceted, and known to have a direct impact on neuronal dynamics. Here we focus specifically on dopaminergic modulation of dMSNs, and will give a brief overview of its effects on dMSN's intrinsic and synaptic conductances (Lindroos et al., 2018).

It is a general consensus that elevated concentrations of dopamine will make a dMSN more excitable, whereas concentrations below normal levels - as occurs for example during Parkinson's disease (PD) - will decrease dMSN excitability (Albin et al., 1989, Mallet, 2006, Planert et al., 2013, Surmeier et al., 2007) (however, in mice models of late-stage PD, compensatory mechanisms may counter this trend; see Fieblinger et al. 2014, Ketzef et al. 2017). The changes in dMSN excitability occur, to a lesser or greater degree, through DA modulation of multiple intrinsic and synaptic ion channels. These modulatory effects have been studied in detail over the past three decades by the neuroscience community, with often mismatching and sometimes even directly conflicting results.

For example, after performing a detailed literature review (Lindroos et al., 2018), we showed that Naf conductance is reported to be down-regulated by DA in a relatively wide range of values (˜20-40 %, Table 3.1). Likewise, Kas, and CaN/P channels are also reported to be down-regulated, while CaL is up-regulated. However, we found conflicting reports on KIR channel, giving a range of values for DA modulation from about $-20\,\%$ to $25\,\%$.

Similarly complex situation could also be found for synaptic conductances. AMPA and NMDA channels are both up-regulated, though the reported values differ from study to study, ranging about 20-60 % for AMPA and 0-30 % for NMDA (Table 3.2). On the other hand, reports for GABA seem to be in direct disagreement with each other, claiming values ranging from about $-20\,\%$ to $40\,\%$.

There are multiple possible reasons for inconsistencies among studies pertaining to DA modulation of ion channels. These span from experimental setups that differed from one laboratory to another, to different types of animals used, different ages of animals, and crucially, different experimental preparations.

Nevertheless, Lindroos et al. (2018) succeeded in creating a complex, biophysically detailed model of a direct-pathway medium spiny neuron that integrates the effects of DA modulation, and expresses dynamics that corresponds well to that of experimentally recorded dMSNs. Here, we use this model to ask the following questions: what

Table 3.1. Summary of the literature study on single channel effect of D1R activation in striatum. Some values given in the Effect column are estimates when there were no exact values given. In the Measure column: *I* stands for current, *IV* stands for current-voltage profile, *Exc* stands for excitability, *pd* stands for plateau duration, and *#APs* stands for number of action potentials. Reproduced from Lindroos et al. (2018).

Chan	Measure	Effect	References	Animal	Preparation
Naf	I	−38±5 %	Schiffmann et al. (1995)	Rat	Culture
Naf	I	−24±2 %	Zhang et al. (1998)	Rat	Dissociated
Naf	I	−22 %	Surmeier et al. (1992)	Rat	Dissociated
Kas	I	−20 %	Kitai and Surmeier (1993)	Rat	Dissociated
KIR	IV	+	Pacheco-Cano et al. (1996)	Rat	Slice
KIR	I	25 %	Zhao et al. (2016)	Mice	Slice
KIR	I	-	Podda et al. (2010)	Mice	Slice
CaN/P	I	−50 %	Zhang et al. (2002)	Rat	Dissociated
CaN/P	I	-	Surmeier et al. (1995)	Rat	Dis./Culture
CaL	I	+	Surmeier et al. (1995)	Rat	Dis./Culture
CaL	Exc	20 %	Galarraga et al. (1997)	Rat	Slice
CaL	Exc	+	Flores-Barrera et al. (2011)	Mice	Slice
CaL	pd, #Aps	20 %, 34 %	Hernandez-Lopez et al. (1997)	Rat	Slice

is the impact of DA-driven alterations of dMSN excitability on trial-by-trial variability? How do changes in DA concentration affect the neural responses when the cell is receiving correlated synaptic input? And what are its effects when a change in input excitation-inhibition (E-I) balance occurs?

3.1.1 Sources of trial-by-trial variability

The spike count variability of neural responses across different trials is a well documented property of the central nervous system (Faisal et al., 2008, Shadlen and Newsome, 1998). Interestingly, this trial-by-trial variability does not seem to be of equal magnitude in all conditions. Probing neural systems with repeated stimuli demonstrated that trial-by-trial variability is larger in the period before a stimulus is presented, and considerably

Table 3.2. Summary of the literature study on synaptic effect of D1R activation given as percentage of control. *I* stands for current, *amp* stands for amplitude, *dur* stands for duration, V_m stands for membrane potential, and *PHOSP* stands for phosphorylation. *I"* indicates current in adult animals (reduced in juvenile). I^* indicates tonic current from low levels in young animals. I^{**} stands for tonic current following application of D1R antagonist in adult animals. Some values are estimated from multiple values or graphs. Reproduced from Lindroos et al. (2018).

Measure	Effect	References	Animal	Preparation
		NMDA (range $20\,\% \rightarrow 60\,\%$**)**		
I (amp, dur)	25 %, 30 %	Flores-Hernández et al. (2002)	Rat and mice	Culture
I (amp, dur)	26±7 %, 5±2 %	Cepeda et al. (1998)	Rat	Slice
I"	45.6±19 %	Tong and Gibb (2008)	Rat	Slice
V_m (amp, dur)	39±14 %, 22±7 %	Levine et al. (1996b)	Mice	Slice
V_m (area)	34±9 %	Levine et al. (1996a)	Rat	Slice
		AMPA (Non-NMDA) (range $0\,\% \rightarrow 30\,\%$**)**		
V_m (area)	6±5 %	Levine et al. (1996a)	Rat	Slice
I	30 %	Umemiya and Raymond (1997)	Rat	Slice
I	11±6 %	Yan et al. (1999)	Rat and mice	Dissociated
I	21±2.5 %	Price et al. (1999)	Rat	Culture
PHOSP	+	Price et al. (1999)	Rat	Culture
PHOSP	300 %	Snyder et al. (2000)	Mice	Slice
PHOSP	200 %	Chao et al. (2002)	Rat	Culture
PHOSP	450 %	Xue et al. (2017)	Rat	*In vivo*
		GABA (range $-20\,\% \rightarrow 40\,\%$**)**		
I	−20 %	Flores-Hernandez et al. (2000)	Rat	Dis./culture
I	−29.7±3.8 %	Flores-Hernandez et al. (2000)	Rat	Dissociated
I	± and no change	Nieto Mendoza and Hernández Echeagaray (2015)	Mice	Slice
I^*	84±34 %	Janssen et al. (2009)	Mice	Slice
I^{**}	44 %	Janssen et al. (2009)	Mice	Slice
I	−14.5±0.7 %	Hernández-Echeagaray et al. (2007)	Mice	Slice

reduced following the presentation (Churchland et al., 2010, Hussar and Pasternak, 2010, Stein et al., 2005). Furthermore, it has been shown in cat visual system that the degree of response variability depended on the stage of sensory processing, increasing from periphery (retina) to cortex (Kara et al., 2000).

Some of the sources of trial-by-trial variability can be traced to synaptic noise (Faisal et al., 2008, Mainen and Sejnowski, 1995), refractory period (Kara et al., 2000), and ongoing neural activity (Arieli et al., 1996). None of these sources however considers

the properties of the synaptic input that arise as a consequence of network dynamics: correlations of synaptic input rates, and the balance between excitatory and inhibitory inputs (E-I balance).

Correlations of neuronal population activity are widespread throughout CNS, and have been investigated both for the inputs to populations (Cafaro and Rieke, 2010, Okun and Lampl, 2008) and for the population outputs (Averbeck et al., 2006, de la Rocha et al., 2007, Engelhard et al., 2013, Riehle et al., 2000, Schneidman et al., 2006). Several theoretical studies thus far have tried to elucidate the function of input correlations in neural processing of information (Bujan et al., 2015, Doiron et al., 2016, Tchumatchenko et al., 2010). At the same time, the balance of excitatory and inhibitory inputs was shown to be one of the deciding factors of neuronal network dynamics and has been the target of much experimental and theoretical research in the previous two decades (Bhatia et al., 2019, Brunel, 2000, Kremkow et al., 2010, Kumar et al., 2008, Haider et al., 2006, Shadlen and Newsome, 1998, van Vreeswijk et al., 1996, Vogels and Abbott, 2009).

Here we hypothesize that one of the potential functions of both input rate correlations and changes in the E-I balance is to regulate the trial-by-trial variability of individual neurons. We investigate the effects of these input modalities on neuronal variability in a model of a striatal direct-pathway medium spiny neuron, which allowed us to explore an additional dimension of response variability issue: that of dopaminergic modulation.

3.2 Methods

3.2.1 dMSN model

In this study we use a biophysically detailed compartmentalized model of a striatal direct-pathway medium spiny neuron with realistic morphology. The dMSN model has been described in detail elsewhere (Lindroos et al., 2018), therefore we focus only on the changes introduced for the purposes of this work.

Intrinsic channels Channel distribution over cell compartments and their parametrization were updated via a Monte Carlo algorithm to improve the fit to the experimental data (primarily to current frequency and to the change of calcium levels in backpropagating action potentials, Table 3.3). Two new channels were introduced to the axon initial segment (AIS), the potassium delayed rectifier (Kdr) and the KCNQ channel responsible for the M-current (Im) (Adams, 1982, Doron et al., 2017). These channels are both normally expressed in the AIS (Petersen et al., 2017).

Table 3.3. Channel distribution over cell compartments as a function of somatic distance (x). Maximal value here stands for permeability (cm/S) for Ca channels, and conductance (S/cm^2) for the rest of the channels. Updated from Lindroos et al. (2018).

Channel	Compartment	Function type	Maximal value (x)
Naf	Soma	Uniform	12
	Dendrite	Sigmoidal	$0.46 \cdot [0.14 + 0.86/(1 + \exp((x - 23.44)/13.11))]$
	Axon	Step	if $(x < 30)$: 9.9; else: 9
Kas	Soma	Uniform	0.016
	Dendrite	Sigmoidal	$0.03 \cdot [0.1 + 0.9/(1 + \exp((x - 10)/6.38))]$
	Axon	Uniform	7×10^{-3}
Kaf	Soma	Uniform	0.15
	Dendrite	Sigmoidal	$0.11 \cdot [1 + 0.21/(1 + \exp(-(x - 42.4)/32.32))$
Kir	Soma/dend.	Uniform	1.2×10^{-3}
Kdr	Soma	Uniform	9.4×10^{-4}
	Dendrite	Uniform	7×10^{-4}
	Axon	Uniform	28.2×10^{-4}
SK	Soma/dend.	Uniform	2×10^{-5}
BK	Soma	Uniform	1.3×10^{-4}
	Dendrite	Uniform	1×10^{-4}
CaL1.2	Soma	Uniform	1.34×10^{-5}
	Dendrite	Uniform	1×10^{-5}
CaL1.3	Soma	Uniform	1.34×10^{-6}
	Dendrite	Uniform	1×10^{-6}
CaN	Soma	Uniform	4×10^{-5}
	Dendrite	Sigmoidal	$8.14 \cdot [0.15 + 0.85/(1 + \exp((x - 36.57)/18.12))]$
CaR	Soma	Uniform	1.34×10^{-4}
	Dendrite	Uniform	1×10^{-4}
CaT3.2	Soma	—	
	Dendrite	Sigmoidal	$1.23e - 7 \cdot [1/(1 + \exp(-(x - 65.54)/18.67))]$
CaT3.3	Soma	—	
	Dendrite	Sigmoidal	$3.81e - 9 \cdot [1/(1 + \exp(-(x - 104.16)/23.8))]$
KM	Axon	Uniform	1×10^{-3}

Synaptic channels Total number of compartments in the model was set to 1010, out of which 1007 were assigned to the dendritic arbor (of the remaining 3 one belonged to the soma and two to the AIS). Each separate dendritic compartment was assigned two synapses: one GABAergic, whose dynamics remained consistent with the previously published model, and one glutamatergic, which unified the activation of AMPA and NMDA synaptic channels. In this way, both excitatory and inhibitory synapses were distributed homogeneously and in equal proportion throughout the dendritic tree.

The excitatory glutamatergic synapse was modified to operate on the base of a summating mechanism, simulating combined contributions of a number of actual synapses.

The ratio between AMPA and NMDA maximal conductances was set to 5 (Ketzef et al., 2017). The remaining synapse model parameters are summarized in Table 3.4.

Each synapse in the model then received an independent and uncorrelated spike train with Poisson-distributed spike times.

Table 3.4. Glutamate synapse model parameters.

Parameter	Value
τ_{AMPA}^{rise}	1.9 ms
τ_{AMPA}^{fall}	4.8 ms
τ_{NMDA}^{rise}	5.52 ms
τ_{NMDA}^{fall}	231 ms
$\bar{g}_{AMPA}$ / $\bar{g}_{NMDA}$	5.0
Mg	1 mmol
α	0.062
Q factor	2

Table 3.5. Maximal dopaminergic modulation of intrinsic and synaptic channels in the dMSN model.

Channel	δ_{max}
Naf	0.75
Kaf	0.8
Kas	0.8
KIR	1.2
CaL1.2	1.3
CaL1.3	0.5
CaN	0.5
CaR	1.0
Glut	1.3
GABA	0.8

Dopaminergic modulation The intracellular signaling cascade triggered by fluctuating DA concentration was removed in this version of the model. Instead, we simulated a steady-state condition of tonic dopaminergic modulation by changing maximal conductances $\bar{g}$ (or permeabilities $\bar{p}$ in the case of calcium channels) of both intrinsic and synaptic channels by a fixed amount. Each of the affected channels was assigned a maximal level of modulation (δ_{max}, Table 3.5), which was then scaled by a fraction (δ_{frac}) in the range from 0 to 1, to determine the final value of the channel's maximal conductance $\bar{g}_{mod}$:

$$\begin{aligned} \delta_{mod} &= 1 + (\delta_{max} - 1) \cdot \delta_{frac} \\ \bar{g}_{mod} &= \bar{g} \cdot \delta_{mod} \end{aligned} \tag{3.1}$$

In our simulations, the DA modulation fraction δ_{frac} was the main determinant of the degree of a channel's modulation. Further in the text, the term "dopaminergic modulation" refers to this fraction of the maximal level of DA modulation. Only those channels previously demonstrated to be modulated by dopamine were manipulated in this way, and the values used in the model were determined either as averages of already published values, or as best fits to currently available experimental data (Table 3.1,

Table 3.2). This fitting process, as well as exploration of DA modulation of Kaf channels which was not previously reported in the literature, was investigated in Lindroos et al. (2018).

Three levels of DA modulation were of particular interest to us: $\delta_{frac} = 0.0$ signifying no presence of dopamine in the system (e.g. due to the lack of DA neuron activity after omission of a predicted reward), $\delta_{frac} = 0.2$ representing "baseline" dopamine concentration, and $\delta_{frac} = 1.0$ as the maximal possible dopaminergic modulation (e.g. peak phasic DA concentration after an unpredicted reward). These levels were determined based on the approximate proportions of dopamine phasic and tonic concentrations found in the literature (Borland et al., 2005, Cheer et al., 2007, Dreyer et al., 2010, Robinson et al., 2001).

The model was developed in NEURON+Python simulation environment (Hines and Carnevale, 1997, Hines, 2009) and simulations ran on resources provided by the Swedish National Infrastructure for Computing (SNIC) at PDC KTH.

3.2.2 Simulation parameters

We performed numerical simulations for a range of input parameters, iterating over synaptic input rates and levels of DA modulation (Table 3.6). 20 trials were run for every input parameter combination, with a separate random number generator (RNG) seed for each trial. RNG seeds were kept constant for the same trial number across different parameter sets. In other words, trial number e.g. 4 would always have the same seed no matter which input parameter set was used.

In each simulation run we calculated the output firing rate (OFR) of the dMSN model. The first 300 ms of a recording were considered to be a transitional period (t_{trans}, Table 3.6), and all spikes that occurred during that time were discarded. Recording spike times during the remaining 2 s of simulation allowed us to reliably detect output firing rates as low as 0.5 Hz. The final output firing rate for each input parameter combination was obtained as an average across all 20 simulation trials.

3.2.3 Sampling of 2D transfer function

Sampling the 2D transfer function with independent input We sampled the dMSN 2D transfer function by firstly dividing the whole transfer space into nine equal regions (Figure 3.2*A*). In each region, we drew 5000 uncorrelated pairs of excitatory and inhibitory input rates from Gaussian distributions and calculated the resulting dMSN output firing rates by using spline interpolation on the underlying 2D transfer function. The standard

Table 3.6. Simulation parameters.

Parameter	Value
General parameters	
t_{sim}	2300 ms
t_{trans}	300 ms
nr. trials	20
Synaptic parameters	
E^I_{rev}	0 mV
E^I_{rev}	−60 mV
J_E	0.5 nS
J_E	1.5 nS
Input parameters	
λ^{in}_E range (per synapse)	0.2-0.45 Hz
λ^{in}_I range (per synapse)	0.2-2.45 Hz
δ_{frac} range	0-1

deviations (SDs) of the marginal Gaussian distributions were $\sigma^{in}_E = 5.035\,\text{Hz}$ for λ^{in}_E and $\sigma^{in}_I = 50.35\,\text{Hz}$ for λ^{in}_I, and their means were located at the centers of each region. This process was then repeated for every dopamine level, resulting in a set of independent OFR distributions for each region.

Each of the sampled E and I pairs represented a single measurement of dMSN's output activity, or a single "trial". Drawing new values for E and I inputs from a distribution in every trial simulated changes in input rates that a biological neuron might see during the course of experimental measurement.

Sampling the 2D transfer function with correlated input We use the term "correlated input" to refer to correlations between excitatory and inhibitory synaptic input rates as they are drawn from their respective distributions, and not to the timing of individual spikes in the incoming spike trains.

In order to have a clear comparison of dispersion in OFR distributions that were the result of correlated synaptic input, we sampled a region of 2D transfer function that was aligned to the 10 Hz OFR contour at baseline DA level (Figure 3.3*A*, means of marginal distributions $\mu^{in}_E = 400.15\,\text{Hz}$, $\mu^{in}_I = 1522.3\,\text{Hz}$). The SDs of marginal distributions were calculated by starting from the value $\sigma^{in}_E = 5.035\,\text{Hz}$ for excitatory input, and determining the the value for the inhibitory input according to the slope of the linear fit of

the 10 Hz OFR contour. We correlated the marginal input distributions by constructing the covariance matrix of the joint distribution as:

$$cov[\lambda_{\mathbf{E}}^{\mathbf{in}}, \lambda_{\mathbf{I}}^{\mathbf{in}}] = \begin{vmatrix} {\sigma_E^{in}}^2 & \rho\, \sigma_E^{in} \sigma_I^{in} \\ \rho\, \sigma_E^{in} \sigma_I^{in} & {\sigma_I^{in}}^2 \end{vmatrix} \tag{3.2}$$

where ρ was the Pearson's coefficient of correlation chosen from the values between 0 and 1, with the step of 0.1. Finally, the OFR distributions were constructed by drawing 5000 data points from a bivariate Gaussian distribution with the appropriate covariance matrix.

Sampling the 2D transfer function while changing the E-I balance Here we define the E-I balance as the relation between the ranges of available excitatory and inhibitory input rates, such that one is proportionate to the other. Starting from marginal λ_E^{in} and λ_I^{in} distributions chosen such that their joint distribution lies on the 10 Hz OFR contour at baseline DA level as described above, but with an additional input correlation value of $\rho = 0.2$ (Figure 3.4*A*, white dots), we change the E-I balance by multiplying the SD of one of the marginal distributions with the coefficient c_b prior to the construction of the joint covariance matrix. The values of c_b are chosen to be positive rational numbers.

To illustrate, we change the E-I balance with respect to the excitatory input rates by starting from the fixed value of σ_E^{in}, calculate the inhibitory SD so that it matches the chosen OFR contour level (σ_I^{cntr}), and proceed to multiply the inhibitory standard deviation with the chosen E-I balance coefficient c_b^E:

$$\sigma_I^{in} = c_b^E \cdot \sigma_I^{cntr}. \tag{3.3}$$

The procedure of changing the E-I balance with respect to the inhibitory input rates is identical, except we fix the value of σ_I^{in} and modify that of the σ_E^{cntr}:

$$\sigma_E^{in} = c_b^I \cdot \sigma_E^{cntr}. \tag{3.4}$$

Finally, we obtain the covariance matrix by applying Equation 3.2.

All data analyses were performed using custom scripts written in Python 2.7.

3.3 Results

Here we examine the variability of the output of a dMSN model under synaptic bombardment, when the neuron dynamics is modulated by different levels of dopamine. We

consider the influence of changes in the input correlation, as well as changes in the balance of excitation (E) and inhibition (I), on the total range of output firing rates (OFRs) available to our dMSN model. We show that these effects, compounded by the dopaminergic modulation, can provide an explanation of trial-by-trial rate variability of dMSNs. Furthermore, we demonstrate how dopamine affects trial-by-trial variability of spikes in time, by exploring the inter-spike interval (ISI) transfer space of the model.

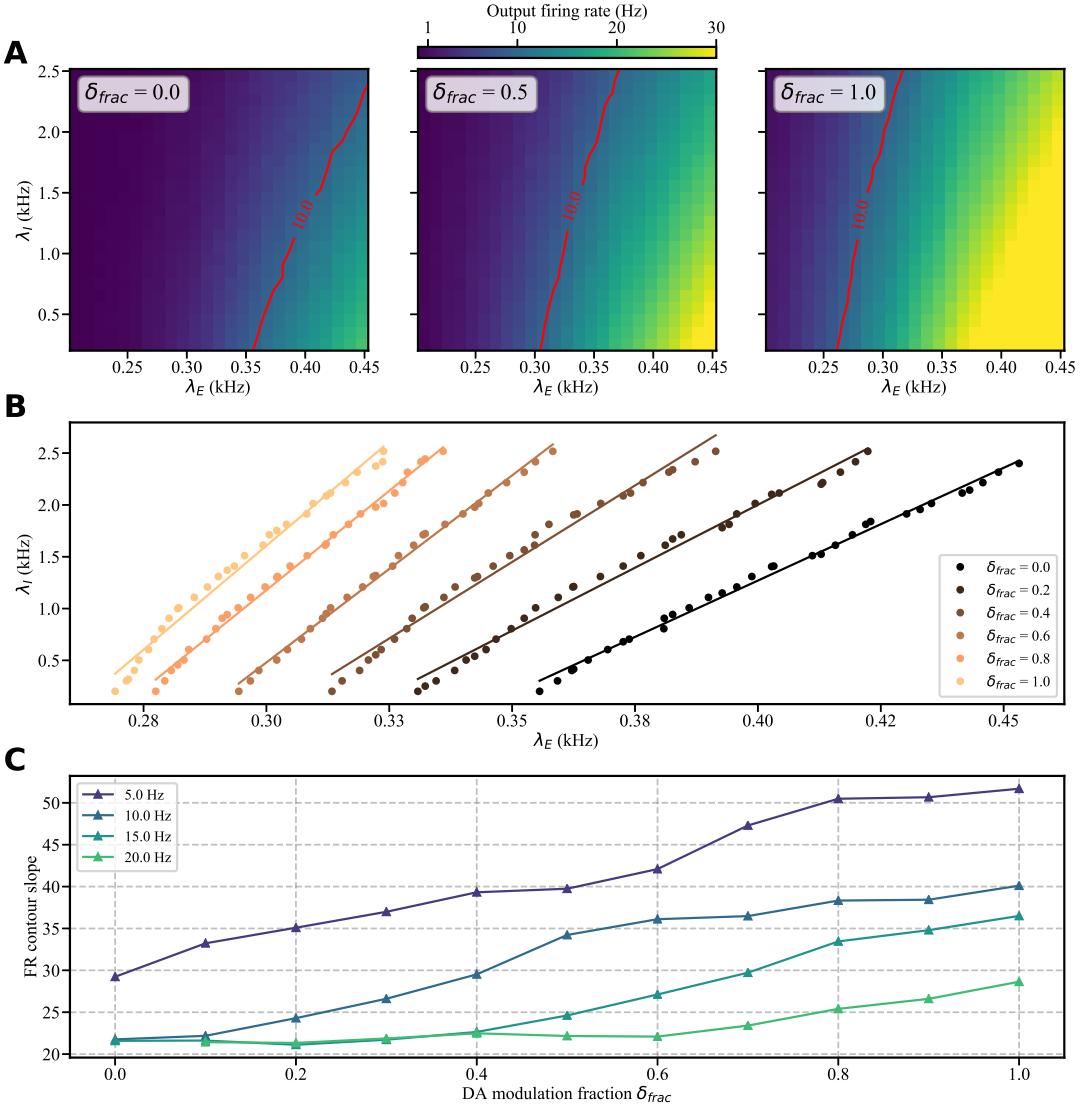

Fig 3.1. dMSN excitability increases with increase in DA levels. ***A*** An example of a dMSN 2D transfer function over three discreet dopamine levels. The red line represents a 10 Hz output firing rate contour. As the dopamine level increases, the total range of available output firing rates also increases. At the same time, the span of excitatory input firing rates needed to maintain the 10 Hz OFR contour shrinks. ***B*** Evolution of 10 Hz OFR contour for different dopamine levels in the same 2D transfer space. Contour data is given as dots, with lines representing linear fits to the data. The slopes of the linear fits increase together with DA levels, indicating a rise of neuronal excitability. ***C*** Evolution of OFR contour slopes across different dopamine levels for four chosen firing rate contours. The overall trend is a dopamine-driven increase of dMSN excitability, as evidenced by the growth of OFR contour slopes.

3.3.1 Dopamine increases excitability of dMSNs

A standard electrophysiological procedure to obtain a neuron's transfer function is to measure the cell's spike frequency for different levels of constant current input (McCormick et al., 1985). However, while this approach allows us to know the voltage needed to elicit a certain output firing rate λ^{out} from a neuron, it disregards the possibility of achieving the same level of output firing for various combinations of excitatory and inhibitory synaptic inputs (Kuhn et al., 2004). This issue is further complicated by the fact that different combinations of E and I input rates will result in different values of the total membrane conductance, thus altering the membrane dynamics in each case while at the same time maintaining the identical output firing rate λ^{out}. Since this effect is not readily apparent from a regular transfer function, here we focus on its two-dimensional (2D) representation.

We constructed the dMSN model's 2D transfer function by recording its output firing rate for every combination of total excitatory and inhibitory synaptic input within our chosen ranges (Figure 3.1*A*, Table 3.6). The synaptic input consisted of uncorrelated and Poisson-distributed spike trains, whose firing rate was independently varied for excitatory and inhibitory synapses (λ_E^{in} and λ_I^{in}, respectively). The points of the transfer function that shared a single output firing rate were designated as "output firing rate (OFR) contours" (Figure 3.1*A*, red line shows 10 Hz OFR contour). We calculated linear fits to all OFR contours and employed their slopes of as a proxy measure of neuronal excitability. Namely, for a contour whose slope had a low value, the range of excitatory input firing rates λ_E^{in} needed to balance the full range of inhibitory input firing rates λ_I^{in} would be wider, indicating low excitability. Correspondingly, high excitability implied a narrower range of λ_E^{in} needed to balance the input inhibition, which was reflected in the higher value of the slope of the linear fit.

We followed the evolution of the firing rate contours as as the steady-state levels of dopamine in the system increased (Figure 3.1*B*). For all OFR contours the general trend was growth of the slope of the linear fit (Figure 3.1*C*), signifying that neuronal excitability increases together with the dopamine levels. This behavior of our dMSN model mimics the well-established dynamics of direct-pathway medium spiny neurons, where an increase in excitability, marked by heightened firing rates, was shown for elevated DA levels, while the lack of dopamine in the system was followed by the decrease in output firing (Albin et al., 1989, Mallet, 2006, Planert et al., 2013, Surmeier et al., 2007).

Thus we demonstrate that our model exhibits similar patterns of behavior as dMSNs recorded in animals for various steady-state levels of dopamine, that the effects of

dopaminergic modulations are clearly visible on 2D transfer functions and that they manifest as shifts of the transfer space. Furthermore, we show that the slope of the linear fit to output firing rate contours is an adequate representation of the neuronal excitability.

3.3.2 Synaptic input and DA level determine trial-by-trial variability

In order to explore how trial-by-trial variability of dMSN output changes with respect to dopamine levels in the system, we repeatedly sampled the 2D transfer function at nine distinct regions (Figure 3.2*A*). For each region, every sample point drawn represented a single "trial", a measurement of the dMSN output activity for a certain combination of E and I input firing rates. A collection of all the sampled points in one region formed an OFR distribution.

OFR distributions showed steady and consistent growth in their mean values with the rise of DA levels across all regions (Figure 3.2*B*, blue lines), demonstrating the general increase of dMSN excitability and output firing as the system saturated with dopamine. This dependency was quite prominent for all input excitation values past the lowest range: for mid-range λ_I^{in} values, output firing rates were 3.5 - 16.3 Hz at mid-range λ_E^{in} (middle row, middle column of Figure 3.2*B*), and 10.8 - 29 Hz at high-range λ_E^{in} (middle row, right column of Figure 3.2*B*). While weaker for low-range λ_E^{in}, it was not negligible, spanning 0.3 - 4.8 Hz across all DA modulation levels (Figure 3.2*B* middle row, left column).

However, OFR distribution means did not provide information necessary to investigate the effects of DA modulation on trial-by-trial variability. For that purpose, we measured the dispersion of distributions with respect to their average values, exemplified by the Fano factor (FF) of their spike count: $FF = \sigma^2_{_{OFR}}/\mu_{_{OFR}}$. We postulated that if dopamine had a perceptible impact on neuronal variability, it would be reflected in the OFR distribution dispersion, or in another words, in changes to the range of output firing rates available to dMSN. Interestingly, the DA effects were not uniform across the nine regions. For low-range λ_E^{in} values we observed a general increase of Fano factor with increased DA levels across the entire range of inhibitory input (Figure 3.2*B* left column, red lines), characteristic of a rise in neuronal variability. However, for high-range λ_E^{in} values, FF-DA profiles were mostly flat. This suggested that the trial-by-trial variability was insensitive to changes in DA concentration, and that the neuron had reliable output for high levels of input excitation. The trend of FF-DA profiles for mid-range excitatory input values was undetermined, and warrants further investigation. The fluctuations within each profile were presumably caused by a combination of non-linearities of the

underlying 2D transfer function, and the finite amount of data we generated in our simulations.

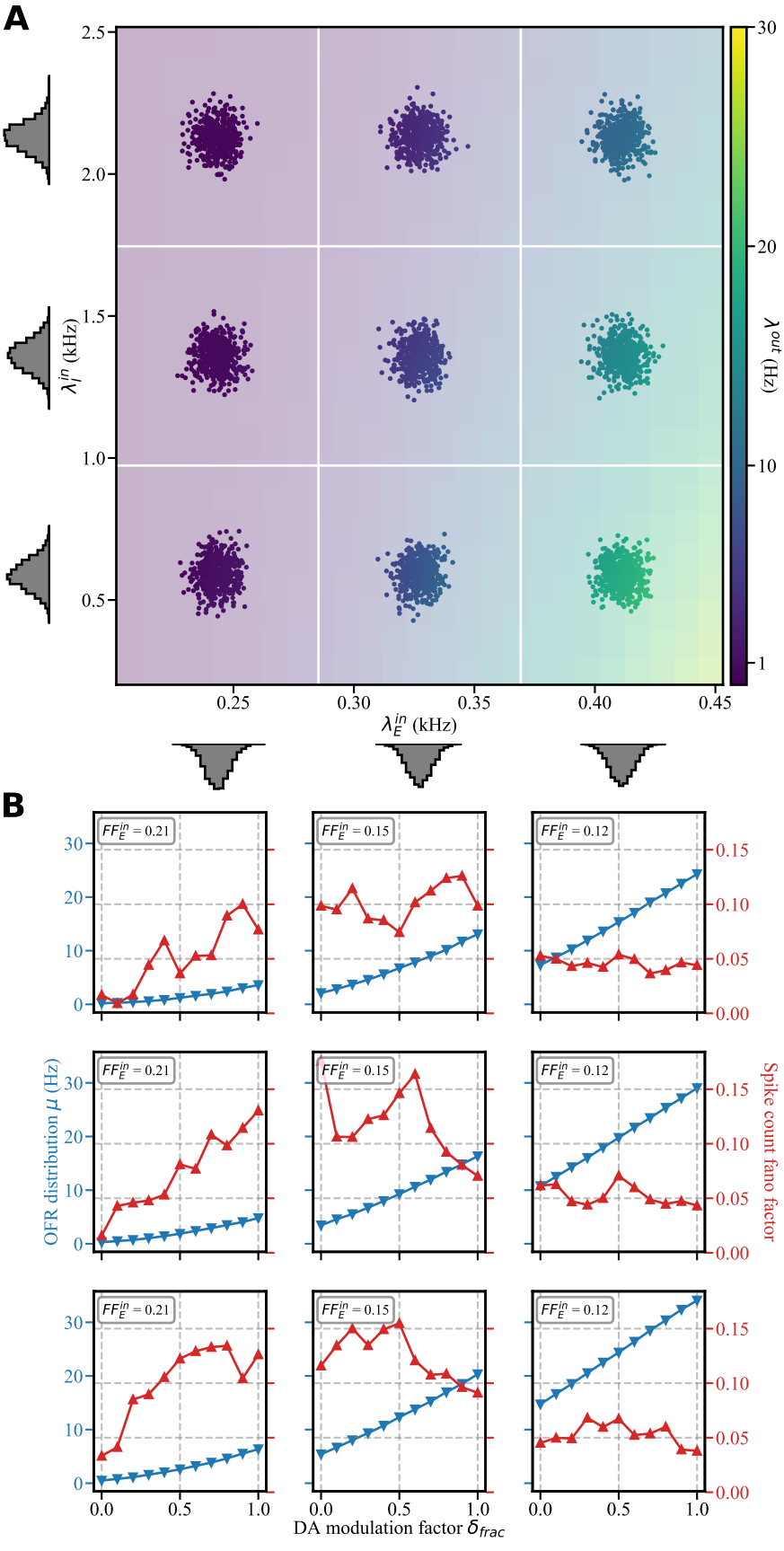

Fig 3.2. ***(preceding page).*** **Response variability depends on amount of synaptic input and DA level.** ***A*** Sampling the output firing rate from nine discreet regions of the 2D transfer function. For each region, 5000 random pairs of λ_E^{in} and λ_I^{in} are drawn from uncorrelated Gaussian distributions and their corresponding output firing rates calculated by spline interpolation from the underlying OFR datasets. The same pairs are then used to calculate OFRs over every DA level. The result is a set of distributions of output firing rates across different levels of DA modulation for each of the sampled regions. The 2D transfer function shown in the panel is for the baseline DA level ($\delta_{frac} = 0.2$), and only every 10^{th} datapoint has been rendered for the sampled OFR distributions. ***B*** Means of sampled OFR distributions (blue lines) grow steadily with heightened concentrations of dopamine. However, distribution Fano factors (red lines) over different DA levels exhibits complex behavior. For low λ_E^{in} (left column) FF is growing, indicating larger than expected response variability. For high λ_E^{in} (right column) FF is more stable, indicating regularized model output. Middle levels of λ_E^{in} are a transition region where FF starts decreasing. For every region, Fano factor of excitatory input distribution is given. The subpanels correspond to the regions sampled in *A*. The grid is aligned to the Fano factor data.

3.3.3 Compound effects of input correlations and DA modulation on trial-by-trial variability

There is significant experimental evidence that neuronal population activity throughout the nervous system is partly correlated. The issue of input correlations is of particular interest to the striatum and its medium spiny neurons, as it was shown that the striatum exhibits active decorrelation properties (Damodaran et al., 2015, Mizrahi-Kliger et al., 2018, Moran et al., 2012, Wilson, 2013). Therefore, we explored how correlated inputs are affecting trial-by-trial variability of a single dMSN under different concentrations of dopamine.

To minimize the contribution of 2D transfer function non-linearities on the range of available output firing rates, we sampled our OFR distributions from a region aligned to an output firing rate contour. We constructed input distributions with different degrees of correlations (see Methods) centered on the 10 Hz OFR contour (Figure 3.3*A*). For a constant level of dopamine, we observed that the dispersion of OFR distributions diminished as the degree of input correlations grew (Figure 3.3*B*). This outcome was not unexpected given the nature of our setup, as very correlated input would result in an OFR distribution that closely follows the OFR contour, which in turn denotes the region of 2D transfer function where the output firing rate was kept constant. Conversely, as the degree of input correlations decreased so had the trial-by-trial variability of dMSN increased, since the range of output firing rates available to the neuron extended past the base contour level. This result persisted across all DA modulation levels, with the higher DA concentrations producing faster decrease of variability (Figure 3.3*B*).

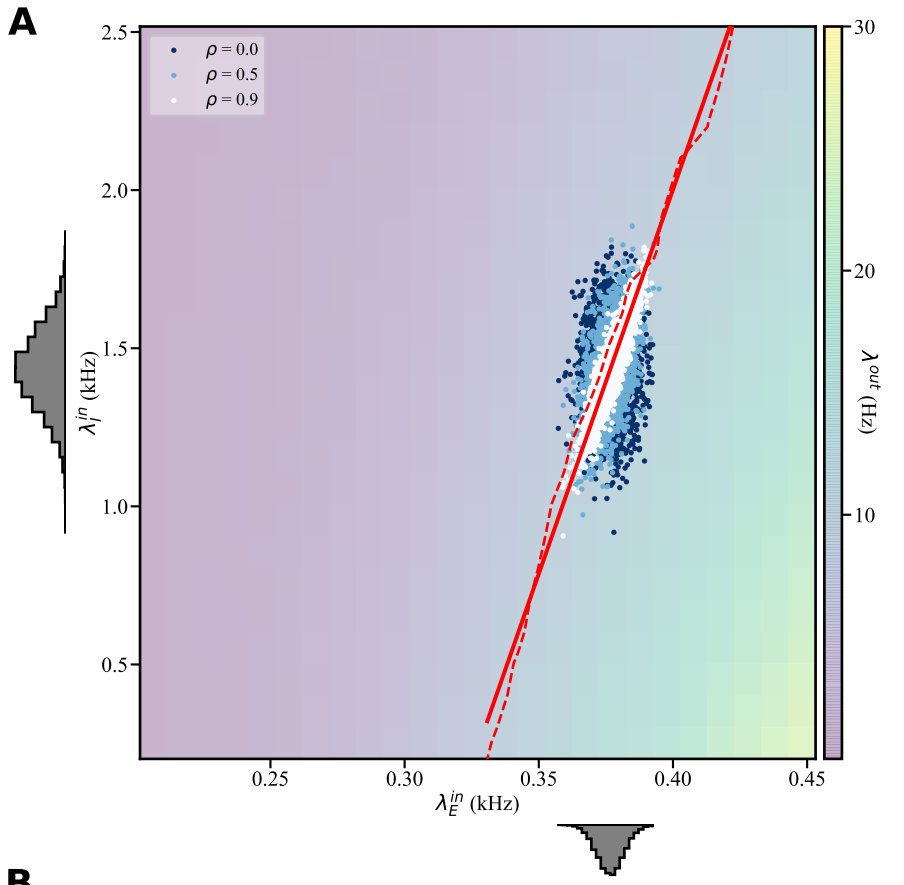
A
ρ = 0.0
ρ = 0.5
ρ = 0.9
2.5
2.0
1.5
1.0
0.5
λ_I^{in} (kHz)
0.25
0.30
0.35
0.40
0.45
λ_E^{in} (kHz)
30
20
10
λ^{out} (Hz)

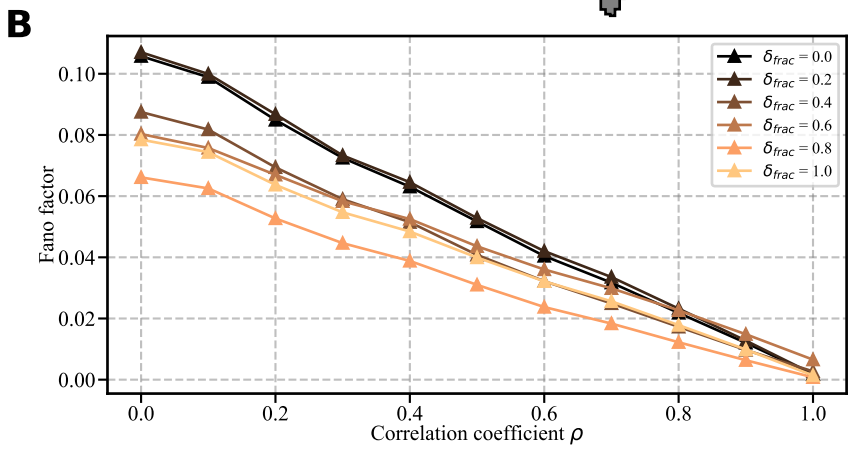
B
δ_{frac} = 0.0
δ_{frac} = 0.2
δ_{frac} = 0.4
δ_{frac} = 0.6
δ_{frac} = 0.8
δ_{frac} = 1.0
Fano factor
0.10
0.08
0.06
0.04
0.02
0.00
0.0
0.2
0.4
0.6
0.8
1.0
Correlation coefficient ρ

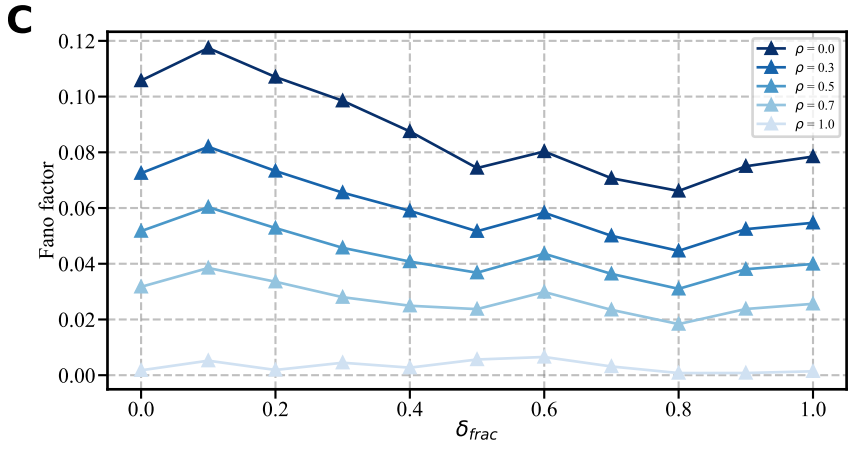
C
ρ = 0.0
ρ = 0.3
ρ = 0.5
ρ = 0.7
ρ = 1.0
Fano factor
0.12
0.10
0.08
0.06
0.04
0.02
0.00
0.0
0.2
0.4
0.6
0.8
1.0
δ_{frac}

Fig 3.3. ***(preceding page).*** **Increase in input correlations is followed by a decrease in trial variability.** ***A*** OFR distributions for three different degrees of input correlations. Marginal distributions are shown for the case of uncorrelated ($\rho = 0.0$) input. The dashed red line is the 10 Hz OFR contour, and the full red line is its linear fit. The 2D transfer function shown in the panel is for the baseline DA level ($\delta_{frac} = 0.2$), and only every 2^{nd} datapoint has been rendered for the sampled OFR distributions. ***B*** Fano factor of OFR distributions decreases linearly with increase in correlations between E and I inputs for a fixed dopamine level. This decrease is faster for lower levels of dopaminergic modulation. ***C*** For fixed degrees of input correlations, OFR distribution FF decreases with an increase in dopamine. However, this effect is greatly diminished for high degrees of correlation.

The evolution of OFR distributions' Fano factors over dopamine concentrations for a fixed degree of input correlations exhibited a general downward trend (Figure 3.3C), indicating that increases in DA levels will have an opposite effect on the neuron's variability. However, this trend was significantly diminished for higher degrees of input correlations. We interpreted this once more as a consequence of the increased alignment of the OFR distribution with the base OFR contour.

Taken together, these results suggest that a change in correlation coefficient between the excitatory and inhibitory synaptic inputs directly affects dMSN's trial-by-trial variability. The neuron will have a more reliable output the higher the degree of correlation between E and I inputs. Moreover, elevated concentration of dopamine in the system will also decrease the output variability, thus limiting the range of output firing rates available to the neuron. An exception to this rule is if the synaptic input to a dMSN is balanced in such a way as to insure the maintenance of a consistent output firing rate, i.e. if it is centered on an OFR contour, and the degree of correlation between excitation and inhibition is very high. In that instance, changes in DA levels will not have an impact on the trial-by-trial variability of dMSN, and the neuron itself will have a very narrow OFR range, ensuring extremely reliable output.

3.3.4 Interplay between E-I balance and DA modulation on trial-by-trial variability

Another source of increased variability in neural outputs is a change in the E-I balance (Nawrot et al., 2008). Here we consider the case of balance in the context of the variability of input rates, while assuming that the timing of input spikes is consistently independent and Poisson distributed.

We start from a baseline OFR distribution that has been aligned to the 10 Hz OFR contour ($\rho = 0.2$, $c_b = 1.0$), and manipulate the E-I balance by modifying the standard deviation of one of the input rate distributions in proportion to the other (Figure 3.4A).

Both in the case of balance change with respect to the excitatory input (c_b^E, Equation 3.3) and with respect to the inhibitory input (c_b^I, Equation 3.4), OFR distribution FFs were increasing together with the E-I balance coefficient c_b (Figure 3.4*B*). Unlike in the previous exploration of the effects of input correlations on the Fano factor, this effect was supra-linear. Additionally, the growth of OFR distribution variance with c_b was faster for the lower DA concentration.

When the E-I balance was fixed (both for c_b^E and c_b^I), comparing the lowest DA modulation levels with the highest revealed a general decline of the Fano factor. That is to say, as the DA levels increased the trial-by-trial variability was decreasing. However, the effect was not monotonic and for low δ_{frac} values was even reversed. This is presumably caused by the non-linear changes in the underlying 2D transfer function when exposed to dopaminergic modulation. Similar to before, the relationship between DA level and Fano factor was negligible for low values of the balance coefficient.

It is of note that both for fixed DA modulation and fixed E-I balance, there was no qualitative difference between the c_b^E and c_b^I cases (Figure 3.4*B*, *left* versus *right*). Any quantitative difference came from disparate values of standard deviations of synaptic input distributions (data not shown).

While excitatory and inhibitory input distributions might not align to an OFR contour in all situations, our example serves to present a concise argument for the importance of E-I balance on the neuronal trial-by-trial variability. Whether through adaptation brought on by synaptic plasticity, reduced membrane integration time due to increased synaptic input, or some other mechanism (Hennequin et al., 2017, Shadlen and Newsome, 1998), alterations of the E-I balance will affect the range of the output firing rates available to a dMSN across different trials. Furthermore, as in the case of input correlations, dopamine proved to have a crucial role in adjusting the trial-by-trial variability, with increased DA levels lowering the dispersion of dMSN OFR distributions.

Fig 3.4. ***(following page).*** **Changes in E-I balance have a direct impact on trial variability.** ***A*** OFR distributions for three different cases of E-I balance, with $\rho = 0.2$. The balance of the distribution in dark blue has been adjusted while keeping σ_E^{in} fixed (see Methods). Conversely, to generate the light blue distribution σ_I^{in} has been kept fixed. Marginal input distributions are shown for the standard balance ($c_b = 1.0$). The dashed red line is the 10 Hz OFR contour, and the full red line is its linear fit. The 2D transfer function shown in the panel is for the baseline DA level ($\delta_{frac} = 0.2$), and only every 2^{nd} datapoint has been rendered for the sampled OFR distributions. ***B*** Fano factor of OFR distributions grows with the E-I balance coefficient c_b for a fixed dopamine level. The growth is faster for lower levels of dopaminergic modulation. There is no qualitative difference between the balance with respect to excitatory input (i.e. for fixed σ_E^{in}, *left*), and the balance with respect to inhibitory input (i.e. for fixed σ_I^{in}, *right*). ***C*** For fixed degrees of E-I balance coefficient, OFR distribution FF drops with the rise of dopamine. However, the relationship is not monotonic, and for low δ_{frac} values it is even reversed. Additionally, this effect is greatly diminished for values of c_b close to the original balance.

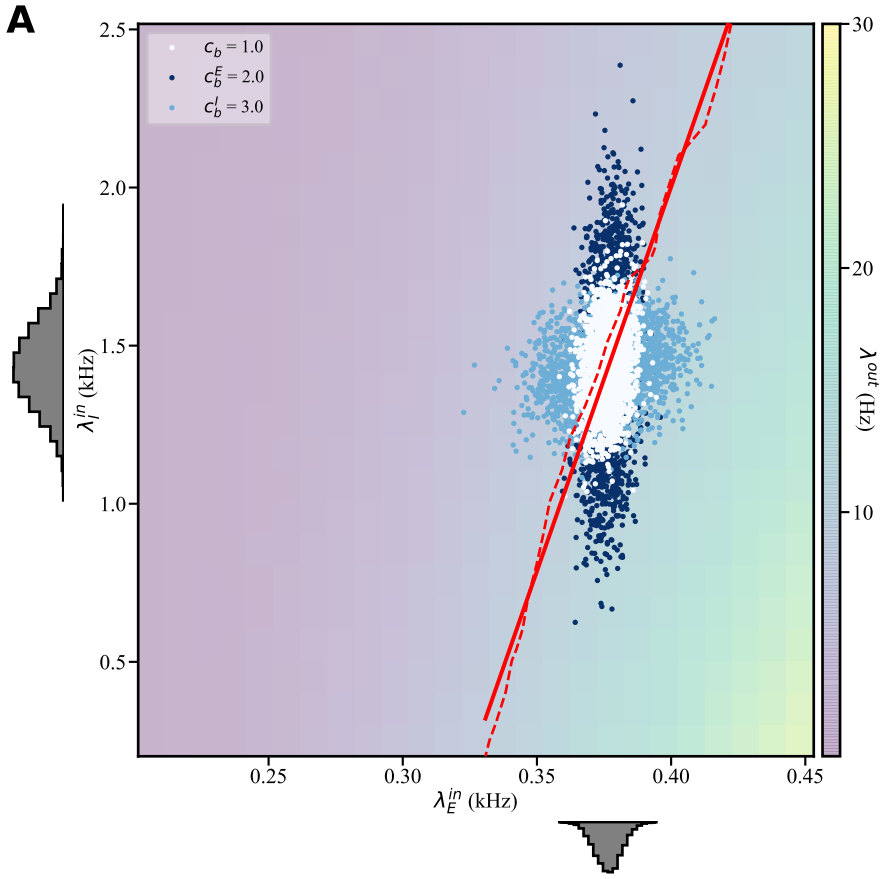
A
$c_b = 1.0$
$c_b^E = 2.0$
$c_b^I = 3.0$
λ_I^{in} (kHz)
λ_E^{in} (kHz)
λ^{out} (Hz)

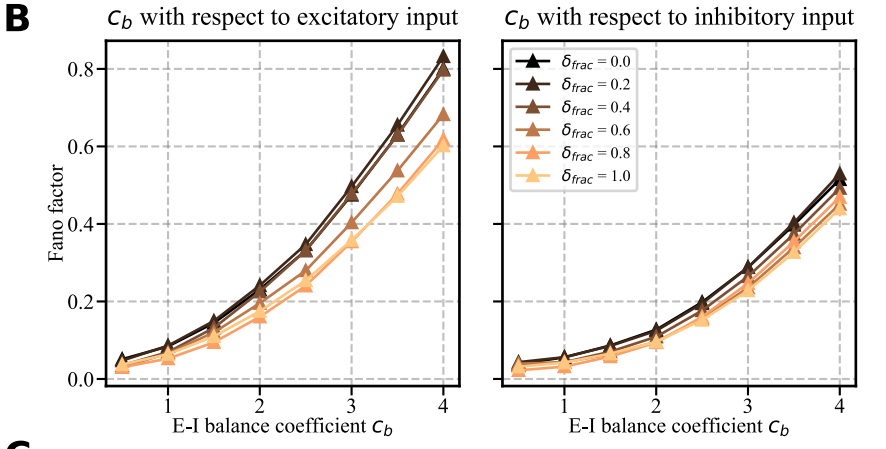
B
c_b with respect to excitatory input
c_b with respect to inhibitory input
$\delta_{frac} = 0.0$
$\delta_{frac} = 0.2$
$\delta_{frac} = 0.4$
$\delta_{frac} = 0.6$
$\delta_{frac} = 0.8$
$\delta_{frac} = 1.0$
Fano factor
E-I balance coefficient c_b

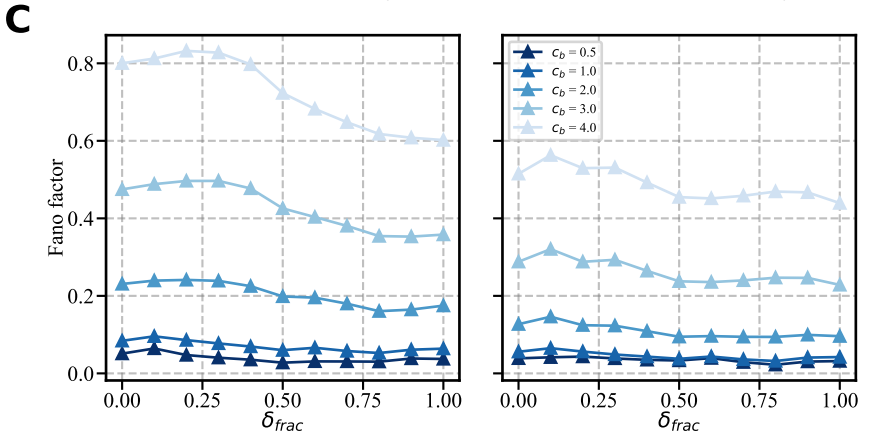
C
$c_b = 0.5$
$c_b = 1.0$
$c_b = 2.0$
$c_b = 3.0$
$c_b = 4.0$
Fano factor
δ_{frac}

3.3.5 Dopamine effect on intra-trial variability depends on the amount of synaptic input

Together with the general DA-driven decrease of trial-by-trial variability in dMSN's output firing rates, we observed that elevated concentrations of dopamine could also have a regularizing effect on spike times for high λ_E^{in} levels. In other words, dopamine could act as a stabilizer of both output firing rate variability, as well as of output spike time ("intra-trial") variability for high levels of excitatory synaptic input. Figure 3.5*A* gives examples of the average coefficient of variation (CV) for dMSN inter-spike intervals (ISIs) in the synaptic input parameter space for three different DA levels. It was evident that for high synaptic input rates an increase in DA modulation led to a decrease in spike timing variability.

Interestingly, overlaying OFR contours onto the ISI CV space revealed that each contour transversed multiple CV values (Figure 3.5*B*). This meant that it was possible to vary excitatory and inhibitory synaptic inputs at a fixed DA level in such a way that the neuron maintained a single output firing rate and at the same time had different values of ISI CV. This effect was more prominent for low-range OFR contours at high levels of DA (Figure 3.5*B left*).

Proceeding to investigate the impact of DA modulation on the ISI CV values lying along an OFR contour, we observed that spike time variability of low-firing rate contours was not uniformly distributed over different dopamine levels. This was illustrated by a small but present increase in mean ISI CV values lying along the 5 Hz OFR contour as the concentration of DA rose (0.67±0.02 at $\delta_{frac} = 0.2$, 0.75±0.04 at $\delta_{frac} = 1.0$, all values given as mean±SD). However, the effect was not evident for mid- (10 Hz, 0.72±0.02 at $\delta_{frac} = 0.2$, 0.74±0.03 at $\delta_{frac} = 1.0$) and high-output firing rate contours (20 Hz, 0.64±0.02 at $\delta_{frac} = 0.2$, 0.66±0.02 at $\delta_{frac} = 1.0$). Please note that due to small number of available data points for 20 Hz OFR contour at $\delta_{frac} = 0.0$, we chose the baseline DA level ($\delta_{frac} = 0.2$) as the starting point for comparison.

Taken together, this result was reminiscent of the effect that dopamine had on Fano factor of OFR distributions (Figure 3.2), and was consistent with the theoretical approach of describing single neuron variability via point process theory (Nawrot et al., 2008).

3.4 Discussion

In this work we explored the effects of dopaminergic modulation on trial-by-trial variability of a dMSN for two conditions: in the presence of correlations of synaptic input

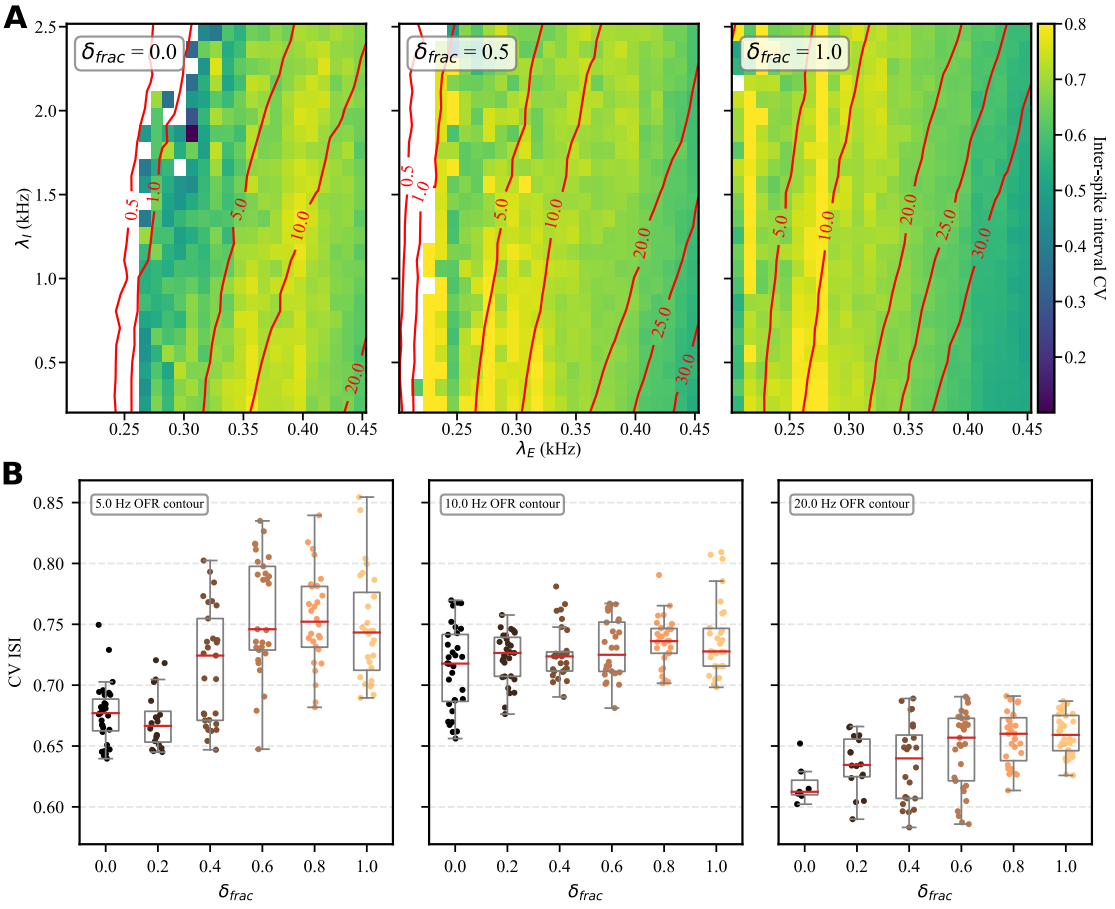

Fig 3.5. Dopaminergic modulation of spike time variability. ***A*** Average CV of inter-spike intervals over multiple trials for three different levels of dopamine. As DA concentration increases, dMSN spike times become more regular for regions with high synaptic input levels. Red curves represent output firing rate contours. The trials where there were less than 5 spikes were discarded from the calculations of the average ISI CV. ***B*** Box-and-whisker plot of ISI CV for each DA level, for three chosen OFR contours. Red lines represents medians of the data. Contours shift position on the 2D transfer function due to DA-driven changes in dMSN excitability, which impacts the ISI CV values they are associated with. For 5 Hz output firing rate DA increases intra-trial variability of dMSNs, reminiscent of the rise of Fano factor for low λ_E^{in} values. The trends for 10 Hz and 20 Hz OFR contours are, however, inconclusive. There is a perceptible drop in average intra-trial variability between 5 Hz OFR, elicited by low- to mid-range λ_E^{in}, and 20 Hz, elicited by high-range λ_E^{in}.

rates, and for the changes in the balance of input excitation and inhibition.

We show that an increase in input correlations ρ reduced the response variability for a fixed DA level, and that this reduction was more prominent for higher DA levels. At the same time, DA modulation by itself also acted to decrease variability when ρ remained unchanged, as long as correlations were relatively weak. Higher degrees of correlations however were mostly insensitive to changes in DA concentration.

The shifts in the E-I balance as well lead to a change in trial-by-trial variability, although the sign of the change depended on the initial combination of synaptic inputs and the final value of balance coefficient c_b. In our examples we demonstrated consistent increases

in spike count variability for a fixed DA level as the balance shifted away from an OFR contour, with lower DA modulation level leading to a higher rate of variability change. Larger degree of contour disalignment allowed DA to have a more prominent impact on the variability, while staying aligned to a contour provided stability necessary to maintain a low range of output firing rates regardless of the DA level.

Given these results we conclude that dopamine is, in general, a significant diminisher of trial-by-trial variability, but that its efficacy in this respect is also dependent on the properties of synaptic input. However, we should not disregard that our chosen output firing rate contour (10 Hz) positioned all the examined OFR distributions in the region of 2D transfer function where we demonstrated dopamine to have either a negative or minor effect on response variability. The extreme steepness of OFR contour slopes for very low firing rates precluded a meaningful analysis in that region of 2D transfer function. That being said, we also found that input rate correlations and changes in E-I balance had by themselves a significant impact on the response variability, and should not be disregarded in future studies related to this subject.

It should be noted that, in the E-I balance paradigm that we examined, changes in a distribution Fano factor were particularly pronounced due to the initial alignment of our sampled OFR distribution to an OFR contour. If a distribution is aligned to a contour, the range of output firing rates it covers will be the smallest possible for a given DA modulation level. Thus, any disalignment with respect to the contour will also result in the rise of the available output firing rates and in the increase in the distribution FF. Nevertheless, our conclusions are general enough to also apply to situations where excitatory and inhibitory synaptic inputs are not aligned to an OFR contour.

A similar line of reasoning can be applied to the case of correlated synaptic input, where very high degrees of correlation between E and I input rates resulted in an OFR distribution constricted to a narrow region around the OFR contour in 2D transfer space, thus severely limiting the range of the model's output activity. However, this shrinking effect due to heightened correlations is present whether an OFR distribution is centered on a contour or not (data not shown).

Another limitation of this study pertains to our implementation of dopaminergic modulation only for the steady-state condition. However, in biological systems phasic dopamine release happens on relative short time scales and has a prominent role in mechanisms such as reinforcement learning and motor control (Howe and Dombeck, 2016, Roitman, 2004, Hamid et al., 2015, Schultz et al., 1997, Schultz, 2007). Thus, an interesting avenue for future investigation would be the time-evolution of dMSN response variability during DA transients.

Finally, we have studied trial-by-trial variability only for direct-pathway MSNs. Canonically, DA has an opposing effect on indirect-pathway MSN (iMSNs) excitability (Planert et al., 2013), and it would be therefore of great interest to investigate whether DA would also have an opposing effect on iMSN trial-by-trial variability.

Experimental verification of our hypothesis presents several problems for future researchers. In an ideal setup, an experimentalist would have a complete control over synaptic input to an MSN, while simultaneously measuring its membrane voltage potential *in vivo*. Recording a single striatal MSN even in behaving animals is something that is possible with today's methods (Sippy et al., 2015), but control over synaptic inputs is not easily achievable. Nevertheless, recent advances in methods such as retrograde labeling and optogenetics may provide an opportunity. For example, using a rabies virus to label all the inputs to a target neural population, and then expressing channelrhodopsin discriminately to labeled excitatory and inhibitory input populations to obtain control over their activity (Osakada et al., 2011).

Here we explored the potential sources of trial-by-trial variability, but a question remains: what is its purpose? It is logical to assume that stability in neural responses is highly desirable for high-fidelity information transfer, and that response variability itself is just noise in the system. Yet, multiple studies reported that variability in the execution of movements and in the motor system in general is closely tied to purposeful exploration of the motor space, and that when coupled with reinforcement it can drive motor learning (for a review see Dhawale et al. 2017). Initial exploratory phase during reinforcement learning implies high variability of movement, but as the learning proceeds this variability decreases until finally the motor system converges on one or more particular actions associated with the highest reward. Variability reduction then is thought to be caused by the strengthening of some synaptic inputs and the pruning of others (Garst-Orozco et al., 2014, Fu et al., 2012, Wang et al., 2011, Xu et al., 2009). Possible consequences of such synaptic reorganization may be precisely the two mechanisms that we demonstrate in this study. Namely, a change in the E-I balance which would produce an alignment in the transfer space to an OFR contour, or an increase in input correlations which would limit the range of output firing rates available to a neuron. The outcome of both of these effects is regularization of a neuron's output firing rate over repeated trials. The benefit of an increase in input rate correlations would additionally be heightened insensitivity to fluctuations of DA concentrations in the system, which might then act as a synaptic "stabilizer" and reduce the occurrences of LTP induction on dMSN synapses (Shen et al., 2008).

Chapter 4

Subthalamic nucleus-globus pallidus externa network model captures beta-band phase heterogeneity as recorded in Parkinson's disease patients

Marko Filipović[1,2], Jyotika Bahuguna[3], Arvind Kumar[1,2]

[1] Dept. of Computational Science and Technology, School of Computer Science and Communication, KTH Royal Institute of Technology, Stockholm, Sweden
[2] Bernstein Center Freiburg and Faculty of Biology, University of Freiburg, Germany
[3] Aix-Marseille University, Institute for Systems Neuroscience, Marseille, France

4.1 Introduction

Amplified beta-band oscillations in cortico-basal ganglia system are a staple of Parkinson's disease (PD; Brown 2007, Hammond et al. 2007, Levy et al. 2002). Increased beta-band activity in PD has been associated with resting state tremor and general issues with movement initiation and execution (Cagnan et al., 2014, Tass et al., 2010). This aberrant synchronization and the associated symptoms can be treated to some extent through dopaminergic therapy (Kühn et al., 2006, Ray et al., 2008).

While the striatum has been implicated in the origin of pathological beta-band oscillations (Kondabolu et al., 2016, Corbit et al., 2016), there is strong experimental (Bevan, 2002, Tachibana et al., 2011) and computational (Kumar et al., 2011, Mirzaei et al., 2017, Pavlides et al., 2015) evidence that the interaction between the subthalamic nucleus (STN) and the globus pallidus pars externa (GPe) plays a key role in their generation. STN and GPe share dense recurrent connections (Shink et al., 1996), with STN sending excitatory projections to GPe which in turn inhibits STN. It is known that such an excitatory-inhibitory network can both generate and sustain persistent oscillatory activity (Brunel, 2000).

In accordance with this hypothesis, the current state-of-the-art model of the STN-GPe network successfully replicates both persistent and transient beta-band oscillations through manipulation of the parameters of the two nuclei alone (Kumar et al., 2011, Mirzaei et al., 2017). It demonstrates that pathological beta-band activity can be induced in several ways: by modifying the strength of synaptic coupling between STN and GPe (Magill et al., 2001), by introducing additional pallidal inhibition from the striatum (due to hyperactivity of indirect pathway medium spiny neurons; Liang et al. 2008, Mallet et al. 2008), or by introducing additional subthalamic excitation from the cortex (Tachibana et al., 2011).

However, the STN-GPe model fails to capture the heterogeneity of the phase alignment of STN and GPe beta-band activities off and on dopaminergic therapy, as recorded in human PD patients (Cagnan et al., 2015). Since both propagation and cessation of beta oscillations have been linked with such phenomena as phase locking and phase slips (Cagnan et al., 2015, Holt et al., 2019, Hurtado et al., 2005), it is of some importance to enable the STN-GPe model to successfully replicate this aspect of the network dynamics.

In this work, we investigate an extension of the STN-GPe model in order to account for the beta-band phase alignment of the two nuclei as recorded in human PD patients. We perform simulations for healthy (control) and pathological (stimulated) conditions, focusing primarily on two parameters: the percentage of STN and GPe neurons that were stimulated, and the synaptic transmission delays between and within the two neuronal populations. By stimulating only a fraction of one of the populations, we observe an increase in STN-GPe phase difference heterogeneity, and find that it is further augmented for shorter synaptic delays. Overall, our results point to the conclusion that a simple adjustment of the model may be enough to explain the discrepancy between the computational approach and the experimental measurements of the phase of beta-band activity.

4.2 Methods

4.2.1 Neuron and network models

Both the neuron model and the basic network have been adapted from Mirzaei et al. (2017) (Table 4.1, Figure 4.1*A*). Individual STN and GPe cells have been modeled as leaky integrate-and-fire neurons with conductance-based synapses where synaptic inputs produced conductance changes described with an alpha function. Initial membrane voltages and spiking thresholds were randomized to introduce greater heterogeneity in model behavior. Total STN neural population consisted of 1000 units, whereas GPe population consisted of 2000 neurons. All neurons received constant uncorrelated Poisson-distributed background excitatory input in order to bring the average population baseline activities close to those previously reported (Bergman et al., 1994, Raz et al., 2000). Synaptic weights for this background input have been randomly drawn from a uniform distribution.

Connections between all neurons were established randomly while keeping their outdegrees fixed. STN-to-STN connections were absent (Sato et al., 2000b, Mirzaei et al., 2017). The base synaptic delays were higher between neural populations than for recurrent connections (Mirzaei et al., 2017).

4.2.2 Simulation design

We explored the dynamics of network beta-band activity for two different conditions: control, i.e. non-stimulated, and stimulated. In non-stimulated condition the network activity was the result of background input only. For stimulated condition we introduced two additional sources of uncorrelated, constant, and Poisson-distributed input: an excitatory one that targeted STN neurons, representing cortical afferents, and an inhibitory one targeting GPe neurons, representing striatal connections. The purpose of this additional input was to simulate an increase in beta-band activity, as can be seen e.g. during Parkinson's disease (Degos et al., 2008, Holgado et al., 2010, Kumar et al., 2011, Mallet et al., 2008, Sato et al., 2000a, Tachibana et al., 2011). Simulations ran for 11 s and over 10 trials. Within each trial, over both conditions and regardless of the input parameters used, random number generator (RNG) seeds were always fixed. However, RNG seeds were different over the different trials.

For the stimulated condition, stimulus rate was fixed at 500 Hz, irrespective of the sign of stimulation or targeted population. Synaptic weights for this additional input were randomly drawn from a uniform distribution between 0.5 nS and 1.5 nS for excitatory

Table 4.1. Neuron and network model parameters.

Parameter	**Value**	**Description**
	Neuron parameters	
V_{th} (mV)	-54	Spiking threshold
V_{reset} (mV)	-70	Reset voltage
t_{ref} (ms)	5	Refractory time
g_L (nS)	10	Leak conductance
C_m (pF)	200	Membrane capacitance
E_{ex} (mV)	0	Excitatory reversal potential
E_{in} (mV)	-80	Inhibitory reversal potential
τ_{ex}^{syn} (ms)	5	Exc. synaptic time constant
τ_{inh}^{syn} (ms)	10	Inh. synaptic time constant
	Network parameters	
N_{STN}	1000	Number of STN neurons
N_{GPe}	2000	Number of GPe neurons
$\delta^{STN\to GPe}$	0.023	STN-to-GPe outdegree
$\delta^{GPe\to STN}$	0.035	GPe-to-STN outdegree
$\delta^{GPe\to GPe}$	0.02	GPe-to-GPe outdegree
$J^{STN\to GPe}$ (nS)	1.2	STN-to-GPe syn. weight
$J^{GPe\to STN}$ (nS)	-0.8	GPe-to-STN syn. weight
$J^{GPe\to GPe}$ (nS)	-0.725	GPe-to-GPe syn. weight
$t_{\Delta}^{STN\to GPe}$ (ms)	6.0	STN-to-GPe syn. delay
$t_{\Delta}^{GPe\to STN}$ (ms)	6.0	GPe-to-STN syn. delay
$t_{\Delta}^{GPe\to GPe}$ (ms)	3.0	GPe-to-GPe syn. delay
λ_{bgr}^{STN} (kHz)	1.5	STN background input
λ_{bgr}^{GPe} (kHz)	1.0	GPe background input

input to STN, and -1.5 nS and -0.5 nS for inhibitory input to GPe. In different simulation setups, we varied independently the percentage of STN and GPe populations that were stimulated, for the following values: 0 %, 25 %, 50 %, 75 %, and 100 %. This produced 25 stimulation combinations, from those where only a single population was receiving varying degrees of additional inputs, to the final one where all of the neurons in both populations were stimulated at the same time (Figure 4.1*B*). We have disregarded

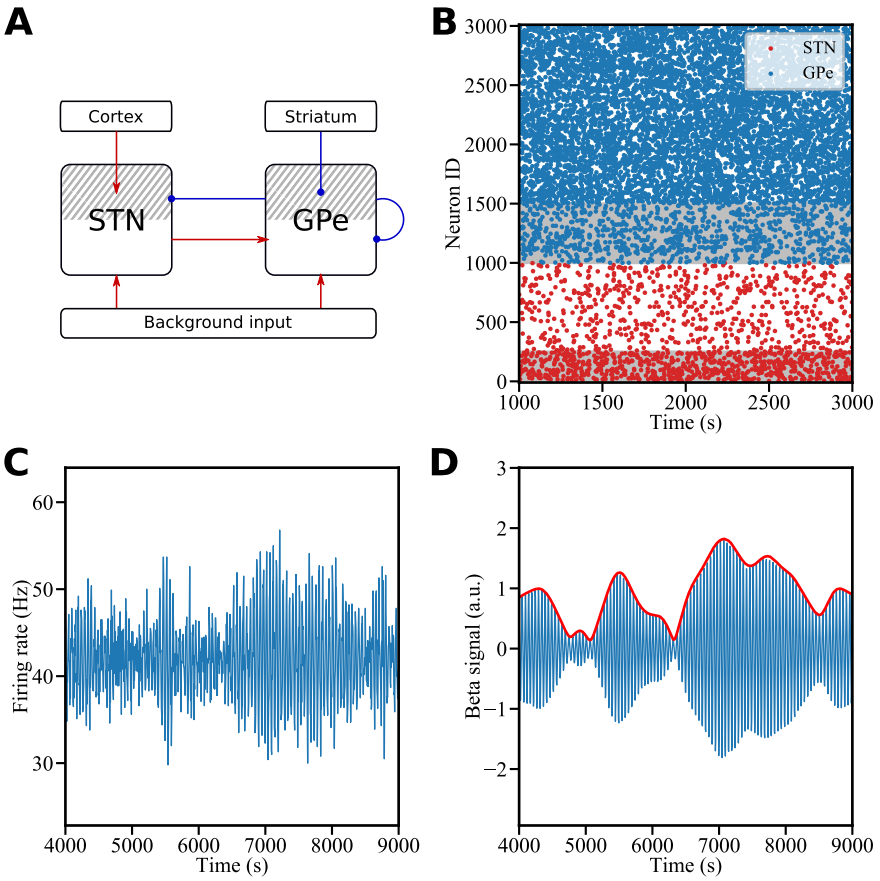

Fig 4.1. STN-GPe network setup and beta signal extraction. ***A*** A schematic of the network architecture. STN neurons send excitatory connections to GPe, and in turn receives inhibitory ones. Recurrent connections are present in GPe but not STN. Both neural populations receive excitatory background input to bring their activities to baseline levels. Depending on the stimulation setup, a percentage of either (or both) of STN and GPe populations may be targeted by additional excitatory (from cortex) or inhibitory (from the striatum) inputs, respectively (patterned grey areas). ***B*** raster plot of 2 s of network activity. Areas shaded grey have received additional stimulation in order to induce increased beta activity. In this case, 25 % of both STN and GPe populations have been stimulated. Every 20^{th} spike has been rendered. ***C*** 5 s of a PSTH trace belonging to non-stimulated GPe subpopulation from *B*. ***D*** Extraction of the beta signal from the PSTH in *C*. The beta signal was obtained by band-pass filtering the PSTH ±1.5 Hz around the peak beta power of the network in stimulated condition. The envelope of the beta signal (red) and the instantaneous phase are obtained by Hilbert transform.

the case where neither of STN or GPe nuclei were stimulated (i.e. where 0 % of each population was stimulated), as this was equivalent to the control condition.

We also varied synaptic delays by introducing "delay scale" factor, which scaled the base delay values up or down by a certain fraction (Table 4.2).

We then performed a parameter search over these two parameter sets: the fraction of STN or GPe populations that were stimulated, and the delay scale factor.

Table 4.2. Values for the scaled synaptic delays in the STN-GPe network. The base values are marked in grey.

Delay scale	**STN⟷GPe (ms)**	**GPe→GPe (ms)**
0.25	1.5	0.75
0.50	3.0	1.5
0.75	4.5	2.25
1.00	6.0	3.0
1.25	7.5	3.75
1.50	9.0	4.5

4.2.3 Beta-band analysis

Envelope and phase extraction Upon the conclusion of simulations, we sampled the activity of 200 randomly chosen neurons from each of the populations, once for every trial. The activity sampled in this way was used to construct a post-stimulus time histograms (PSTH) for STN and GPe. The first 400 ms were removed from the start of each PSTH in order to account for the network transition period. To extract the beta signal, we band-pass filtered PSTHs ±1.5 Hz around the reference peak power in the beta region (12-35 Hz) using zero-phase third order Butterworth filter. The reference peak beta power was defined as the highest power in the beta region of a stimulated population, and that value was applied in the analysis of both conditions in a "control-stimulated" simulation pair. Finally, we employed Hilbert transform in order to estimate instantaneous envelopes and phases of the band-pass filtered beta signals (Figure 4.1, *C* and *D*).

Envelope-phase dependency We performed the analysis of the difference between STN and GPe beta-band instantaneous phases as described in Cagnan et al. (2015). Briefly, the STN-GPe phase difference (further on, just "phase difference") was calculated for sampled STN and GPe neurons in each condition separately, wrapped to the interval $[-\pi, \pi)$, and then binned into 20 bins. The final phase difference profiles for each condition were obtained by averaging over all trials, and normalized to obtain their probability mass functions.

Information entropy We quantified phase heterogeneity in each normalized profile by calculating their information (Shannon) entropies:

$$S = -\sum_i P_i \log_e(P_i) \tag{4.1}$$

where P_i is the probability mass for each of the 20 bins i, and S is entropy measured in nats ("natural units").

Relative error We compared the STN-GPe phase difference profiles from our simulations to those obtained from human patient recordings, reproduced from Cagnan et al. (2015) by WebPlotDigitizer (`https://automeris.io/WebPlotDigitizer/`). To this purpose, we devised a measure of similarity based on scaled residual sum of squares (RSS) which we named "relative error" (RE):

$$RSS = \sum_{i=1}^{n} (y_i - x_i)^2$$
$$RE = \frac{RSS}{n \sum_{i=1}^{n} |y_i|} \tag{4.2}$$

where y_i and x_i are probability masses of the i^{th} bin of the phase difference profiles for human patient data and simulation data, respectively, and $n = 20$ is the number of bins in each profile. The final RE value was obtained as an average of RE of the control condition and RE of the stimulated condition.

All network simulations were written in Python, using PyNN and NEST simulator (version 2.14, Peyser et al. (2017)). Analysis of the simulation results were performed using custom scripts written in Python (version 2.7).

4.3 Results

We explored the dynamics of beta-band activity of an STN-GPe network in two conditions: control, where we recorded the spontaneous network activity (representing non-pathological state), and stimulated, where a portion of neurons in either of STN and GPe populations received additional input to promote heightened levels of beta activity (representing pathological state). Our focus was on investigating factors which would enable the model network to exhibit as rich beta-band phase heterogeneity as is seen in human patients. Namely, Cagnan et al. (2015) have shown in LFP data acquired from PD patients, both OFF and ON dopaminergic medication, that the beta-band phase difference between STN and GPe nuclei is distributed over all the phases between $-\pi$ and π(Figure 4.2*A*). In contrast, while the best current model of the STN-GPe network can replicate many of the characteristic features of both healthy and pathological beta-band activity (Kumar et al., 2011, Mirzaei et al., 2017), its phase difference profile is very narrow. This is illustrated in Figure 4.2*B*, where the same methodology described in Cagnan et al. (2015) was used on sampled PSTH data instead of LFP measurements in order to construct the phase difference profiles. In these simulations, spontaneous

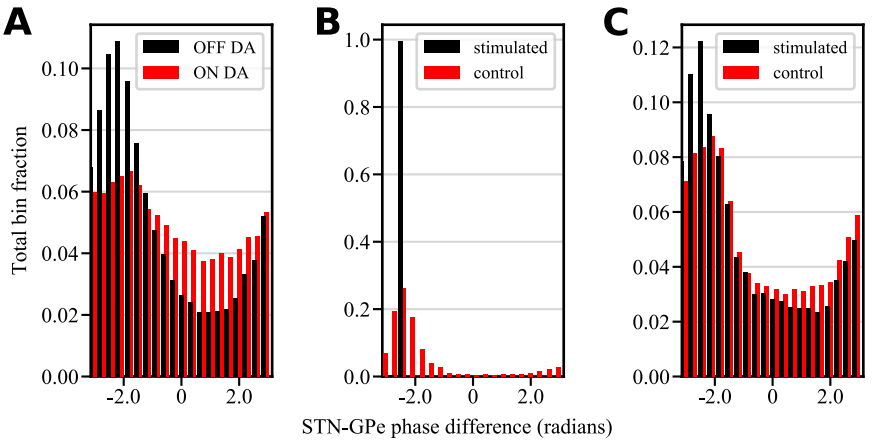

Fig 4.2. Modified STN-GPe network improves correspondence to the PD patient data. ***A*** Distribution of the phase difference between STN and GPe from LFP recordings in human PD patients. Black bars correspond to recordings acquired when the patients were OFF dopaminergic medication, and red bars to those when the patients were receiving L-DOPA treatment. Reproduced from Cagnan et al. (2015). ***B*** STN-GPe phase difference obtained from the established computational model of the STN-GPe network (Kumar et al., 2011, Mirzaei et al., 2017). Entire GPe population has been stimulated. Beta-band phases were derived from PSTHs of sampled populations in both groups of neurons. The "control" condition corresponds to "ON DA" activity in *A*, whereas "stimulated" condition was used to induce pathological beta-band activity analogous to the "OFF dopamine" case. Notice the different scale of the y-axis. ***C*** Phase difference produced from an iteration of the modified STN-GPe network. This particular result was obtained by decreasing the synaptic delays from the original network by half, and by stimulating only 50 % of GPe population.

activity of the network ("control") was analogous to ON DA medication state in human patients, while OFF DA condition was represented through stimulation of the network ("stimulated"), which promoted heightened levels of beta activity. It can be seen that the STN-GPe phase difference, especially in the stimulated condition, is mostly constrained to a very limited range of values.

Through extensive parameter search using the established network model, we have concluded that at least two variables influence phase difference heterogeneity in the STN-GPe circuit: the percentage of population stimulated, and the synaptic delays within and between neuronal populations represented through "delay scales" (see Methods). By examining different combinations of these two variables, we were able to construct phase difference profiles that were qualitatively closer to those as seen in human patients (Figure 4.2*C*). However, we were unable to fully capture the difference between control/ON DA and stimulated/OFF DA profiles.

4.3.1 Higher percentage of population stimulated decreases STN-GPe phase difference heterogeneity

In order to ascertain the impact of the investigated variables on phase difference heterogeneity, we described phase difference profiles through information entropy (Equation 4.1). High entropy values signified rich information content and were associated with wider distributions of phase difference (e.g. Figure 4.2C), whereas low entropy values were characteristic of phase difference that was concentrated in a smaller number of available bins (e.g. Figure 4.2B).

We found that for delay scales below 1.0 (i.e. for synaptic delays that were lower or equal to the base values) there was a perceptible decrease of entropy as the percentage of stimulated neurons in a population grew (Figure 4.3). This effect didn't seem to depend on which of the STN or GPe populations were stimulated. However, it did appear that the entropy was decreasing faster when both nuclei were stimulated at the same time. For delay scales above 1.0 entropy of phase difference profiles was uniformly low regardless of the portion of neural population stimulated, suggesting a significant impact of larger synaptic delays on beta-band activity.

We postulate that the mechanism behind the dependence of entropy on the percentage of population stimulated is as follows: as the number of stimulated neurons grows, it becomes easier to entrain the remaining neural population to the evoked activity and thus to lock the phases of STN and GPe to an increasingly similar pattern. It follows that when the entire population of a nuclei is stimulated, phases of beta-band activity for both STN and GPe become nearly identical and the entropy of their phase difference profiles becomes minimal.

We also observed that for some combinations of input parameters — large delay scales and high percentages of population stimulated — the entropy of the network in control condition grew even though it did not receive any stimulation whatsoever. The most likely reason for this behavior was a change in frequency of peak beta-band power, which was always derived solely from the network in stimulated condition for every "control-stimulated" pair of simulations (see Methods). As the peak beta-band power decreased in frequency, so did the content of the filtered beta signal change, which then affected the results of the phase analysis. However, this effect was mostly constrained to the region of the parameter space that was not biologically relevant, with synaptic delays between STN and GPe nuclei being over 7 ms (Table 4.2).

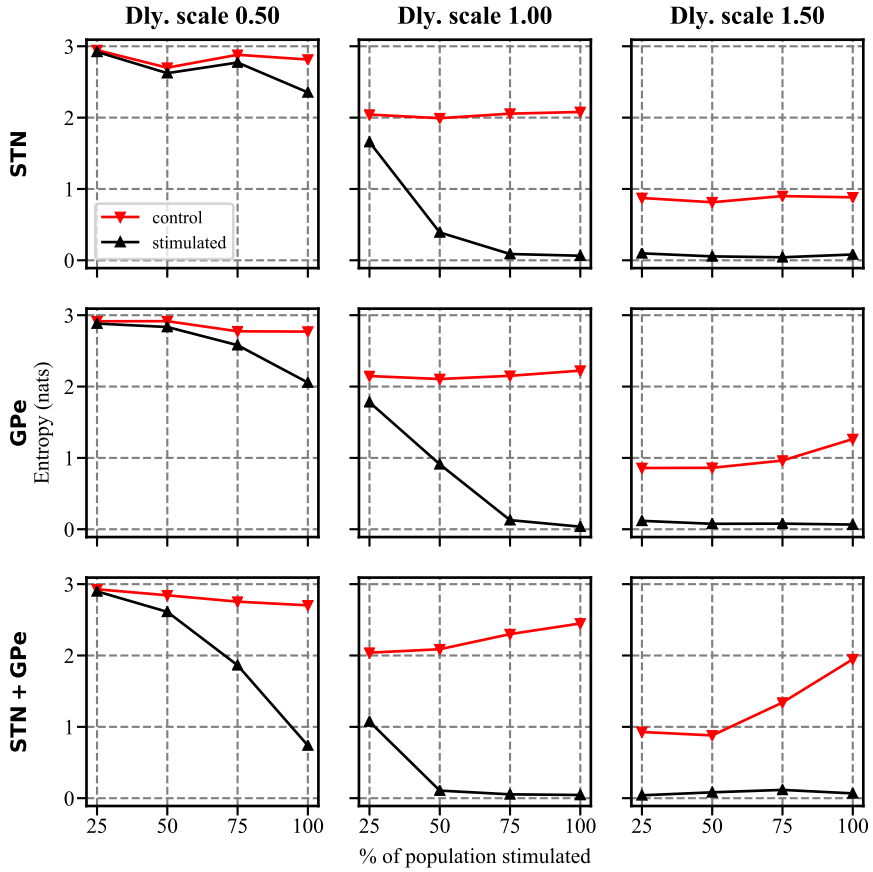

Fig 4.3. Increase in percentage of stimulated population reduced phase difference heterogeneity. For standard or low values of synaptic delays information entropy of phase difference profiles is reduced as the portion of the total neuronal population stimulated rises. For high synaptic delays entropy is always close to zero. Rows represent simulation iterations where only the indicated population (or both of them simultaneously in the third row) has received additional input. Each column corresponds to a fixed value of delay scale, with three different scales chosen as representative.

4.3.2 Lower synaptic delays increase STN-GPe phase difference heterogeneity

We proceeded to investigate the evolution of the phase difference distribution entropy across the whole range of synaptic delay scales used in our simulations, for three representative percentages of population stimulated. We observed that for each column of Figure 4.4 the entropy tended to assume lower values as the synaptic delays in STN-GPe circuit increased. Indeed, this effect was evident for both control and stimulated conditions, but was more prominent when stimulatory input was applied.

It should be noted that while the maximal entropy in each case was obtained for the lowest delay scale, for most combinations of stimulation using that delay scale the phase difference distributions were mostly flat (data not shown). That is to say, while the phase heterogeneity exemplified through entropy was at the maximum, the phase difference

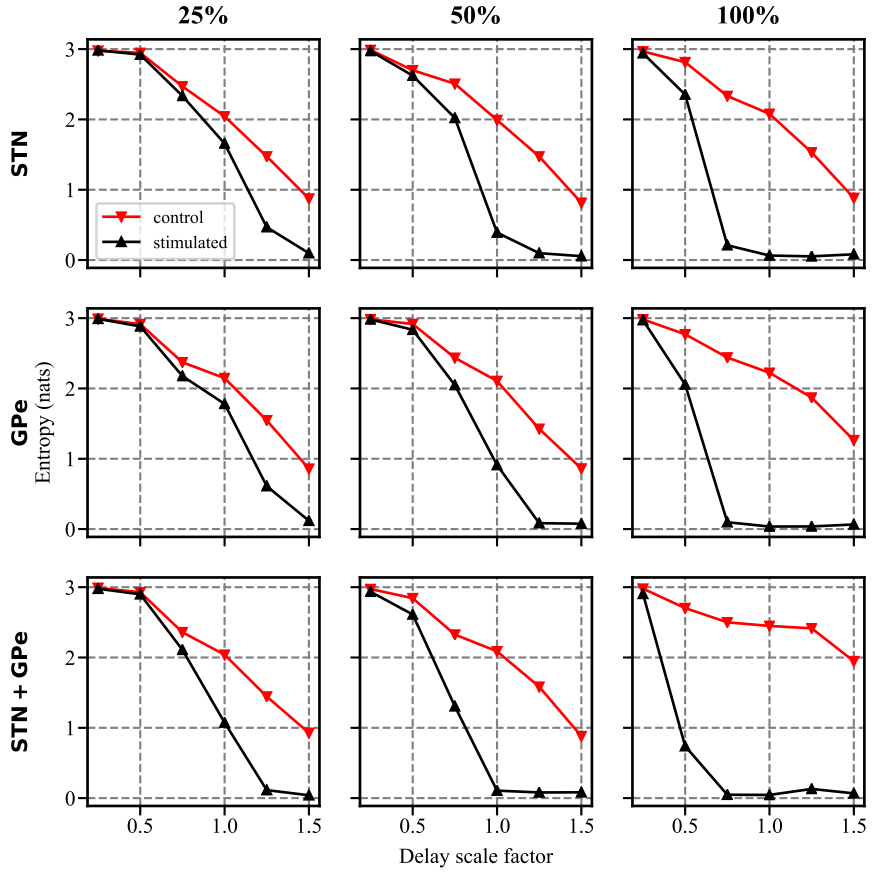

Fig 4.4. Decrease in synaptic delays augmented phase difference heterogeneity. For all examined percentages of population stimulated (three representative values are given column-wise), entropy of phase difference profiles is at the highest for low delay scales and decreases as synaptic delays grow. This effect is stronger for the stimulated than for the control condition.

profiles themselves were distributed over the available bins relatively equally, thus losing the structure that was evident in human patient recordings (Figure 4.2*A*).

While we are not explicitly concerned with beta-band oscillations in this study, their presence and effects on STN-GPe network dynamics are nevertheless crucial, and especially pertinent to explain the mechanism behind the dependence of entropy on synaptic delays. Namely, the stronger the oscillations in an excitatory-inhibitory network, the more neurons are entrained into a synchronous state, thereby reducing the variability of instantaneous phases they assume. This has a direct effect on the phase difference between STN and GPe, and therefore on the entropy of phase difference profiles. For in order for network oscillations to occur, there needs to be an adequate delay between the individual nuclei in that network Holgado et al. (2010). To illustrate with an example, there has to be an adequate amount of time for STN to achieve high enough firing rates to excite large enough portion of GPe neurons, which then likewise need time to build up their activity and in turn suppress the STN population. The decrease in STN firing would reduce the excitatory input to GPe, which then disinhibits STN and leads to a

new cycle of oscillations. However, if the synaptic delay between STN and GPe is too short, not enough activity can build up in one nucleus to sufficiently affect the other and thus initiate oscillatory behavior, which would finally result in a network converging to an equilibrium (Brunel, 2000, Holgado et al., 2010). As discussed above, such a network would indeed have a very high phase heterogeneity and thus high entropy, but its phase difference distribution would be flat. Conversely, very long synaptic delays allow for larger build-up of activity in the nuclei, leading to more intense oscillations, stronger coupling of activity between the two nuclei, and therefore to a much narrower distribution of phase differences.

4.3.3 Quantifying similarity of modified network output to human patient data

Finally, taking into account both the synaptic delay scale and the percentage of populations stimulated, we performed comparison of the STN-GPe phase difference profiles generated by our simulations to those obtained from human data patients. To this end we defined "relative error" (RE, Equation 4.2) that quantified the correspondence between the simulated profiles and the ones reproduced from Cagnan et al. (2015).

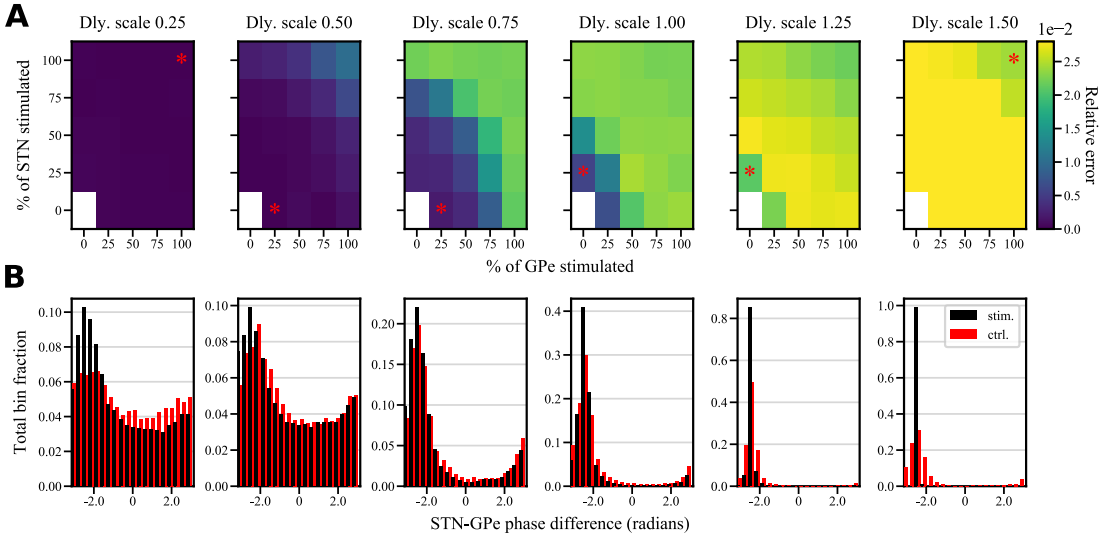

Fig 4.5. Exploring the parameter space to find the best match with human data. ***A*** Color plot of relative error values measuring similarity of simulation-obtained phase difference profiles to Figure 4.2*A* for different combinations of synaptic delay scales and percentages of STN and GPe populations stimulated. Red asterisk denotes the parameter combination that produced the best match. ***B*** STN-GPe phase difference profile corresponding to the red asterisk in *A*.

In Figure 4.5*A* we show how the relative error depends on the fraction of neurons that were stimulated in STN and GPe populations separately, and how this dependence changes for different delay scales. Generally, RE was the smallest for low delay scale

values, in line with the previous consideration about the effect of short synaptic delay times on phase difference heterogeneity. As the delay scale increased, low REs were concentrated in the region of the least fractions of population stimulated.

For each delay scale we located the parameter combination that produced the smallest REs, i.e. the best match with the human patient data, and plotted its corresponding phase difference profile (Figure 4.5*B*). It is striking that the best match was obtained for the values of synaptic delays that were around only 1 ms (Table 4.2). What is more, this particular parameter combination even reproduced the difference in distributions between control/ON DA and stimulated/OFF DA conditions that was evident in Figure 4.2*A*, but which we failed to achieve for higher delay scales. However, the current physiological evidence points to delays of synaptic transmission between STN and GPe nuclei to be of higher values (Holgado et al., 2010, Kita and Jaeger, 2016).

For larger delay scales, the best matches were obtained for the simulations in which only one of the STN or GPe populations were stimulated at the same time, and with the lowest fraction of neurons at that. Among these simulations, based on the comparison of entropy, the phase difference heterogeneity was at its maximum for synaptic delays that were only half of those used in the original iteration of the STN-GPe network (Mirzaei et al., 2017) (Figure 4.5*B*, second panel), and whose values lie firmly in the biologically relevant range (Kita and Jaeger, 2016).

Taken together, these results point to the importance of the way stimulation of STN and GPe is implemented in simulations of their circuitry, and that imposing additional input to only a portion of the neural populations may result in phase difference profiles similar to those as seen in human patients. Furthermore, we conclude that the choice of synaptic delays is crucial when exploring beta-band activity in the STN-GPe network, both in the healthy and the pathological state.

4.4 Discussion

Currently the most successful computational interpretation of the STN-GPe network reproduces in a realistic way both persistent and transient beta-band oscillations in healthy and Parkinsonian conditions. Nevertheless, it fails to capture the full spectrum of values of beta-band phase alignments between the two nuclei, as has been observed in human PD patients. This is especially evident for simulations of the Parkinsonian state, where one or both of the populations were receiving stimulatory input in order to promote pathological levels of beta-band activity. Here we address this issue and show that the heterogeneity of STN-GPe beta-band phase differences can be improved through

manipulation of two main variables: synaptic transmission delays, and the fraction of neuronal population that receives stimulation. Our results show that the model can achieve a greater correspondence with experimental results if not all the neurons in the target population(s) are stimulated. Indeed, those simulations where only a quarter of the neurons in a population were targeted by additional input proved to bear the highest degree of resemblance to the human patient data. This effect becomes even more prominent for very short synaptic delays, and conversely, disappears if the delays are overly long.

In this study we have approached the manipulation of synaptic delays by starting from the base values used in the previous version of the model (Mirzaei et al., 2017) and scaling both the within-population (GPe→GPe only) and between-population (STN↔GPe) ones by the same factor. This caused the within- and between-population delays to grow progressively further apart as the delay scale factor increased. To verify that the results we obtained were not due to this effect, we performed a set of simulations where both GPe→GPe and STN↔GPe delays were modified simultaneously by addition or subtraction of a constant value. However, there was no qualitative difference between the two approaches (data not shown).

It should be noted that the scope and the results of this study are limited in several aspects. Firstly, only a single value of the stimulus rate was employed, regardless of the percentage of the population affected or the target nucleus. The strength of the additional input to the network affects its dynamics directly, as too weak a stimulus would not be able to elicit significantly higher levels of beta-band activity, whereas too strong one would result in beta oscillations of unrealistic proportions. Nevertheless, there is a range of possible stimulus rates between these two extremes that warrant further investigation. Furthermore, it has been shown in a recent study by Bahuguna et al. (2019a) that the same network setup, but utilizing a neuron model where the firing rates and bursting can be independently controlled, responds in a different manner depending on whether the STN or GPe was stimulated. More precisely, the beta oscillations were more sensitive to changes in STN firing rates (induced by additional excitatory input), than to changes in GPe firing rates (induced by inhibitory stimulus). Therefore, it might be of interest to explore how the STN-GPe network dynamics might change during those simulations where both of the nuclei are stimulated, when the stimulus rates are different for each of them.

Secondly, a significant shortcoming of our model is its failure to replicate the characteristic relation of OFF DA and ON DA phase difference profiles as recorded in humans (Figure 4.2*A*). While the model does successfully capture the overall shape of the OFF DA/stimulated condition profile for several different combinations of input parameters

investigated in this study, the same cannot be said for the case of ON DA/control condition distribution. A possible reason for this issue lies in our choice of the background inputs to the STN and GPe neurons. Namely, the excitatory-inhibitory nature of the STN-GPe network model makes it prone to oscillatory behavior (Brunel, 2000), and one of the parameters that has a significant impact on the network dynamics is the balance of rates of the background input that the neurons of the two nuclei receive. We strived to balance those rates in such a way that the model, in the absence of additional stimulation, did not exhibit excessive beta-band oscillations, while at the same time allowed the STN and GPe populations to maintain average output levels close to physiological ones. Nevertheless, these two conditions could also be met for a different choice of background rates, and our tuning might not have been optimal enough to allow for the proper differentiation of phase difference profiles. As part of the future work, we will perform a detailed parameter search in order to verify this hypothesis.

Additionally, improved representation of STN-GPe phase alignments in our network allows us to direct future efforts towards further examination of beta-band phase properties. For example, it is known that beta-band activity is not continuously elevated, even during PD, but rather fluctuates and gives rise to beta bursts (Feingold et al., 2015, Tinkhauser et al., 2017b). However, the relationship of the beta bursts and phase-related phenomena such as phase locking or phase slips (Cagnan et al., 2015, Hurtado et al., 2005) remains to be explored.

Finally, a question may be asked: what would be the neurological basis for the assumption that only a part of STN or GPe may be stimulated? One answer to this issue might lie in the somatotopic organization of the basal ganglia in general, which is also reflected in both STN and GPe (Nambu, 2011). Thus, depending on the source of the input to the two structures, it is perfectly conceivable for some neurons of one of the nuclei to be temporarily more active than their neighbors. Another answer could be related to studies of action selection and neuronal ensembles within the basal ganglia, or more specifically, within the striatum. One of the functions of the BG is action selection, and several theoretical studies approached this subject by considering "action channels" — neural populations within the striatum that process individual upstream inputs (Bogacz and Gurney, 2007, Gurney et al., 2015, Bahuguna et al., 2019b). Moreover, there are both theoretical and experimental indications of the existence of localized groupings of neurons forming ensembles that also map the action space (Barbera et al., 2016, Humphries et al., 2009, Klaus et al., 2017, Spreizer et al., 2017). If action channels and localized neuronal ensembles exist also in the downstream BG nuclei, then their effects could perhaps be seen in subpopulations of different levels of activity in STN or GPe, similar to our own approach in this work.

Chapter 5

Discussion

As the principal cells of the striatum, GABAergic medium spiny neurons are at the center of both function and dysfunction of the basal ganglia. The proper balance of their activity is responsible, through direct and indirect pathways of the BG, for motor execution, action selection, habit formation, reinforcement learning, and others. When this balance is disturbed, for example through dopaminergic depletion in the striatum or increased selective apoptosis of MSNs, the results manifest as pathologies of the entire basal ganglia system. The goal of this thesis was to further our understanding of MSN activity through study of their inputs and their outputs. To this purpose, I used signal processing tools to analyze *in vivo* recorded MSN membrane potentials and examine their inputs (Chapter 2), biophysically complex dMSN model to investigate trial-by-trial output variability of a single neuron (Chapter 3), and a network of point neurons to observe the effects of pathological striatal activity on phase alignment of subthalamic nucleus and globus pallidus externa (Chapter 4).

5.1 Increased total input to dMSNs

In Chapter 2 I analyzed sub-threshold and supra-threshold dynamics of recorded MSN membrane potentials, to verify the presence of increased amounts of total input to one of the two MSN types.

Previously, Wall et al. (2013) gave a comprehensive overview of MSN afferents from various cortical and thalamic regions, and showed that limbic and sensory cortices preferentially target dMSNs, while motor cortex preferentially targets iMSNs. Over the past decade, several research groups were involved in a dispute concerning differential innervation of the two MSN types by intratelencephalic (IT) and pyramidal (PT) cortical

tracts. One side provided evidence that a higher percentage of IT-type neurons contacted dMSNs than iMSNs, and that iMSNs received more connections from PT-type than dMSNs (Deng et al., 2015, Lei et al., 2004). Other groups responded with their own results showing no such difference (Arias-García et al., 2017, Doig et al., 2010, Wall et al., 2013). More recently, Parker et al. (2016) demonstrated *in vitro* that both cortical and thalamic inputs are biased to dMSNs. Differences in both lateral MSN connectivity, as well as in the connections from fast spiking interneurons (FSIs) to MSNs, have also been demonstrated (Taverna et al., 2008, Planert et al., 2010); in both cases dMSNs were receiving more inhibitory inputs than iMSNs. Summating all the previous research, a theoretical study by Bahuguna et al. (2015) found that dMSNs have to receive stronger overall input in order for the activities of the two MSN types to be balanced.

In our own work, we show for the first time *in vivo* that dMSNs indeed receive stronger total input in healthy mice, and that this difference is lost for 6OHDA lesioned animals. Our conclusions rest on two key observations. First, by analyzing power spectral densities (PSD) of the sub-threshold MSN membrane potential, we demonstrate that dMSNs exhibit significantly higher spectral power than iMSNs in up-states for a wide range of high-frequency bands. Comparison of the estimates of the effective membrane time constant τ_m indicated that this effect was not the product of different membrane dynamics. Second, dMSN spike-triggered average (STA) traces clearly showed faster depolarization toward spiking threshold for stimulus-induced spikes compared to iMSN STAs.

Furthermore, PSD analysis revealed no difference in spectral power between dMSNs and iMSNs in 6OHDA lesioned mice, and values of τ_m that were comparable between the two groups. Together, these results indicate that in DA-depleted condition dMSNs and iMSNs receive similar amounts of total input.

Finally, we also found through effective membrane time constant estimation that up-state τ_m is significantly shorter than in the down-states, indicating that MSNs in the up-states operate in a high-conductance regime.

5.2 Dopamine as a modulator of response variability

In Chapter 3 I investigated the effects of dopaminergic modulation on output spike count variability of a biophysically complex dMSN model. I focused on two main modalities of synaptic input: when the input excitatory (E) and inhibitory (I) rates are correlated, and when a change in E-I balance occurs.

Variability of neuronal responses across different trials is a general characteristic of the central nervous system, and its sources have been tracked to synaptic noise, refractory period, and ongoing neural activity (Arieli et al., 1996, Faisal et al., 2008, Kara et al., 2000, Mainen and Sejnowski, 1995). Here we explored for the first time dMSN trial-by-trial variability in the context of a 2D transfer function, where excitatory and inhibitory inputs have been manipulated independently to produce a landscape of dMSN output firing rates. We found that dopaminergic modulation has a distinctly non-linear effect on dMSN response variability. In our setup, rise in dopamine levels would increase response variability when excitatory input rates were low, have a non-monotonic but generally diminishing effect on variability when excitatory input rates were mid-range, and have no perceptible effect for high excitatory input rates. Changes in inhibitory input rates mostly served to modulate the magnitude of these results.

When we restricted the independency of E and I inputs, either through imposing correlations of E and I input rates over different trials or through changes of E-I balance, we observed a complex interplay of synaptic bombardment and dopaminergic modulation. If a DA level remained fixed, an increase in input correlations would reduce trial-by-trial variability; this reduction would be more prominent for higher concentrations of dopamine. When input correlation value was fixed, dMSN trial-by-trial variability in the examined region of the 2D transfer function diminished as DA concentration grew. However, for high degrees of input correlations changes in DA level would have no perceptible effect. Shifts in E-I balance were more involved to interpret as our analysis revolved around so-called output firing rate (OFR) contours (see Chapter 3). Any changes in the E-I balance that would move sampled OFR distribution away from a contour would result in an increase in response variability for a fixed level of dopamine, and vice versa. At the same time, dopamine acted to decrease variability in the examined region of the 2D transfer function, as long as OFR distribution was sufficiently displaced from the contour; otherwise its effects were negligible.

Taken together, the model predicts that dopaminergic effect on dMSN trial-by-trial variability depends heavily on the proportion and the covariance of excitatory and inhibitory synaptic input, and that any changes in the E-I balance will have perceptible impact on the dispersion of dMSN output firing rates.

As a final note, in this study we sampled 2D dMSN transfer function by drawing samples from distributions of excitatory and inhibitory input rates. Each E and I rate drawn would produce a single dMSN output firing rate, which we considered a single trial. Multiple drawings would then represent multiple trials, and thus would the variance of MSN output firing rates (scaled by the mean OFR) represent trail-by-trial variability. However, we could also look at this sampling procedure from a network perspective. In

this situation, each sample would not represent a single trial, but rather an output firing rate of a single neuron in a pool of neurons. Thus all the samples taken together would constitute OFR distribution of a collection of cells recorded from a network, and the measured variability would be the response variability of the network itself. Of course, this would be only an approximation, as effects of lateral connectivity between dMSNs would not be included.

5.3 Partial stimulation of STN-GPe network improves phase alignment between the nuclei

In Chapter 4 I extended the existing STN-GPe network model in order to obtain an STN and GPe phase alignment profile more similar to that recorded in human PD patients.

The network model we used is able to successfully reproduce other aspects of STN and GPe beta band activity, such as transient and persistent beta oscillations in both healthy and Parkinsonian conditions (Kumar et al., 2011, Mirzaei et al., 2017), but it fails to fully capture the beta-band phase relationship of the two nuclei (Cagnan et al., 2015). This was especially true PD state, which we simulated by applying additional inhibitory input to GPe (representing increased iMSN activity that occurs during PD), and/or additional excitatory input to STN (representing increased cortical drive) (Degos et al., 2008, Holgado et al., 2010, Kumar et al., 2011, Mallet et al., 2008, Sato et al., 2000a, Tachibana et al., 2011). In this condition the STN-GPe phase difference distributions were very narrow, indicating that the two nuclei were perpetually phase-locked.

We were able to achieve a degree of correspondence of the network model output and the human patient recordings through manipulation of two model parameters: synaptic transmission delays, and percentages of populations stimulated. Our model predicts that a partial stimulation of one of the nuclei is enough to recover a portion of the STN-GPe phase difference heterogeneity. Indeed, we obtained the greatest correspondence to patient data when only a quarter of either STN or GPe neurons were stimulated. Furthermore, we showed that the heterogeneity of STN-GPe beta-band phase alignments was greatest for short synaptic delays, and that it decreased significantly as synaptic delay grew. While some of the values that we have used for delays fall outside of confines of physiology (being either too short or too long), the literature is not fully consistent on this subject and provides a range of values to choose from (Holgado et al., 2010, Kita and Jaeger, 2016).

5.4 Future work

Each of the projects I have described in this thesis lends itself to extensions and improvements, and offers multiple opportunities for future studies. Here I describe some of the possibilities.

5.4.1 Differentiating inputs to MSNs in health and disease

While our analysis of MSN membrane potentials comprises a well-rounded story, there are aspects of it that could be extended in a future work. The biggest remaining question is that of the differentiation of excitatory and inhibitory inputs to the MSNs. However, to the best of my knowledge, there exists no method to discern the type of input activity from a recorded membrane potential alone, and a more involved experimental setup would be needed to answer this problem.

Another aspect that is lacking in our work is STA treatment of DA-depleted traces. Unfortunately, we didn't have access to enough data from 6OHDA-lesioned animals to perform this analysis, but it would be of great interest to compare MSN STA traces between healthy and DA-depleted conditions. In our setup, we were able to follow the effects of mouse barrel cortex activation on outputs of healthy MSNs and show the difference between spontaneous and evoked activities, demonstrating increased inputs to dMSNs. When it comes to dopamine depletion however, there is a complex rewiring of all connections in the striatum, both afferent and recurrent ones. Namely, it has been shown that iMSNs suffer a widespread loss of dendritic spines and glutamatergic synapses in DA-depleted animals, while dMSNs remain relatively unchanged in this regard (Day et al., 2006, Taverna et al., 2008). Additionally, thalamo-striatal — but not cortico-striatal — neurons start targeting iMSNs preferentially in Parkinsonian condition (Parker et al., 2016). Changes in connectivity from FSIs to MSNs driven by the lack of dopamine are also asymmetrical, with the number of connections to iMSNs nearly doubling, while at the same time remaining largely unchanged for dMSNs (Gittis et al., 2011). Finally, lateral MSN connectivity is reported to be profoundly decreased in 6OHDA lesioned mice for both direct- and indirect-pathway neurons (Taverna et al., 2008). Therefore, it is difficult to estimate the cumulative effect of these changes on the amount of total input dMSNs and iMSNs receive without direct measurements, and further investigation in this direction is necessary. Our STA approach is straightforward to implement once *in vivo* recordings are obtained, and could provide further valuable insight into the changes to MSN processing brought about by the lack of dopaminergic modulation.

Lastly, we could also apply our novel approach for estimation of effective membrane time constant to other electrophysiological data, and measure its effectiveness versus a more traditional time constant measurement. While our method is relative, in the sense that it doesn't return true values for τ_m but that it can be used to compare all the data obtained in the same way, it is also fast and simple to apply to a post-processed membrane potential recording, and works without a need for additional specialized experiments.

5.4.2 Generalizing MSN response variability

The compartmental dMSN model that we have used to investigate the impact dopamine has on neural trial-by-trial variability is state-of-the-art. It integrates all the known MSN channel dynamics, and includes dMSN-specific dopaminergic modulation of intrinsic and synaptic channels. However, it has been constructed and tuned with respect to MSN data recorded from healthy animals, and thus does not allow for investigations of behavior under Parkinsonian conditions. It is known that due to adaptations of brain circuits during PD, both MSN types undergo changes in their intrinsic properties (Ketzef et al., 2017), as well as their connectivity (described in the previous section). Alterations in DA levels in the system and the changes of dopaminergic modulation dynamics also need to be taken into account. Therefore, in order to explore dMSN response variability under PD conditions, future efforts necessitate the complete re-tuning of all model parameters and creation of a parallel "PD dMSN".

Indirect-pathway MSNs should also not be forgotten. Different inputs they receive (Chapter 2 of this thesis, and Parker et al. 2016) as well as their different electrophysiological and anatomical properties compared to dMSNs (Gertler et al., 2008) indicate that iMSN 2D transfer function will have a distinct landscape. This of course will have a direct impact on its trial-by-trial variability profiles. Currently, such an iMSN model is in development and will be available for use in the near future (unpublished personal correspondence with R. Lindroos).

Ultimately, we have examined only two possible modes of synaptic input, and fairly limited at that. We can also wonder what would be the effects of input spike train correlations or a combination of changes in E-I balance and rate correlations on MSN response variability, and what role would dopamine play in those cases. We have also only touched the subject of intra-trial variability and regularization of output spike times. It would be then interesting in the future to consider these questions more thoroughly in the framework of point process theory (Nawrot et al., 2008).

Finally, while the overall subject of this thesis concerns medium spiny neurons, the approach that we used in Chapter 3 can be applied also to a more generic neuron

model. Indeed, we are currently investigating response variability of a large-scale neural network comprised of a more simple, leaky integrate and fire neuron.

5.4.3 Phase locking of beta bursts in STN-GPe circuit

While we succeeded in improving the correspondence of the network model and the human patient data for STN-GPe beta-band phase differences, we failed to reproduce the particular relationship between the OFF dopamine and ON dopamine conditions. A possible reason for this lies in the specific tuning of the STN-GPe network that we used, and as the first step in the future work we will address this issue by performing a thorough search for the optimal network parameters.

Improving the model in this way would open the door to further research on the subject of beta-band phase properties. Cagnan et al. (2015) has postulated, based on observations of STN and GPe beta-band phase locking duration, that synchronization of beta activity of the two nuclei spreads in waves within the populations until a phase slip occurs. While experimental verification of this hypothesis might demand complex recordings of a large number of neurons in both STN and GPe, it would be comparatively simple to test it in a computational environment.

5.5 Implications for the function and dysfunction of the basal ganglia

The analysis that we have performed in *in vivo* MSN recordings provides a valuable insight into how the extrinsic inputs are processed within the striatum, and gives experimental support to the conclusions of a previous computational model (Bahuguna et al., 2015). Nevertheless, other important aspects of striatal inputs remain to be studied in a living brain: the relative strengths of total excitatory and inhibitory inputs to MSNs; their balance, and the degree of correlation between them; spike time correlation within excitatory and inhibitory inputs separately; the difference in these variables depending on the MSN type; their evolution in time; and finally, the changes in the properties of inputs during Parkinson's disease. Some of these questions have been addressed by various *in vitro* studies, but limitations inherent in that approach preclude generalization of their results to the *in vivo* case. Ultimately, we are lacking hard values that describe distributions of input rates to individual MSNs and that discriminate between sources of that input.

We have shown here on the example of a dMSN model that properties of synaptic inputs affect its processing significantly, and that relatively small changes in the balance or in the correlation between incoming excitation and inhibition, combined with dopaminergic modulation, can have a large impact on neuronal response variability. These variations in MSN outputs will in turn reflect on the dynamics of the downstream nuclei, especially after synaptic rewiring that occurs in the striatum after dopamine depletion. To illustrate, it has recently been demonstrated in 6OHDA-lesioned rats that iMSNs in particular tend to lock to cortical beta oscillations, and that cortical beta-band bursts are closely associated with phase locking between the striatum, the subthalamic nucleus, the globus pallidus externa, and the cortex (Cagnan et al., 2019, Sharott et al., 2017). This locking of beta phase activity plays a significant role in propagation of BG-wide pathological beta oscillations, and further underscores the importance of the research into striatal medium spiny neurons.

5.6 Importance of collaboration between experimental and theoretical groups

It bears mentioning that for the study of MSN inputs (Chapter 2) we have used an archival dataset, that was recorded for the express purpose of a previous, related work (Ketzef et al., 2017). While in Ketzef et al. (2017) most of the analyses were performed on MSN down-states, we have complemented its results with our own investigation into the dynamics of up-states. This is a good illustration of two particular points: (1) even already used datasets have a lot to offer, and (2) their further examination could serve as the basis of collaboration between an experimental and a theoretical group, something that is of crucial importance for the future of neuroscience. Here I would like to very briefly focus on the second point, with a personal note.

During the course of my PhD I have come to the conclusion that a lot of experimentalists do not understand what is it that theoretical neuroscientists do, and that theoreticians do not appreciate the complexities of even the simplest experimental study. On the theoreticians' side, there is often a lack of proper interpretation of experimentally-obtained results. I have known computational neuroscientists (myself included) to ignore the differences between experimental setups while browsing through the literature for appropriate parameters to use for tuning of their models. They would not realize that a variable might vary wildly in its value depending on whether the recording was performed in brain slices or *in vivo*, or that even for the same type of recording different chemicals used in the process will have different impact on the results. The most illustrative example of this issue I have come across is that of an established and very

complex model of a neuron, that evolved and was upgraded over the years, sometimes used as a benchmark for other theoretical studies. However, after a detailed examination of the experimental studies that informed construction of the original model, it was discovered that a few of its parameters — which were also inherited in its newer versions — had actually wrong values, because the authors didn't interpret experimental findings properly.

On the other hand, I have regularly observed experimentalists outright ignoring theoretical work. Partly, it is due different levels of abstractions. A large fraction of computational studies concerns dynamics of neural networks that are larger than what experimentalists usually work with. They can also employ somewhat abstract mathematical concepts and analyses in order to describe the models and make predictions. Nevertheless, these computational models do make testable predictions, and it can be quite frustrating to see an experimental paper come to the same conclusions as a theoretical study, only years after the latter has already been published. Another part of the reason for shunning computation comes from a somewhat puzzling mindset that the only good model is the one which replicates biology perfectly. An aphorism of George Box, "all models are wrong, but some are useful", is often quoted by scientists who share this mindset. However, they tend to ignore the rest of the quote (Box, 1976):

> Since all models are wrong the scientist cannot obtain a "correct" one by excessive elaboration. On the contrary following William of Occam he should seek an economical description of natural phenomena. Just as the ability to devise simple but evocative models is the signature of the great scientist so overelaboration and overparameterization is often the mark of mediocrity.

Therefore, scientists who hold to the opinion that every model should strive to be as biologically precise as possible should dedicate some time to think about the actual purpose of modeling.

That being said, the cause of these misunderstandings is simple — a lack of communication between the two groups of researchers. Having said that, I do not believe that any amount of conferences and seminars is likely to fully bridge the gap between theoreticians and experimentalists. I do believe though, that the most effective way to achieve this is to force a prolonged co-mingling of the two groups of researchers, and make them dependent on each other. In other words, something scientific collaborations are known to do. Similar to our own efforts (see Chapter 2), there is a wealth of data obtained from different experiments that can be further studied and analyzed, maybe serve as a basis for a new model explaining an aspect of brain dynamics whose cause is currently unknown. Conversely, there are many computational models already published that would

benefit greatly from having their predictions tested experimentally. And the results of such efforts are certain to provide us all, no matter our approach to neuroscience, with new knowledge.

Bibliography

Adams, P. (1982). Voltage-dependent conductances of vertebrate neurones. *Trends in Neurosciences*, 5(C):116–119.

Adey, W. and Dunlop, C. (1960). Amygdaloid and peripheral influences on caudate and pallidal units in the cat and effects of chlorpromazine. *Experimental Neurology*, 2(4):348–363.

Albin, R. L. and Mink, J. W. (2006). Recent advances in Tourette syndrome research. *Trends in Neurosciences*, 29(3):175–182.

Albin, R. L., Young, A. B., and Penney, J. B. (1989). The functional anatomy of basal ganglia disorders. *Trends in Neurosciences*, 12(10):366–375.

Alexander, G. E. and Crutcher, M. D. (1990). Functional architecture of basal ganglia circuits: neural substrates of parallel processing. *Trends in Neurosciences*, 13:266–271.

Alexander, G. E., DeLong, M. R., and Strick, P. L. (1986). Parallel organization of functionally segregated circuits linking basal ganglia and cortex. *Annual Review of Neuroscience*, 9(1):357–381.

Anderson, B. A., Kuwabara, H., Wong, D. F., Roberts, J., Rahmim, A., Brašić, J. R., and Courtney, S. M. (2017). Linking dopaminergic reward signals to the development of attentional bias: A positron emission tomographic study. *NeuroImage*, 157(May):27–33.

Andre, V. M., Cepeda, C., Fisher, Y. E., Huynh, M., Bardakjian, N., Singh, S., Yang, X. W., and Levine, M. S. (2011). Differential Electrophysiological Changes in Striatal Output Neurons in Huntington's Disease. *Journal of Neuroscience*, 31(4):1170–1182.

Arias-García, M. A., Tapia, D., Laville, J. A., Calderón, V. M., Ramiro-Cortés, Y., Bargas, J., and Galarraga, E. (2017). Functional comparison of corticostriatal and thalamostriatal postsynaptic responses in striatal neurons of the mouse. *Brain Structure and Function*.

Arieli, A., Sterkin, A., Grinvald, A., and Aertsen, A. (1996). Dynamics of Ongoing Activity: Explanation of the Large Variability in Evoked Cortical Responses. *Science*, 273(5283):1868–1871.

Averbeck, B. B. and Costa, V. D. (2017). Motivational neural circuits underlying reinforcement learning. *Nature Neuroscience*, 20(4):505–512.

Averbeck, B. B., Latham, P. E., and Pouget, A. (2006). Neural correlations, population coding and computation. *Nature Reviews Neuroscience*, 7(5):358–366.

Bahuguna, J. (2017). Homologous Basal Ganglia Network Models in Physiological and Parkinsonian Conditions. *Frontiers in Computational Neuroscience*, 11(August):1–21.

Bahuguna, J., Aertsen, A., and Kumar, A. (2015). Existence and Control of Go/No-Go Decision Transition Threshold in the Striatum. *PLOS Computational Biology*, 11(4):e1004233.

Bahuguna, J., Sahasranamam, A., and Kumar, A. (2019a). Uncoupling the roles of firing rates and spike bursts in shaping the GPe-STN beta band oscillations. *bioRxiv doi: 10.1101/707471*.

Bahuguna, J., Weidel, P., and Morrison, A. (2019b). Exploring the role of striatal D1 and D2 medium spiny neurons in action selection using a virtual robotic framework. *European Journal of Neuroscience*, 49(6):737–753.

Balleine, B. W., Delgado, M. R., and Hikosaka, O. (2007). The Role of the Dorsal Striatum in Reward and Decision-Making. *Journal of Neuroscience*, 27(31):8161–8165.

Barbera, G., Liang, B., Zhang, L., Gerfen, C. R., Culurciello, E., Chen, R., Li, Y., and Lin, D.-T. (2016). Spatially Compact Neural Clusters in the Dorsal Striatum Encode Locomotion Relevant Information. *Neuron*, 92(1):202–213.

Barlow, R. L., Gorges, M., Wearn, A., Niessen, H. G., Kassubek, J., Dalley, J. W., and Pekcec, A. (2018). Ventral Striatal D2/3 Receptor Availability Is Associated with Impulsive Choice Behavior As Well As Limbic Corticostriatal Connectivity. *International Journal of Neuropsychopharmacology*, 21(7):705–715.

Barry, J., Akopian, G., Cepeda, C., and Levine, M. S. (2018). Striatal Direct and Indirect Pathway Output Structures Are Differentially Altered in Mouse Models of Huntington's Disease. *The Journal of Neuroscience*, 38(20):4678–4694.

Bergman, H., Wichmann, T., Karmon, B., and DeLong, M. R. (1994). The primate subthalamic nucleus. II. Neuronal activity in the MPTP model of parkinsonism. *Journal of neurophysiology*, 72(2):507–20.

Bevan, M. (2002). Move to the rhythm: oscillations in the subthalamic nucleus–external globus pallidus network. *Trends in Neurosciences*, 25(10):525–531.

Bhatia, A., Moza, S., and Bhalla, U. S. (2019). Precise excitation-inhibition balance controls gain and timing in the hippocampus. *eLife*, 8.

Bissonette, G. B. and Roesch, M. R. (2015). Rule encoding in dorsal striatum impacts action selection. *European Journal of Neuroscience*, 42(8):2555–2567.

Bogacz, R. and Gurney, K. (2007). The Basal Ganglia and Cortex Implement Optimal Decision Making Between Alternative Actions. *Neural Computation*, 19(2):442–477.

Borland, L. M., Shi, G., Yang, H., and Michael, A. C. (2005). Voltammetric study of extracellular dopamine near microdialysis probes acutely implanted in the striatum of the anesthetized rat. *Journal of Neuroscience Methods*, 146(2):149–158.

Box, G. E. P. (1976). Science and Statistics. *Journal of the American Statistical Association*, 71(356):791–799.

Brown, P. (2007). Abnormal oscillatory synchronisation in the motor system leads to impaired movement. *Current Opinion in Neurobiology*, 17(6):656–664.

Brown, P., Oliviero, A., Mazzone, P., Insola, A., Tonali, P., and Di Lazzaro, V. (2001). Dopamine Dependency of Oscillations between Subthalamic Nucleus and Pallidum in Parkinson's Disease. *The Journal of Neuroscience*, 21(3):1033–1038.

Brunel, N. (2000). Dynamics of sparsely connected networks of excitatory and inhibitory neurons. *Journal of Computational Neuroscience*, 8:183–208.

Bujan, A. F., Aertsen, A., and Kumar, A. (2015). Role of Input Correlations in Shaping the Variability and Noise Correlations of Evoked Activity in the Neocortex. *Journal of Neuroscience*, 35(22):8611–8625.

Buzsáki, G. (2006). *Rhythms of the Brain*. Oxford University Press.

Cafaro, J. and Rieke, F. (2010). Noise correlations improve response fidelity and stimulus encoding. *Nature*, 468(7326):964–967.

Cagnan, H., Duff, E. P., and Brown, P. (2015). The relative phases of basal ganglia activities dynamically shape effective connectivity in Parkinson's disease. *Brain*, 138(6):1667–1678.

Cagnan, H., Little, S., Foltynie, T., Limousin, P., Zrinzo, L., Hariz, M., Cheeran, B., Fitzgerald, J., Green, A. L., Aziz, T., and Brown, P. (2014). The nature of tremor circuits in parkinsonian and essential tremor. *Brain*, 137(12):3223–3234.

Cagnan, H., Mallet, N., Moll, C. K. E., Gulberti, A., Holt, A. B., Westphal, M., Gerloff, C., Engel, A. K., Hamel, W., Magill, P. J., Brown, P., and Sharott, A. (2019). Temporal evolution of beta bursts in the parkinsonian cortical and basal ganglia network. *Proceedings of the National Academy of Sciences*, 116(32):16095–16104.

Carvalho, M. M., Campos, F. L., Marques, M., Soares-Cunha, C., Kokras, N., Dalla, C., Leite-Almeida, H., Sousa, N., and Salgado, A. J. (2017). Effect of Levodopa on Reward and Impulsivity in a Rat Model of Parkinson's Disease. *Frontiers in Behavioral Neuroscience*, 11(August):1–13.

Cepeda, C., Colwell, C. S., Itri, J. N., Chandler, S. H., and Levine, M. S. (1998). Dopaminergic modulation of NMDA-induced whole cell currents in neostriatal neurons in slices: contribution of calcium conductances. *Journal of neurophysiology*, 79(1):82–94.

Chao, S. Z., Lu, W., Lee, H. K., Huganir, R. L., and Wolf, M. E. (2002). D1 dopamine receptor stimulation increases GluR1 phosphorylation in postnatal nucleus accumbens cultures. *Journal of Neurochemistry*, 81(5):984–992.

Cheer, J. F., Aragona, B. J., Heien, M. L., Seipel, A. T., Carelli, R. M., and Wightman, R. M. (2007). Coordinated Accumbal Dopamine Release and Neural Activity Drive Goal-Directed Behavior. *Neuron*, 54(2):237–244.

Churchland, M. M., Yu, B. M., Cunningham, J. P., Sugrue, L. P., Cohen, M. R., Corrado, G. S., Newsome, W. T., Clark, A. M., Hosseini, P., Scott, B. B., Bradley, D. C., Smith, M. A., Kohn, A., Movshon, J. A., Armstrong, K. M., Moore, T., Chang, S. W., Snyder, L. H., Lisberger, S. G., Priebe, N. J., Finn, I. M., Ferster, D., Ryu, S. I., Santhanam, G., Sahani, M., and Shenoy, K. V. (2010). Stimulus onset quenches neural variability: a widespread cortical phenomenon. *Nature Neuroscience*, 13(3):369–378.

Corbit, V. L., Whalen, T. C., Zitelli, K. T., Crilly, S. Y., Rubin, J. E., and Gittis, A. H. (2016). Pallidostriatal Projections Promote Oscillations in a Dopamine-Depleted Biophysical Network Model. *Journal of Neuroscience*, 36(20):5556–5571.

Cox, S. M., Frank, M. J., Larcher, K., Fellows, L. K., Clark, C. A., Leyton, M., and Dagher, A. (2015). Striatal D1 and D2 signaling differentially predict learning from positive and negative outcomes. *NeuroImage*, 109:95–101.

Cui, G., Jun, S. B., Jin, X., Pham, M. D., Vogel, S. S., Lovinger, D. M., and Costa, R. M. (2013). Concurrent activation of striatal direct and indirect pathways during action initiation. *Nature*, 494(7436):238–242.

Damodaran, S., Cressman, J. R., Jedrzejewski-Szmek, Z., and Blackwell, K. T. (2015). Desynchronization of Fast-Spiking Interneurons Reduces Beta-Band Oscillations and

Imbalance in Firing in the Dopamine-Depleted Striatum. *Journal of Neuroscience*, 35(3):1149–1159.

Daw, N. D., Niv, Y., and Dayan, P. (2005). Uncertainty-based competition between prefrontal and dorsolateral striatal systems for behavioral control. *Nature Neuroscience*, 8(12):1704–1711.

Day, M., Wang, Z., Ding, J., An, X., Ingham, C. A., Shering, A. F., Wokosin, D., Ilijic, E., Sun, Z., Sampson, A. R., Mugnaini, E., Deutch, A. Y., Sesack, S. R., Arbuthnott, G. W., and Surmeier, D. J. (2006). Selective elimination of glutamatergic synapses on striatopallidal neurons in Parkinson disease models. *Nature Neuroscience*, 9(2):251–259.

de la Rocha, J., Doiron, B., Shea-Brown, E., Josić, K., and Reyes, A. (2007). Correlation between neural spike trains increases with firing rate. *Nature*, 448(7155):802–806.

Degos, B., Deniau, J.-M., Le Cam, J., Mailly, P., and Maurice, N. (2008). Evidence for a direct subthalamo-cortical loop circuit in the rat. *European Journal of Neuroscience*, 27(10):2599–2610.

DeLong, M. R. (1971). Activity of pallidal neurons during movement. *Journal of Neurophysiology*, 34(3):414–427.

DeLong, M. R. (1990). Primate models of movement disorders of basal ganglia origin. *Trends in Neurosciences*, 13(7):281–285.

Deng, Y., Lanciego, J., Goff, L. K.-L., Coulon, P., Salin, P., Kachidian, P., Lei, W., Del Mar, N., and Reiner, A. (2015). Differential organization of cortical inputs to striatal projection neurons of the matrix compartment in rats. *Frontiers in systems neuroscience*, 9(April):51.

Denny-Brown (1962). *The Basal Ganglia*. London: Oxford Univ. Press.

Deserno, L., Schlagenhauf, F., and Heinz, A. (2016). Striatal dopamine, reward, and decision making in schizophrenia. *Dialogues in Clinical Neuroscience*, 18(1):77–89.

Destexhe, A., Hughes, S. W., Rudolph, M., and Crunelli, V. (2007). Are corticothalamic 'up' states fragments of wakefulness? *Trends in Neurosciences*, 30(7):334–342.

Destexhe, A., Paré, D., Willmore, B. D. B., Cooke, J. E., King, A. J., and Physiol, J. (1999). Impact of Network Activity on the Integrative Properties of Neocortical Pyramidal Neurons In Vivo. *Journal of Neurophysiology*, 81(4):1531–1547.

Destexhe, A., Rudolph, M., and Paré, D. (2003). The high-conductance state of neocortical neurons in vivo. *Nature Reviews Neuroscience*, 4(12):1019–1019.

Dhawale, A. K., Smith, M. A., and Ölveczky, B. P. (2017). The Role of Variability in Motor Learning. *Annual Review of Neuroscience*, 40(1):479–498.

Doig, N. M., Moss, J., and Bolam, J. P. (2010). Cortical and Thalamic Innervation of Direct and Indirect Pathway Medium-Sized Spiny Neurons in Mouse Striatum. *Journal of Neuroscience*, 30(44):14610–14618.

Doiron, B., Litwin-Kumar, A., Rosenbaum, R., Ocker, G. K., and Josić, K. (2016). The mechanics of state-dependent neural correlations. *Nature Neuroscience*, 19(3):383–393.

Doron, M., Chindemi, G., Muller, E., Markram, H., and Segev, I. (2017). Timed Synaptic Inhibition Shapes NMDA Spikes, Influencing Local Dendritic Processing and Global I/O Properties of Cortical Neurons. *Cell Reports*, 21(6):1550–1561.

Dreyer, J. K., Herrik, K. F., Berg, R. W., and Hounsgaard, J. D. (2010). Influence of Phasic and Tonic Dopamine Release on Receptor Activation. *Journal of Neuroscience*, 30(42):14273–14283.

Engelhard, B., Ozeri, N., Israel, Z., Bergman, H., and Vaadia, E. (2013). Inducing Gamma Oscillations and Precise Spike Synchrony by Operant Conditioning via Brain-Machine Interface. *Neuron*, 77(2):361–375.

Faisal, A. A., Selen, L. P. J., and Wolpert, D. M. (2008). Noise in the nervous system. *Nature Reviews Neuroscience*, 9(4):292–303.

Feingold, J., Gibson, D. J., DePasquale, B., and Graybiel, A. M. (2015). Bursts of beta oscillation differentiate postperformance activity in the striatum and motor cortex of monkeys performing movement tasks. *Proceedings of the National Academy of Sciences*, 112(44):13687–13692.

Fieblinger, T., Graves, S. M., Sebel, L. E., Alcacer, C., Plotkin, J. L., Gertler, T. S., Chan, C. S., Heiman, M., Greengard, P., Cenci, M. A., and Surmeier, D. J. (2014). Cell type-specific plasticity of striatal projection neurons in parkinsonism and L-DOPA-induced dyskinesia. *Nature Communications*, 5:5316.

Flores-Barrera, E., Vizcarra-Chacón, B. J., Bargas, J., Tapia, D., and Galarraga, E. (2011). Dopaminergic modulation of corticostriatal responses in medium spiny projection neurons from direct and indirect pathways. *Frontiers in systems neuroscience*, 5(March):15.

Flores-Hernández, J., Cepeda, C., Hernández-Echeagaray, E., Calvert, C. R., Jokel, E. S., Fienberg, A. A., Greengard, P., and Levine, M. S. (2002). Dopamine Enhancement of NMDA Currents in Dissociated Medium-Sized Striatal Neurons: Role of D1 Receptors and DARPP-32. *Journal of Neurophysiology*, 88(6):3010–3020.

Flores-Hernandez, J., Hernandez, S., Snyder, G. L., Yan, Z., Fienberg, A. A., Moss, S. J., Greengard, P., and Surmeier, D. J. (2000). D(1) dopamine receptor activation reduces GABA(A) receptor currents in neostriatal neurons through a PKA/DARPP-32/PP1 signaling cascade. *Journal of neurophysiology*, 83(5):2996–3004.

Frank, M. J. (2004). By Carrot or by Stick: Cognitive Reinforcement Learning in Parkinsonism. *Science*, 306(5703):1940–1943.

Fu, M., Yu, X., Lu, J., and Zuo, Y. (2012). Repetitive motor learning induces coordinated formation of clustered dendritic spines in vivo. *Nature*, 483(7387):92–95.

Fucke, T., Suchanek, D., Nawrot, M. P., Seamari, Y., Heck, D. H., Aertsen, A., and Boucsein, C. (2011). Stereotypical spatiotemporal activity patterns during slow-wave activity in the neocortex. *Journal of Neurophysiology*, 106(6):3035–3044.

Galarraga, E., Hernández-López, S., Reyes, A., Barral, J., and Bargas, J. (1997). Dopamine facilitates striatal EPSPs through an L-type Ca2+ conductance. *Neuroreport*, 8(9-10):2183–6.

Garofalo, S., Justicia, A., Arrondo, G., Ermakova, A. O., Ramachandra, P., Tudor-Sfetea, C., Robbins, T. W., Barker, R. A., Fletcher, P. C., and Murray, G. K. (2017). Cortical and Striatal Reward Processing in Parkinson's Disease Psychosis. *Frontiers in Neurology*, 8(APR):1–11.

Garst-Orozco, J., Babadi, B., and Ölveczky, B. P. (2014). A neural circuit mechanism for regulating vocal variability during song learning in zebra finches. *eLife*, 3:e03697.

Gerfen, C. R. and Scott Young, W. (1988). Distribution of striatonigral and striatopallidal peptidergic neurons in both patch and matrix compartments: an in situ hybridization histochemistry and fluorescent retrograde tracing study. *Brain Research*, 460(1):161–167.

Gertler, T. S., Chan, C. S., and Surmeier, D. J. (2008). Dichotomous Anatomical Properties of Adult Striatal Medium Spiny Neurons. *Journal of Neuroscience*, 28(43):10814–10824.

Gittis, A. H., Hang, G. B., LaDow, E. S., Shoenfeld, L. R., Atallah, B. V., Finkbeiner, S., and Kreitzer, A. C. (2011). Rapid target-specific remodeling of fast-spiking inhibitory circuits after loss of dopamine. *Neuron*, 71(5):858–868.

Gittis, A. H., Nelson, A. B., Thwin, M. T., Palop, J. J., and Kreitzer, A. C. (2010). Distinct Roles of GABAergic Interneurons in the Regulation of Striatal Output Pathways. *Journal of Neuroscience*, 30(6):2223–2234.

Groenewegen, H. J. (2003). The Basal Ganglia and Motor Control. *Neural Plasticity*, 10(1-2):107–120.

Gurney, K., Prescott, T. J., and Redgrave, P. (2001a). A computational model of action selection in the basal ganglia. I. A new functional anatomy. *Biological Cybernetics*, 84(6):401–410.

Gurney, K., Prescott, T. J., and Redgrave, P. (2001b). A computational model of action selection in the basal ganglia. II. Analysis and simulation of behaviour. *Biological Cybernetics*, 84(6):411–423.

Gurney, K. N., Humphries, M. D., and Redgrave, P. (2015). A New Framework for Cortico-Striatal Plasticity: Behavioural Theory Meets In Vitro Data at the Reinforcement-Action Interface. *PLoS Biology*, 13(1):e1002034.

Gusel'nikov, V. I. (1957). Methods of recording encephalograms in small laboratory animals in chronic experiments with the help of microelectrodes. *Zhurnal vfsshei nervmei deyatelnosti imeni*, 1:626–628.

Guthrie, M., Myers, C. E., and Gluck, M. A. (2009). A neurocomputational model of tonic and phasic dopamine in action selection: A comparison with cognitive deficits in Parkinson's disease. *Behavioural Brain Research*, 200(1):48–59.

Haider, B., Duque, A., Hasenstaub, A. R., and McCormick, D. A. (2006). Neocortical Network Activity In Vivo Is Generated through a Dynamic Balance of Excitation and Inhibition. *Journal of Neuroscience*, 26(17):4535–4545.

Haider, B., Häusser, M., and Carandini, M. (2013). Inhibition dominates sensory responses in the awake cortex. *Nature*, 493(7430):97–100.

Hamid, A. A., Pettibone, J. R., Mabrouk, O. S., Hetrick, V. L., Schmidt, R., Vander Weele, C. M., Kennedy, R. T., Aragona, B. J., and Berke, J. D. (2015). Mesolimbic dopamine signals the value of work. *Nature Neuroscience*, 19(1):117–126.

Hammond, C., Bergman, H., and Brown, P. (2007). Pathological synchronization in Parkinson's disease: networks, models and treatments. *Trends in Neurosciences*, 30(7):357–364.

Hennequin, G., Agnes, E. J., and Vogels, T. P. (2017). Inhibitory Plasticity: Balance, Control, and Codependence. *Annual Review of Neuroscience*, 40(1):557–579.

Hernández-Echeagaray, E., Cepeda, C., Ariano, M. A., Lobo, M. K., Sibley, D. R., and Levine, M. S. (2007). Dopamine Reduction of GABA Currents in Striatal Medium-sized Spiny Neurons is Mediated Principally by the D1 Receptor Subtype. *Neurochemical Research*, 32(2):229–240.

Hernandez-Lopez, S., Bargas, J., Surmeier, D. J., Reyes, A., Galarraga, E., Hernández-López, S., Bargas, J., Surmeier, D. J., Reyes, A., and Galarraga, E. (1997). D1 receptor activation enhances evoked discharge in neostriatal medium spiny neurons by modulating an L-type Ca2+ conductance. *J Neurosci*, 17(9):3334–3342.

Hienert, M., Gryglewski, G., Stamenkovic, M., Kasper, S., and Lanzenberger, R. (2018). Striatal dopaminergic alterations in Tourette's syndrome: a meta-analysis based on 16 PET and SPECT neuroimaging studies. *Translational Psychiatry*, 8(1):143.

Hines, M. (2009). NEURON and Python. *Frontiers in Neuroinformatics*, 3(January):1–12.

Hines, M. L. and Carnevale, N. T. (1997). The NEURON Simulation Environment. *Neural Computation*, 9(6):1179–1209.

Holgado, A. J. N., Terry, J. R., and Bogacz, R. (2010). Conditions for the Generation of Beta Oscillations in the Subthalamic Nucleus-Globus Pallidus Network. *Journal of Neuroscience*, 30(37):12340–12352.

Holm, S. (1979). A simple sequentially rejective multiple test procedure. *Scandianvian Journal of Statistics*, 6(2):65–70.

Holt, A. B., Kormann, E., Gulberti, A., Pötter-Nerger, M., McNamara, C. G., Cagnan, H., Baaske, M. K., Little, S., Köppen, J. A., Buhmann, C., Westphal, M., Gerloff, C., Engel, A. K., Brown, P., Hamel, W., Moll, C. K., and Sharott, A. (2019). Phase-Dependent Suppression of Beta Oscillations in Parkinson's Disease Patients. *The Journal of Neuroscience*, 39(6):1119–1134.

Howard, C. D., Li, H., Geddes, C. E., and Jin, X. (2017). Dynamic Nigrostriatal Dopamine Biases Action Selection. *Neuron*, 93(6):1436–1450.e8.

Howe, M. W. and Dombeck, D. A. (2016). Rapid signalling in distinct dopaminergic axons during locomotion and reward. *Nature*, 535(7613):505–510.

Hubel, D. H. (1957). Single unit activity in visual cortex of the unanesthetized cat. *Federation Proceedings*, 16(1):63–63.

Huerta-Ocampo, I., Mena-Segovia, J., and Bolam, J. P. (2014). Convergence of cortical and thalamic input to direct and indirect pathway medium spiny neurons in the striatum. *Brain Structure and Function*, 219(5):1787–1800.

Humphries, M. D., Wood, R., and Gurney, K. (2009). Dopamine-modulated dynamic cell assemblies generated by the GABAergic striatal microcircuit. *Neural Networks*, 22(8):1174–1188.

Hurtado, J. M., Rubchinsky, L. L., Sigvardt, K. A., Wheelock, V. L., and Pappas, C. T. E. (2005). Temporal Evolution of Oscillations and Synchrony in GPi/Muscle Pairs in Parkinson's Disease. *Journal of Neurophysiology*, 93(3):1569–1584.

Hussar, C. and Pasternak, T. (2010). Trial-to-trial variability of the prefrontal neurons reveals the nature of their engagement in a motion discrimination task. *Proceedings of the National Academy of Sciences*, 107(50):21842–21847.

Ikemoto, S. (2010). Brain reward circuitry beyond the mesolimbic dopamine system: A neurobiological theory. *Neuroscience & Biobehavioral Reviews*, 35(2):129–150.

Janssen, M. J., Ade, K. K., Fu, Z., and Vicini, S. (2009). Dopamine Modulation of GABA Tonic Conductance in Striatal Output Neurons. *Journal of Neuroscience*, 29(16):5116–5126.

Jones, E. G. (1999). MAKING BRAIN CONNECTIONS: Neuroanatomy and the Work of TPS Powell, 1923–1996. *Annual Review of Neuroscience*, 22(1):49–103.

Jung, R. and Hassler, R. (1960). The extrapyramidal motor system. In *Handbook of Physiology*, chapter 35, pages 863–927. American Physiological Society, Wahsington, D.C.

Kara, P., Reinagel, P., and Reid, R. (2000). Low Response Variability in Simultaneously Recorded Retinal, Thalamic, and Cortical Neurons. *Neuron*, 27(3):635–646.

Kasanova, Z., Ceccarini, J., Frank, M. J., van Amelsvoort, T., Booij, J., Heinzel, A., Mottaghy, F., and Myin-Germeys, I. (2017). Striatal dopaminergic modulation of reinforcement learning predicts reward—oriented behavior in daily life. *Biological Psychology*, 127(April):1–9.

Katz, Y., Yizhar, O., Staiger, J., and Lampl, I. (2013). Optopatcher-An electrode holder for simultaneous intracellular patch-clamp recording and optical manipulation. *Journal of Neuroscience Methods*, 214(1):113–117.

Keiflin, R. and Janak, P. H. (2015). Dopamine Prediction Errors in Reward Learning and Addiction: From Theory to Neural Circuitry. *Neuron*, 88(2):247–263.

Ketzef, M., Spigolon, G., Johansson, Y., Bonito-Oliva, A., Fisone, G., and Silberberg, G. (2017). Dopamine Depletion Impairs Bilateral Sensory Processing in the Striatum in a Pathway-Dependent Manner. *Neuron*, 94(4):855–865.e5.

Kita, H. and Jaeger, D. (2016). Organization of the Globus Pallidus. In Steiner, H. and Tseng, K. Y., editors, *Handbook of basal ganglia structure and function*, pages 259–276. Academic Press, 2nd edition.

Kitai, S. and Surmeier, D. (1993). Cholinergic and dopaminergic modulation of potassium conductances in neostriatal neurons. *Advances in Neurology*, 60:40–52.

Klaus, A., Martins, G. J., Paixao, V. B., Zhou, P., Paninski, L., and Costa, R. M. (2017). The Spatiotemporal Organization of the Striatum Encodes Action Space. *Neuron*, 95(5):1171–1180.e7.

Kondabolu, K., Roberts, E. A., Bucklin, M., McCarthy, M. M., Kopell, N., and Han, X. (2016). Striatal cholinergic interneurons generate beta and gamma oscillations in the corticostriatal circuit and produce motor deficits. *Proceedings of the National Academy of Sciences*, 113(22):E3159–E3168.

Kremkow, J., Aertsen, A., and Kumar, A. (2010). Gating of Signal Propagation in Spiking Neural Networks by Balanced and Correlated Excitation and Inhibition. *Journal of Neuroscience*, 30(47):15760–15768.

Kress, G. J., Yamawaki, N., Wokosin, D. L., Wickersham, I. R., Shepherd, G. M. G., and Surmeier, D. J. (2013). Convergent cortical innervation of striatal projection neurons. *Nature Neuroscience*, 16(6):665–667.

Kuhn, A., Aertsen, A., and Rotter, S. (2004). Neuronal Integration of Synaptic Input in the Fluctuation-Driven Regime. *Journal of Neuroscience*, 24(10):2345–2356.

Kühn, A. A., Kupsch, A., Schneider, G. H., and Brown, P. (2006). Reduction in subthalamic 8-35 Hz oscillatory activity correlates with clinical improvement in Parkinson's disease. *European Journal of Neuroscience*, 23(7):1956–1960.

Kumar, A., Cardanobile, S., Rotter, S., and Aertsen, A. (2011). The Role of Inhibition in Generating and Controlling Parkinson's Disease Oscillations in the Basal Ganglia. *Frontiers in Systems Neuroscience*, 5(October):1–14.

Kumar, A., Rotter, S., and Aertsen, A. (2008). Conditions for Propagating Synchronous Spiking and Asynchronous Firing Rates in a Cortical Network Model. *Journal of Neuroscience*, 28(20):5268–5280.

Lammel, S., Ion, D. I., Roeper, J., and Malenka, R. C. (2011). Projection-Specific Modulation of Dopamine Neuron Synapses by Aversive and Rewarding Stimuli. *Neuron*, 70(5):855–862.

Léger, J., Stern, E., Aertsen, A., and Heck, D. (2005). Synaptic integration in rat frontal cortex shaped by network activity. *Journal of Neurophysiology*, 93(93):281–293.

Lei, W., Jiao, Y., Del Mar, N., and A, R. (2004). Evidence for Differential Cortical Input to Direct Pathway versus Indirect Pathway Striatal Projection Neurons in Rats. *Journal of Neuroscience*, 24(38):8289–8299.

Levine, M. S., Altemus, K. L., Cepeda, C., Cromwell, H. C., Crawford, C., Ariano, M. A., Drago, J., Sibley, D. R., and Westphal, H. (1996a). Modulatory actions of dopamine on NMDA receptor-mediated responses are reduced in D1A-deficient mutant mice. *J Neurosci*, 16(18):5870–5882.

Levine, M. S., Li, S., Cepeda, C., Cromwell, H. C., and Altemus, K. L. (1996b). Neuromodulatory actions of dopamine on synaptically-evoked neostriatal responses in slices. *Synapse*, 24(1):65–78.

Levy, R., Ashby, P., Hutchison, W. D., Lang, A. E., Lozano, A. M., and Dostrovsky, J. O. (2002). Dependence of subthalamic nucleus oscillations on movement and dopamine in Parkinson's disease. *Brain*, 125(6):1196–1209.

Liang, L., DeLong, M. R., and Papa, S. M. (2008). Inversion of Dopamine Responses in Striatal Medium Spiny Neurons and Involuntary Movements. *Journal of Neuroscience*, 28(30):7537–7547.

Lindroos, R., Dorst, M. C., Du, K., Filipović, M., Keller, D., Ketzef, M., Kozlov, A. K., Kumar, A., Lindahl, M., Nair, A. G., Pérez-Fernández, J., Grillner, S., Silberberg, G., and Hellgren Kotaleski, J. (2018). Basal Ganglia Neuromodulation Over Multiple Temporal and Structural Scales—Simulations of Direct Pathway MSNs Investigate the Fast Onset of Dopaminergic Effects and Predict the Role of Kv4.2. *Frontiers in Neural Circuits*, 12(February):1–23.

Lynd-Balta, E. and Haber, S. (1994). The organization of midbrain projections to the striatum in the primate: Sensorimotor-related striatum versus ventral striatum. *Neuroscience*, 59(3):625–640.

Magill, P., Bolam, J., and Bevan, M. (2001). Dopamine regulates the impact of the cerebral cortex on the subthalamic nucleus–globus pallidus network. *Neuroscience*, 106(2):313–330.

Maia, T. V. and Frank, M. J. (2011). From reinforcement learning models to psychiatric and neurological disorders. *Nature Neuroscience*, 14(2):154–162.

Mainen, Z. F. and Sejnowski, T. J. (1995). Reliability of Spike Timing in Neocortical Neurons. *Science*, 268:1503–1506.

Mallet, N. (2006). Cortical Inputs and GABA Interneurons Imbalance Projection Neurons in the Striatum of Parkinsonian Rats. *Journal of Neuroscience*, 26(14):3875–3884.

Mallet, N., Pogosyan, A., Marton, L. F., Bolam, J. P., Brown, P., and Magill, P. J. (2008). Parkinsonian Beta Oscillations in the External Globus Pallidus and Their Relationship with Subthalamic Nucleus Activity. *Journal of Neuroscience*, 28(52):14245–14258.

McCormick, D. A., Connors, B. W., Lighthall, J. W., and Prince, D. A. (1985). Comparative electrophysiology of pyramidal and sparsely spiny stellate neurons of the neocortex. *Journal of Neurophysiology*, 54(4):782–806.

McGeorge, A. J. and Faull, R. L. M. (1989). The organization of the projection from the cerebral cortex to the striatum in the rat. *Neuroscience*, 29(3):503–537.

McGregor, M. M. and Nelson, A. B. (2019). Circuit Mechanisms of Parkinson's Disease. *Neuron*, 101(6):1042–1056.

Miller, R. (2007). *A Theory of the Basal Ganglia and Their Disorders*. CRC Press.

Mirzaei, A., Kumar, A., Leventhal, D., Mallet, N., Aertsen, A., Berke, J., and Schmidt, R. (2017). Sensorimotor Processing in the Basal Ganglia Leads to Transient Beta Oscillations during Behavior. *The Journal of Neuroscience*, 37(46):11220–11232.

Mizrahi-Kliger, A. D., Kaplan, A., Israel, Z., and Bergman, H. (2018). Desynchronization of slow oscillations in the basal ganglia during natural sleep. *Proceedings of the National Academy of Sciences*, page 201720795.

Moran, A., Stein, E., Tischler, H., and Bar-Gad, I. (2012). Decoupling neuronal oscillations during subthalamic nucleus stimulation in the parkinsonian primate. *Neurobiology of Disease*, 45(1):583–590.

Morita, K., Jitsev, J., and Morrison, A. (2016). Corticostriatal circuit mechanisms of value-based action selection: Implementation of reinforcement learning algorithms and beyond. *Behavioural Brain Research*, 311:110–121.

Mukovski, M., Chauvette, S., Timofeev, I., and Volgushev, M. (2007). Detection of active and silent states in neocortical neurons from the field potential signal during slow-wave sleep. *Cerebral Cortex*, 17(2):400–414.

Nambu, A. (2004). A new dynamic model of the cortico-basal ganglia loop. In *Neuroscience Research*, volume 43, pages 461–466. Elsevier.

Nambu, A. (2011). Somatotopic Organization of the Primate Basal Ganglia. *Frontiers in Neuroanatomy*, 5(April):26.

Nawrot, M. P., Boucsein, C., Rodriguez Molina, V., Riehle, A., Aertsen, A., and Rotter, S. (2008). Measurement of variability dynamics in cortical spike trains. *Journal of Neuroscience Methods*, 169(2):374–390.

Nieto Mendoza, E. and Hernández Echeagaray, E. (2015). Dopaminergic Modulation of Striatal Inhibitory Transmission and Long-Term Plasticity. *Neural Plasticity*, 2015:1–15.

Nisenbaum, E. S. and Wilson, C. J. (1995). Potassium currents responsible for inward and outward rectification in rat neostriatal spiny projection neurons. *The Journal of neuroscience : the official journal of the Society for Neuroscience*, 15(6):4449–4463.

Okun, M. and Lampl, I. (2008). Instantaneous correlation of excitation and inhibition during ongoing and sensory-evoked activities. *Nature Neuroscience*, 11(5):535–537.

Osakada, F., Mori, T., Cetin, A. H., Marshel, J. H., Virgen, B., and Callaway, E. M. (2011). New Rabies Virus Variants for Monitoring and Manipulating Activity and Gene Expression in Defined Neural Circuits. *Neuron*, 71(4):617–631.

Pacheco-Cano, M., Bargas, J., Hernandez-Lopez, S., Tapia, D., and Galarraga, E. (1996). Inhibitory action of dopamine involves a subthreshold Cs+-sensitive conductance in neostriatal neurons. *Experimental Brain Research*, 110(2):205–211.

Papoulis, A. and Pillai, S. U. (2002). *Probability, Random Variables and Stochastic Processes*. Tata McGraw-Hill Education, 4th edition.

Paré, D., Shink, E., Gaudreau, H., Destexhe, A., and Lang, E. J. (1998). Impact of spontaneous synaptic activity on the resting properties of cat neocortical pyramidal neurons In vivo. *Journal of neurophysiology*, 79(3):1450–1460.

Parent, A. (2012). The History of the Basal Ganglia: The Contribution of Karl Friedrich Burdach. *Neuroscience and Medicine*, 03(04):374–379.

Parker, P. R. L., Lalive, A. L., and Kreitzer, A. C. (2016). Pathway-Specific Remodeling of Thalamostriatal Synapses in Parkinsonian Mice. *Neuron*, 89(4):734–740.

Parkinson, J. (2002). An Essay on the Shaking Palsy. *Journal of Neuropsychiatry*, 14(2):223–236.

Pavlides, A., Hogan, S. J., and Bogacz, R. (2015). Computational Models Describing Possible Mechanisms for Generation of Excessive Beta Oscillations in Parkinson's Disease. *PLoS Computational Biology*, 11(12):1–29.

Paxinos, G. and Franklin, K. B. (2004). *The mouse brain in stereotaxic coordinates*. Gulf professional publishing.

Percheron, G., Fenelon, G., Leroux-Hugon, V., and Feve, A. (1994). The history of basal ganglia. The slow development of a major cerebral system. *Revue Neurologique*, 150(8):543–554.

Petersen, A. V., Cotel, F., and Perrier, J.-F. (2017). Plasticity of the Axon Initial Segment: Fast and Slow Processes with Multiple Functional Roles. *The Neuroscientist*, 23(4):364–373.

Peyser, A., Sinha, A., Vennemo, S. B., Ippen, T., Jordan, J., Graber, S., Morrison, A., Trensch, G., Fardet, T., Mørk, H., Hahne, J., Schuecker, J., Schmidt, M., Kunkel, S., Dahmen, D., Eppler, J. M., Diaz, S., Terhorst, D., Deepu, R., Weidel, P., Kitayama, I., Mahmoudian, S., Kappel, D., Schulze, M., Appukuttan, S., Schumann, T., Tunç, H. C., Mitchell, J., Hoff, M., Müller, E., Carvalho, M. M., Zajzon, B., Plesser, H. E., Itayama, I., Mahmoudian, S., Kappel, D., Schulze, M., Appukuttan, S., Schumann, T., Tunç, H. C., Mitchell, J., Hoff, M., Müller, E., Carvalho, M. M., and Zajzon, Barna Plesser, H. E. (2017). NEST 2.14.0.

Planert, H., Berger, T. K., and Silberberg, G. (2013). Membrane properties of striatal direct and indirect pathway neurons in mouse and rat slices and their modulation by dopamine. *PloS one*, 8(3):e57054.

Planert, H., Szydlowski, S. N., Hjorth, J. J. J., Grillner, S., and Silberberg, G. (2010). Dynamics of Synaptic Transmission between Fast-Spiking Interneurons and Striatal Projection Neurons of the Direct and Indirect Pathways. *Journal of Neuroscience*, 30(9):3499–3507.

Podda, M., Riccardi, E., D'Ascenzo, M., Azzena, G., and Grassi, C. (2010). Dopamine D1-like receptor activation depolarizes medium spiny neurons of the mouse nucleus accumbens by inhibiting inwardly rectifying K+ currents through a cAMP-dependent protein kinase A-independent mechanism. *Neuroscience*, 167(3):678–690.

Price, C. J., Kim, P., and Raymond, L. a. (1999). D1 dopamine receptor-induced cyclic AMP-dependent protein kinase phosphorylation and potentiation of striatal glutamate receptors. *Journal of neurochemistry*, 73(6):2441–6.

Ray, N., Jenkinson, N., Wang, S., Holland, P., Brittain, J., Joint, C., Stein, J., and Aziz, T. (2008). Local field potential beta activity in the subthalamic nucleus of patients with Parkinson's disease is associated with improvements in bradykinesia after dopamine and deep brain stimulation. *Experimental Neurology*, 213(1):108–113.

Raz, A., Vaadia, E., and Bergman, H. (2000). Firing Patterns and Correlations of Spontaneous Discharge of Pallidal Neurons in the Normal and the Tremulous 1-Methyl-4-Phenyl-1,2,3,6-Tetrahydropyridine Vervet Model of Parkinsonism. *The Journal of Neuroscience*, 20(22):8559–8571.

Redgrave, P., Prescott, T. J., and Gurney, K. (1999). The basal ganglia: A vertebrate solution to the selection problem?

Reig, R. and Silberberg, G. (2014). Multisensory Integration in the Mouse Striatum. *Neuron*, 83(5):1200–1212.

Ricci, G., Doane, B., and Jasper, H. (1957). Microelectrode studies of conditioning: technique and preliminary results. In *Premier congres international des sciences neurologiques*, pages 401–415.

Riehle, A., Grammont, F., Diesmann, M., and Grün, S. (2000). Dynamical changes and temporal precision of synchronized spiking activity in monkey motor cortex during movement preparation. *Journal of Physiology-Paris*, 94:569–582.

Robinson, D. L., Phillips, P. E. M., Budygin, E. A., Trafton, B. J., Garris, P. A., and Wightman, R. M. (2001). Sub-second changes in accumbal dopamine during sexual behavior in male rats. *Neuroreport*, 12(11):2549–2552.

Roitman, M. F. (2004). Dopamine Operates as a Subsecond Modulator of Food Seeking. *Journal of Neuroscience*, 24(6):1265–1271.

Santini, E., Valjent, E., Usiello, A., Carta, M., Borgkvist, A., Girault, J.-A., Herve, D., Greengard, P., and Fisone, G. (2007). Critical Involvement of cAMP/DARPP-32 and Extracellular Signal-Regulated Protein Kinase Signaling in L-DOPA-Induced Dyskinesia. *Journal of Neuroscience*, 27(26):6995–7005.

Sato, F., Lavallée, P., Lévesque, M., and Parent, A. (2000a). Single-axon tracing study of neurons of the external segment of the globus pallidus in primate. *The Journal of Comparative Neurology*, 417(1):17–31.

Sato, F., Parent, M., Lévesque, M., and Parent, A. (2000b). Axonal branching pattern of neurons of the subthalamic nucleus in primates. *The Journal of Comparative Neurology*, 424(1):142–152.

Schiffmann, S. N., Lledo, P.-M., and Vincent, J.-D. (1995). Dopamine D1 receptor modulates the voltage-gated sodium current in rat striatal neurones through a protein kinase A. *Journal of Physiology*, 483(1):95–107.

Schneidman, E., Berry, M. J., Segev, R., and Bialek, W. (2006). Weak pairwise correlations imply strongly correlated network states in a neural population. *Nature*, 440(7087):1007–1012.

Schreiber, S., Fellous, J.-M., Tiesinga, P., and Sejnowski, T. J. (2004). Influence of Ionic Conductances on Spike Timing Reliability of Cortical Neurons for Suprathreshold Rhythmic Inputs. *Journal of Neurophysiology*, 91(1):194–205.

Schultz, W. (2007). Multiple Dopamine Functions at Different Time Courses. *Annual Review of Neuroscience*, 30(1):259–288.

Schultz, W. (2016). Dopamine reward prediction error coding. *Dialogues in Clinical Neuroscience*, 18:23–32.

Schultz, W., Dayan, P., and Montague, P. R. (1997). A Neural Substrate of Prediction and Reward. *Science*, 275(June 1994):1593–1600.

Shadlen, M. N. and Newsome, W. T. (1998). The variable discharge of cortical neurons: implications for connectivity, computation, and information coding. *The Journal of neuroscience : the official journal of the Society for Neuroscience*, 18(10):3870–96.

Sharott, A., Vinciati, F., Nakamura, K. C., and Magill, P. J. (2017). A population of indirect pathway striatal projection neurons is selectively entrained to parkinsonian beta oscillations. *The Journal of Neuroscience*, 37(41):0658–17.

Shen, W., Flajolet, M., Greengard, P., and Surmeier, D. J. (2008). Dichotomous Dopaminergic Control of Striatal Synaptic Plasticity. *Science*, 321(5890):848–851.

Shink, E., Bevan, M., Bolam, J., and Smith, Y. (1996). The subthalamic nucleus and the external pallidum: two tightly interconnected structures that control the output of the basal ganglia in the monkey. *Neuroscience*, 73(2):335–357.

Silberberg, G. and Bolam, J. P. (2015). Local and afferent synaptic pathways in the striatal microcircuitry. *Current Opinion in Neurobiology*, 33:182–187.

Sippy, T., Lapray, D., Crochet, S., and Petersen, C. C. H. (2015). Cell-Type-Specific Sensorimotor Processing in Striatal Projection Neurons during Goal-Directed Behavior. *Neuron*, 88(2):298–305.

Snyder, G. L., Allen, P. B., Fienberg, a. a., Valle, C. G., Huganir, R. L., Nairn, a. C., and Greengard, P. (2000). Regulation of phosphorylation of the GluR1 AMPA receptor in the neostriatum by dopamine and psychostimulants in vivo. *The Journal of neuroscience : the official journal of the Society for Neuroscience*, 20(12):4480–4488.

Spreizer, S., Angelhuber, M., Bahuguna, J., Aertsen, A., and Kumar, A. (2017). Activity Dynamics and Signal Representation in a Striatal Network Model with Distance-Dependent Connectivity. *eneuro*, 4(4):ENEURO.0348–16.2017.

Stein, R. B., Gossen, E. R., and Jones, K. E. (2005). Neuronal variability: noise or part of the signal? *Nature Reviews Neuroscience*, 6(5):389–397.

Stern, E. a., Kincaid, A. E., and Wilson, C. J. (1997). Spontaneous subthreshold membrane potential fluctuations and action potential variability of rat corticostriatal and striatal neurons in vivo. *Journal of neurophysiology*, 77(4):1697–1715.

Surmeier, D. J., Bargas, J., Hemmings, H. C., Nairn, a. C., and Greengard, P. (1995). Modulation of calcium currents by a D1 dopaminergic protein kinase/phosphatase cascade in rat neostriatal neurons. *Neuron*, 14(2):385–97.

Surmeier, D. J., Ding, J., Day, M., Wang, Z., and Shen, W. (2007). D1 and D2 dopamine-receptor modulation of striatal glutamatergic signaling in striatal medium spiny neurons. *Trends in Neurosciences*, 30(5):228–235.

Surmeier, D. J., Eberwine, J., Wilson, C. J., Cao, Y., Stefani, A., and Kitai, S. T. (1992). Dopamine receptor subtypes colocalize in rat striatonigral neurons. *Proceedings of the National Academy of Sciences of the United States of America*, 89(21):10178–82.

Surmeier, D. J., Plotkin, J., and Shen, W. (2009). Dopamine and synaptic plasticity in dorsal striatal circuits controlling action selection. *Current Opinion in Neurobiology*, 19(6):621–628.

Tachibana, Y., Iwamuro, H., Kita, H., Takada, M., and Nambu, A. (2011). Subthalamo-pallidal interactions underlying parkinsonian neuronal oscillations in the primate basal ganglia. *European Journal of Neuroscience*, 34(9):1470–1484.

Tai, L.-H., Lee, A. M., Benavidez, N., Bonci, A., and Wilbrecht, L. (2012). Transient stimulation of distinct subpopulations of striatal neurons mimics changes in action value. *Nature Neuroscience*, 15(9):1281–1289.

Tass, P., Smirnov, D., Karavaev, A., Barnikol, U., Barnikol, T., Adamchic, I., Hauptmann, C., Pawelcyzk, N., Maarouf, M., Sturm, V., Freund, H.-J., and Bezruchko, B. (2010). The causal relationship between subcortical local field potential oscillations and Parkinsonian resting tremor. *Journal of Neural Engineering*, 7(1):016009.

Taverna, S., Ilijic, E., and Surmeier, D. J. (2008). Recurrent Collateral Connections of Striatal Medium Spiny Neurons Are Disrupted in Models of Parkinson's Disease. *Journal of Neuroscience*, 28(21):5504–5512.

Tchumatchenko, T., Malyshev, A., Geisel, T., Volgushev, M., and Wolf, F. (2010). Correlations and synchrony in threshold neuron models. *Physical Review Letters*, 104(5):5–8.

Tinkhauser, G., Pogosyan, A., Little, S., Beudel, M., Herz, D. M., Tan, H., and Brown, P. (2017a). The modulatory effect of adaptive deep brain stimulation on beta bursts in Parkinson's disease. *Brain*, 140(4):1053–1067.

Tinkhauser, G., Pogosyan, A., Tan, H., Herz, D. M., Kühn, A. A., and Brown, P. (2017b). Beta burst dynamics in Parkinson's disease OFF and ON dopaminergic medication. *Brain*, 140(11):2968–2981.

Tomkins, A., Vasilaki, E., Beste, C., Gurney, K., and Humphries, M. D. (2014). Transient and steady-state selection in the striatal microcircuit. *Frontiers in Computational Neuroscience*, 7(January):1–16.

Tong, H. and Gibb, A. J. (2008). Dopamine D1 receptor inhibition of NMDA receptor currents mediated by tyrosine kinase-dependent receptor trafficking in neonatal rat striatum. *The Journal of Physiology*, 586(19):4693–4707.

Travis, R. P. and Sparks, D. L. (1967). Changes in unit activity during stimuli associated with food and shock reinforcement. *Physiology & Behavior*, 2(2):171–177.

Tremblay, L., Worbe, Y., and Hollerman, J. R. (2009). The ventral striatum. In *Handbook of Reward and Decision Making*, pages 51–77. Elsevier.

Tritsch, N. X. and Sabatini, B. L. (2012). Dopaminergic Modulation of Synaptic Transmission in Cortex and Striatum. *Neuron*, 76(1):33–50.

Umemiya, M. and Raymond, L. A. (1997). Dopaminergic modulation of excitatory postsynaptic currents in rat neostriatal neurons. *Journal of Neurophysiology*, 78(3):1248–1255.

van Vreeswijk, C., Sompolinsky, H., Vreeswijk, C. v., and Sompolinsky, H. (1996). Chaos in neuronal networks with balanced excitatory and inhibitory activity. *Science*, 274(5293):1724–1726.

Vogels, T. P. and Abbott, L. F. (2009). Gating multiple signals through detailed balance of excitation and inhibition in spiking networks. *Nature Neuroscience*, 12(4):483–491.

Wall, N. R., De La Parra, M., Callaway, E. M., and Kreitzer, A. C. (2013). Differential innervation of direct- and indirect-pathway striatal projection neurons. *Neuron*, 79(2):347–360.

Wang, L., Conner, J. M., Rickert, J., and Tuszynski, M. H. (2011). Structural plasticity within highly specific neuronal populations identifies a unique parcellation of motor learning in the adult brain. *Proceedings of the National Academy of Sciences*, 108(6):2545–2550.

Waters, J. and Helmchen, F. (2006). Background Synaptic Activity Is Sparse in Neocortex. *Journal of Neuroscience*, 26(32):8267–8277.

Wilson, C. J. (2013). Active decorrelation in the basal ganglia. *Neuroscience*, 250:467–482.

Wilson, C. J. and Kawaguchi, Y. (1996). The origins of two-state spontaneous membrane potential fluctuations of neostriatal spiny neurons. *The Journal of neuroscience : the official journal of the Society for Neuroscience*, 16(7):2397–410.

Xu, T., Yu, X., Perlik, A. J., Tobin, W. F., Zweig, J. A., Tennant, K., Jones, T., and Zuo, Y. (2009). Rapid formation and selective stabilization of synapses for enduring motor memories. *Nature*, 462(7275):915–919.

Xue, B., Chen, E. C., He, N., Jin, D. Z., Mao, L. M., and Wang, J. Q. (2017). Integrated regulation of AMPA glutamate receptor phosphorylation in the striatum by dopamine and acetylcholine. *Neuropharmacology*, 112:57–65.

Yager, L., Garcia, A., Wunsch, A., and Ferguson, S. (2015). The ins and outs of the striatum: Role in drug addiction. *Neuroscience*, 301:529–541.

Yan, Z., Hsieh-Wilson, L., Feng, J., Tomizawa, K., Allen, P. B., Fienberg, a. a., Nairn, a. C., and Greengard, P. (1999). Protein phosphatase 1 modulation of neostriatal AMPA channels: regulation by DARPP-32 and spinophilin. *Nature neuroscience*, 2(1):13–17.

Zhai, S., Tanimura, A., Graves, S. M., Shen, W., and Surmeier, D. J. (2018). Striatal synapses, circuits, and Parkinson's disease. *Current Opinion in Neurobiology*, 48:9–16.

Zhang, X.-F., Cooper, D. C., and White, F. J. (2002). Repeated cocaine treatment decreases whole-cell calcium current in rat nucleus accumbens neurons. *Journal Of Pharmacology And Experimental Therapeutics*, 301(3):1119–1125.

Zhang, X. F., Hu, X. T., and White, F. J. (1998). Whole-cell plasticity in cocaine withdrawal: reduced sodium currents in nucleus accumbens neurons. *The Journal of neuroscience : the official journal of the Society for Neuroscience*, 18(1):488–98.

Zhao, B., Zhu, J., Dai, D., Xing, J., He, J., Fu, Z., Zhang, L., Li, Z., and Wang, W. (2016). Differential dopaminergic regulation of inwardly rectifying potassium channel mediated subthreshold dynamics in striatal medium spiny neurons. *Neuropharmacology*, 107(169):396–410.